Data Assimilation for Off site Nuclear Emergency Management

FINAL REPORT

DAONEM

FIKR-CT-2000-00025

F I N A L

V e r s i o n 1 . 0

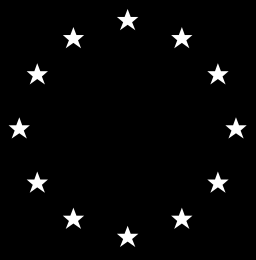

RODOS

REPORT

DECISION SUPPORT FOR NUCLEAR EMERGENCIES

RODOS(RA5)-RE(04)-01

DAONEM Final Report

RODOS(RA5)-RE(04)-01

Carlos Rojas Palma (ed.)

Belgian Nuclear Research Center (SCK•CEN)
Radiation Protection Division
Boeretang 200
B-2400 Mol, Belgium
Email: crojas@sckcen.be

Final, 02 September 2005

Table of Contents

Executive Summary[1]

There is an imperative need for developing a methodology that enables radiological advisors to use observations to update the predictions of models; hence reducing the uncertainty associated with model-based dose and consequence assessments, in the light of available monitoring data. Such a methodology is known as data assimilation. Application of data assimilation in a model spreads the information obtained from point measurements to the entire domain in a consistent manner, according to the model dynamics (interpolation in space). Furthermore, by updating the modelling system whenever measurements are available ensures that the model will not drift away from the measurements (interpolation in time).

In the 4th Framework Programme, a considerable amount of effort has been devoted to integrating a suite of computer codes, with different degrees of complexity, into a European real-time, on-line decision support system for off-site management of nuclear emergencies (the RODOS system). The modelling system describes the transport and dispersion of radionuclides in both atmospheric and aquatic systems, as well as their impact on the food chain.

RODOS predicts the values of many quantities that are likely to be of interest to decision makers after an accident (e.g. activity concentration in air, deposition, concentration in foods, external dose rates, concentrations in water bodies). The predictions will not exactly reflect the situation after an accident, as the models use a number of assumptions that are appropriate to the average situation across large areas of Europe, rather than to the particular conditions of the area affected by the accident. In the period immediately after the accident there will be a limited amount of information available from monitoring programmes. To make the best use of this information, it is necessary to correct the RODOS predictions in light of the available measurements.

In general, in off-site emergency management, data assimilation will prove useful throughout the different stages of the accident. In the assessment of the consequences during the early phase, in the improvement of prior assumptions based solely on expert judgement, and when there is a clear need for longer-term predictions to assess the radiological impact on the food chain.

The core of the proposed work was to develop data assimilation tools for off-site nuclear emergency management, and integrate these tools into the real-time, on-line decision support system RODOS. The work consisted of three main components, which are associated with the main pathways through which radioactivity will reach the biosphere. These include:

[1] The work described in this report has been performed with support of the European Commission under the contract “Data Assimilation for Off-site Nuclear Emergency Management” (DAONEM), contract no. FIKR-CT-2000-00025

• Data assimilation in the early phase of a nuclear accident, including atmospheric transport and dispersion.
• Data assimilation in the late phase after the deposition of radionuclides from the atmosphere has ceased, including food chain and dose assessment.
• Data assimilation in the hydrological model chain, including runoff of radionuclides from watersheds and transport and dispersion in rivers, lakes, reservoirs and coastal areas.

For all three components, a common methodology based on Bayes' theorem and Kalman filtering has been adopted for assimilation of data. The use of a common data assimilation approach in the different pathways and the subsequent implementation in the RODOS decision support system guaranteed a harmonised and coherent methodology to handle and to propagate uncertainties from one model into the other. However, due to the different nature and complexity of the models involved, the Kalman filter needed to be adapted differently in the various models, and hence different methodological developments were required in each of the three components.

Uncertainty assessment procedures were developed as an integrated part of the data assimilation schemes. This included assessment of uncertainties of measured quantities as well as modelling uncertainties. For all three components a common Monte Carlo based technique was adopted for identifying the most sensitive model and initialisation parameters and to quantify their uncertainty under specific environmental conditions.
Besides the data assimilation activities, the DAONEM project was extended through the participation of two newly associated states: the Slovak Republic and Romania. Their activities concentrated on the implementation of the RODOS hydrological model chain and posterior customization, with the aim of reporting back to the developers their findings and bugs. They also evaluated some of the proposed data assimilation techniques using simulated environmental measurements for their water sheds.

Since this project covers data assimilation in three areas, namely: early phase, late phase and in the RODOS hydrological model chain, the results will subdivided in the same order.

Data assimilation in the early phase

The data assimilation module, ADUM (Atmospheric Dispersion Updating Module), for the meso-scale atmospheric dispersion program RIMPUFF (Risø Mesoscale Puff model) – part of the early-phase programs of RODOS – has been developed. It is built on the Kalman filtering algorithm and it assimilates 10-minute averaged gamma dose rates measured at ground level stations. Since the gamma rates are non-linear functions of the state vector variables, the applied Kalman filter is the so-called Extended Kalman filter. Simulations showed that given reasonable conditions, i.e. a spatially dense distribution of gamma monitors and a realistic wind field, the developed ADUM module is found to be able to enhance the prediction of the gamma dose field.
Based on some of the Kalman filtering parameters, another module, ToDeMM, has been developed for providing the late-phase DeMM

(Deposition Monitoring Module) of RODOS with an ensemble of fields of ground level air concentrations and wet deposited material. This accounts for the uncertainty estimation of this kind of quantities as calculated by RIMPUFF for use by DeMM.

Data assimilation in the late phase

For the improvement of data assimilation tools in the deposition and the food chain modeling, a comprehensive testing of a variety of advanced Kalman filter approaches was accomplished. The Ensemble Kalman filter (EnKF) was identified as the most promising approach for data assimilation in both the deposition model and the food chain model. In the EnKF the uncertainty of the state vector (which represents the considered system) is described by an ensemble of state vectors, where each state vector is a possible representation of the system. New versions of the Deposition Monitoring Module (DeMM) and the Food Monitoring Module (FoMM) on the basis of the EnKF have been developed and integrated into the RODOS system.
DeMM assimilates measured data of gamma dose rate and predictions of radionuclide depositions onto different surfaces. The EnKF required integrating a stochastic uncertainty modelling into the deposition model, which considers uncertainty of model forcing (i.e. input from the ADUM module), uncertainty of model parameters and uncertainty of measurement data.
FoMM makes use of measured food and feed contaminations in order to improve the respective predictions and to reduce their uncertainty. Updates of the food chain modelling parameters (and optionally of the deposition pattern) are derived in FoMM which can be used by the Food chain and Dose Module FDMT for an improvement of feed and food contaminations as well as of doses from different pathways. Submodules have been developed for FoMM which quantify the estimated uncertainty of model predictions and of the measurement data.
For both modules, DeMM and FoMM, twin experiments with simulated measurement data, as well as tests with real measurements from the time after the Chernobyl accident were carried out in order to test their performance. These tests have shown that the Ensemble Kalman filter is a suitable data assimilation tool for improving results of the deposition and the food chain model, since the information from the model inter- and extrapolates the information coming from the measurements in several respects:

- measurements taken at any time can lead to an update of the predictions of past and future contaminations,
- measurements at individual locations can improve the predictions at the whole calculation grid,
- measurements of certain foodstuff's contamination allow an update also of other products,
- measurement of activity concentrations of one nuclide can update the predictions for other radionuclides.

Data assimilation in the RODOS hydrological model chain

Data assimilation and uncertainty assessment procedures have been develop and implemented into the different models in the Hydrological Dispersion

Module (HDM) of RODOS. These include the watershed model RETRACE, the 1D river model RIVTOX, the 2D model COASTOX, and the 3D model THREETOX.

For the RETRACE model an uncertainty assessment module has been developed (RETRACE ASUN). The implementation is based on a Monte Carlo simulation approach that propagates the main uncertainty sources, including the radionuclide depositions, wash-off coefficients and precipitation. For the radionuclide depositions the uncertainty given by the ensemble approximation in the Deposition Monitoring Module (DeMM) is used. The output from RETRACE ASUN includes uncertainties in the runoff and radionuclide wash-off to the river model RIVTOX in terms of ensemble approximations.

For the RIVTOX model two different sub-optimal variants of the Kalman filter, the EnKF and the reduced rank square root (RRSQRT) filter, have been further developed. In the EnKF different enhancements have been made that reduces the impact of statistical noise caused by applying a finite ensemble size. For the RRSQRT filter a new algorithm has been developed that provides a more efficient truncation of the low-rank approximation of the covariance matrix. This new filter, denoted Subspace Parsing Enhanced RRSQRT, is especially tailored for use in a multi-phase system such as RIVTOX. The implemented data assimilation methods have been tested on a setup of the Dnieper river for simulation of the transport and dispersion of ^{90}Sr caused by inundation of the contaminated floodplains in the Chernobyl zone in 1999. The test showed that both filters are suitable tools for improving the prediction skills in RIVTOX, and, importantly, provide an estimate of the prediction uncertainty.

For data assimilation in COASTOX and THREETOX the EnKF and RRSQRT filter cannot be directly applied due to the high computational load of these models. Instead more cost-effective procedures have been developed and tested. These include different sub-optimal variants of the Kalman filter that assume constant, time-independent uncertainty in the model forecast and the measurements, and hence do not require propagation of the covariance (or rather its ensemble approximation) between measurement updates. These techniques are only slightly more expensive than a normal model run. Twin-test experiments with simulated measurements based on model setups of the Kiev and Kakhovka reservoirs were applied for testing the methods. In addition, a test has been conducted based on ^{137}Cs dispersion in the Black Sea caused by Chernobyl fallout. These tests have shown that the implemented data assimilation procedures enhance the prediction capabilities of the models.

Implementation of the RODOS HDM in Slovakia

In line with the collected databases, the hydro models were adapted to the conditions of the river watershed of the developed river network Váh-Hron-Žitava-Danube and the reservoir Kráľová. Subsequent testing of the modules was performed by means of created set of files with hypothetical unit parameters. Based on the verification scenarios selected for the models, also the verification of simulated prediction data was performed on the basis of

comparison of this data with the physically expected one for the model and site given.
The verification done in 2003 highlighted the fact that the results of calculations strongly depend on the values of certain model parameters for which no exact data are available – e.g., the value of sediment deposition rates, the average amount of bottom sediments in the river bed. These parameters were set for the Dudváh River on the basis of existing empirical data obtained during monitoring an accidentally elevated ^{137}Cs discharges from the Bohunice Nuclear Power Plant (NPP) A1 (being under decommissioning). These values for the other then Dudvah river sections (e.g. Hron river) can be set more accurately only on the basis of processing and evaluation of future accidental monitoring data. Proper data assimilation techniques using the initial phase of an accidental data sequence seems to be appropriate for such adjusting of the mentioned model parameters.

Implementation of the RODOS HDM in Romania

The implementation of the RODOS-HDM for the Danube river was a complex task, due to the topology of Danube in the Cernavoda segment, which contains loops and multiple outlets. Consequently a simplified model of flow was adopted and further implemented into RODOS.
The customisation work focused on the RIVTOX model for which the connection to the RODOS aquatic food dose and chain module (FDMA) was also realised. The data assimilation methodology was tested via the ADM-RIVTOX chain, based on a simulated CANDU nuclear accident scenario.
The modelling of a river like Danube has to pay a special attention from the developers, in order to address in a better way the real topology, containing loops and multiple outlets.
For the further customisation of HDM modules in case of the complex hydrology of the Danube Delta, containing a mixture of lakes and channels, there is a need for simplification, due to the large amount of hydrological data required.
Since tritium is a very important radionuclide in case of accidental CANDU NPP releases in Danube river, it should be included in the RODOS-database.
On the other hand, it would be useful to extend the capabilities of the FDMA module for the assessment of radionuclide concentrations in predatory and non-predatory fish.
The FDMA grid has also to be extended to more than 160 km because the effects of a release in water and, consequently, the radioactive pollution of the water withdraw regions propagate downstream on a larger area.
Having in mind that many NPPs, potential nuclear pollutants, are situated on the Danube river and its tributaries, a complete stream of river is needed. A special database has to be developed by participation of all countries that are passed by the river, addressing the peculiarities of this river such as dams or the delta. This would also allow to estimate the nuclear pollution even for an accidental release that would occur outside the national territory.

Objectives and strategic aspects

The main objective of this project was to improve the predictive capabilities of the RODOS system by developing and implementing data assimilation tools. More specifically:

- To investigate data assimilation techniques based on Bayes theorem and Kalman filtering methods to identify those aspects, which can be used in the project and where common developments are required.
- To incorporate appropriate data assimilation tools in the existing (EURATOM 4th Framework Programme) RODOS atmospheric dispersion model, for application during the early phase of a nuclear accident.
- Improve existing data assimilation algorithms in the deposition estimation and in the food chain modelling, to assess their limitations by testing them against existing data sets, and to define ways to improve them.
- To incorporate appropriate data assimilation tools in the existing RODOS hydrological model chain.

The work performed clearly contributes to the program and key action objectives by improving existing models and introducing the possibility of assimilating available information. All of this will translate in a more coherent and efficient decision support system for off-site management of nuclear emergencies in Europe.

The knowledge derived from this project could also be transferred to research efforts in updating numerical weather forecasts of local wind with monitoring data, this way predicted wind field around the release point used to predict the dispersion of radioactivity in the atmosphere, would be more accurate. Such an application of data assimilation and uncertainty modelling on wind forecasts could also significantly improve the uncertainty estimates from atmospheric dispersion models, thus enabling an improved performance of all data assimilation tools developed within the DAONEM project.
Testing the developed data assimilation tools has proven their ability to improve the quality and reliability of predictions. But it became also obvious that problems may occur in practical application due to imperfect uncertainty estimation, e.g. if measurement or prediction errors exceed the estimated uncertainty of measurements or models. For this reason, further testing and application of the developed data assimilation tools in realistic off-site emergency management situations is necessary in order to make the methodologies more robust in operational application.
The knowledge on data assimilation is there, a remaining task is to find its applicability on responding to nuclear or radiological emergencies through its implementation and the feedback from the user community.

Scientific and technical description of the results

The project work-plan was divided into 5 major work packages:

WP1Harmonization of the data assimilation and uncertainty assessment approaches
WP2 Development of data assimilation in the early phase modeling
WP3 Development of data assimilation in the late phase modeling
WP4 Development of data assimilation in the hydrological modeling
WP5 Synopsis and post-audit of the integrated models in the RODOS system

The division into these five work packages acknowledges both the adaptation of common methodologies as well as the need for individual developments in the different modeling components, together with the final integration within the RODOS decision support system. WP1 aimed at ensuring that coherent methodologies were applied in the different fields of radiological assessment modeling, and at avoiding duplicate developments. The major work packages WP2-WP4 were divided into several sub-work packages as outlined in the technical annex. WP5 performed an evaluation of the developments in the three areas and made the findings available to generic decision support systems.

The following sub-sections describe the results of the individual work packages as well as those associated with the NAS-DAONEM extension of the project, namely the implementation and evaluation of data assimilation techniques associated with the RODOS Hydrological model chain (HDM).

Data assimilation in the early phase (WP2)

During the early phase of an atmospheric release of radioactivity, spanning from the pre-release and extending not beyond 24 hours from its onset, the decision making process will concentrate on sheltering, distribution of stable iodine, and, if need be, evacuation. All these countermeasures will be strongly supported by model predictions, which are prone to errors and uncertainties. After some time, monitoring teams and radiological networks will start populating a database; however, these data may be sparse in both time and space and therefore model predictions will still be needed.

The present report describes the Atmospheric Dispersion Updating Module (ADUM), i.e. the data assimilation module developed for the atmospheric dispersion model RIMPUFF, Risø Mesoscale Puff Model, Mikkelsen et al. (1984), Thykier-Nielsen et al. (1998), one of the dispersion models in the Local Scale Model Chain of RODOS. The prescribed data assimilation method in DAONEM is the so-called Kalman filtering, Kalman (1960), which updates selected state variables of the prediction on the basis of differences between predicted and measured quantities and on uncertainty estimates for both prediction and measurements. Because of the nonlinearity between the selected state variables: puff position and inventory, and the

available measurement quantities: gamma dose rates, the so-called Extended Kalman Filter has been applied.

More than just being post-processed by other early-phase RODOS modules, the RIMPUFF/ADUM results are also needed by the later phase Deposition Monitoring Module (DeMM), Gering et al. (2000). In DeMM, Kalman filtering is also being applied, for which reason uncertainty estimates have to follow the fields passed to it. DeMM does this estimation itself based on an ensemble of probable fields, and for the calculation of this ensemble of fields, the ToDeMM module has been created, a module also described in the present report.

The early-phase atmospheric dispersion model used in this project is the Risø Mesoscale Puff model, RIMPUFF, Mikkelsen et al. (1984), Thykier-Nielsen et al. (1998), which is driven by a meteorological preprocessor. RIMPUFF models the plume of released material as a number of individual puffs, every 10 minutes releasing a puff that holds 10 minutes of released material. A puff can be visualized as a kind of spherical or ellipsoidal cloud, a body of air and suspended released material, having a certain size. For the sake of calculation, the suspended material is given a 3D-Gaussian concentration distribution. This is an approximation to the real fluctuating distribution in a plume, and at its tails it is not describing reality very well. For this reason RIMPUFF cuts it off at a user specified distance from the puff centre, the point of maximum concentration. The recommended cut-off distance is 3.7 standard deviations, where the concentration equals 0.001 times the centre concentration, and with this value RIMPUFF accounts for 97% of the specified release, far within any real release uncertainty.

Each puff is advected with the local wind speed at its centre, it grows in size due to the local turbulence - i.e. the concentration distribution flattens - its centre is raised as the puff strikes the ground in order to model the rise of the plume centre of mass, and its inventory holds up to 15 different nuclides, the amount of which change due to radioactive decay and due to deposition to ground, the latter due to both dry processes and to rain. All meteorological parameters needed by the model are obtained from the meteorological pre-processor of RODOS.

RIMPUFF delivers fields of time integrated ground concentrations, time integrated gamma dose rates (i.e. gamma doses) from the puffs, time integrated deposition rates (i.e. deposited amount) split on dry and wet deposition, and instantaneous gamma dose rates from deposited material, all for each of the up to 15 nuclides. Iodine is further treated as a mix of differently depositing elementary, organic, and aerosol bound iodine. And more than just the fields, RIMPUFF also calculates the same parameters for specific points, detector points, specified within the computation area.

Kalman filtering

Kalman filtering, Kalman (1960), is a statistically based method for improving model predictions by real time assimilation of measurements. It works by updating the state vector, i.e. a set of important state variables in the model being filtered, by applying a correction based on the difference between measured and model calculated data and on specified uncertainties associated with the state vector update and with the measurements. The

methodology and the used nomenclature are described in detail in Puch and Astrup (2002).

For normal Kalman filtering of a well posed system, the state vector is a constant set of parameters, the Kalman update takes place at every time step based on instantaneous measurements, and the P-matrix, the error covariance matrix, settles after a number of time steps and becomes more or less constant in time, holding values that do not depend on its initial setting.

For the Kalman filtering of RIMPUFF the state vector has been selected to hold the centre position (*x,y,z*) and the total radioactive content *q* of each puff within the given computation domain, whereas the data used for the Kalman filtering are the calculated and measured gamma radiation dose rates at the specified ground based detector points.

Already here two things make this use of Kalman filtering non standard: 1) The state vector variables are not a fixed set but change whenever a new puff is released, a puff leaves the calculational area, or a puff splits into more puffs, and 2) measured gamma dose rates shall only be available as 10-minute average values, i.e. the Kalman filter has to update "instantaneous" puff positions and contents based on calculated and measured 10-minute average values.

Using 10-minute average gamma dose rates is not necessarily a draw back. In fact the calculated instantaneous gamma dose rates to the detector points on ground shall be artificially fluctuating due to the split of the plume into puffs, which at least close to the release point are so small that they do not really overlap if there is just a bit of wind. The 10-minute average values can be considered more reliably calculated quantities. But the determination of the needed derivatives of the 10-minute average dose rates with respect to the final puff positions is not unique.

A third untypical element comes in, if the detector points are sparse and puffs may travel several time steps before getting sufficiently close to the next detector point to add to the dose rate there. In this case different parts of the state vector may get Kalman updated at different times and not necessarily often.

Error covariance matrix initialization

The behaviour of the Kalman filtering is very much dependent upon the so-called *P*-matrix, the error covariance matrix, which is updated during the Kalman procedure, but needs to be initialized. For normal well-behaved Kalman filtering, the *P*-matrix stabilizes after some update sequences, and the initial value is not critical, but, as mentioned above, the actual use of Kalman filtering is not standard, and the initial *P*-matrix is very influential.

As the Kalman state vector contains the center position *(x,y,z)* and the inventory *q* of each puff, and the P-matrix holds the error covariances of all state vector variables, the *P*-matrix expands, whenever a new puff is released. All new parameters, i.e. all parameters refering to the new puff, need to be initialized. The covariance elements for the new puff itself, the submatrix P_{init}, is set as

$$P_{init} = \begin{pmatrix} S_{xy}^2 & 0 & 0 & 0 \\ 0 & S_{xy}^2 & 0 & 0 \\ 0 & 0 & S_z^2 & 0 \\ 0 & 0 & 0 & (a \cdot q)^2 \end{pmatrix}$$

where S_{xy}, S_z, and a are user specified numbers, while q is the also user specified total puff activity for the new puff.

The S_{xy} and S_z values represent the standard deviation of the initial puff position, i.e. the uncertainty of the release point position, horizontally and vertically.

The coefficient $a=S_q/q$ specifies the ratio of the puff inventory standard deviation S_q to the specified puff inventory q, i.e. it is the relative uncertainty in the estimation/specification of the release rate.

The covariances between new puff and old puff state vector variables also form submatrices in the P-matrix, which need initialization. The off-diagonal terms are again set to 0.0, while the diagonal terms are set as half the sum of the corresponding P-matrix diagonal terms multiplied with a factor going smoothly from 1 to 0 for the puff-to-puff distance going from 0 to twice the Lagrangian length scale of the local atmospheric turbulence.

Prediction update covariances

The Kalman filter needs an error covariance estimate for the prediction update of the state vector. A method for estimating these error covariances for the state vector variables of a single puff and of different puffs is presented in appendix B. With a single adjustment the method presented there is the one being used.

The adjustment is due to the fact, that the approach is based on wind speed and direction uncertainties due only to turbulence, any meteorological bias thus being neglected. Bias as such cannot be dealt with, but the uncertainties can be increased due to the expectation of other uncertainty sources than just turbulence. Presently a hardwired minimum wind direction uncertainty (standard deviation) is applied: $\sigma_\varphi \geq 15°$, while for a neutrally stable atmosphere the appendix B formulas give $\sigma_\varphi \approx 6°$.

Measurement covariances

Kalman filtering also needs an estimation of the measurement uncertainties, or more precisely, it needs a covariance matrix for the measurements. For the present implementation zero covariance is assumed between different measurements thus reducing the problem to the vector of the matrix diagonal, i.e. the measurement variances. Radiation monitoring devices are different and so are their uncertainties/variances. For the time being the RODOS system is not set up to provide uncertainty information for which reason it is necessary to specified it via file input. This has been made simple and it is based on an instrument at Risø National Laboratory, Denmark. The measurement standard deviation is set as the maximum of a fraction f of the measured gamma dose rate y and a minimum uncertainty value m:

$$\sigma = \max(f * y, m)$$

The applied variances equal σ^2

f and *m* are user specified, and only a single set can be given. This is then used for all specified detectors.

Averaging details

The Kalman filtering on measured 10-minute average gamma dose rates requires that the predicted gamma dose rates are also 10- minute average values. When a puff passes a detector point the calculated dose rate there can vary rather quickly, and a single instantaneous dose rate per minute, as calculated by RIMPUFF, may be inappropriate for the averaging. To obtain better gamma dose rate averages, the puff positions and inventories are therefore interpolated into 6 seconds steps, i.e. 10 steps per puff advection step, and the gamma dose rates so averaged over 100 instantaneous values in stead of 10. This is performed in a complex of routines not being part of RIMPUFF although with calls to the RIMPUFF gamma dose rate routines, and called from within the RIMPUFF one-minute timestep advection loop.

The matrix elements holding derivatives of the gamma dose rates at the detector points with respect to puff positions and inventories are calculated in parallel to the gamma dose rates and also averaged over 100 six-second values.

Test cases

Test cases are necessary for the development of simulation tools. In the present development of Kalman filtering for the RIMPUFF dispersion model, the "measurement data" have mostly had to be produced by the code itself and then used for the filtering in tests with slightly changed wind or release conditions.

Proof of concept

The first test case was a kind of proof of concept . It was not carried out with RIMPUFF but with a small purpose built program using a straightforward implementation of an extended Kalman filter based on instantaneous gamma dose rates and updating after every 60-second time step. It involved a single puff only, and the state vector only comprised the puff centre coordinates, not the inventory.

A dry run (no Kalman filtering) was performed with a specified pure westerly wind, i.e. wind direction 270°. At three detector points 1000 m right east of the release point and with 20 m north/south separation the received instantaneous gamma dose rates were calculated and stored for use as "measurements" in following calculations.

The next calculation was still without Kalman filtering but with a wind direction 10° south of west, i.e. 260°. No calculated gamma dose rates were stored, just the track of the puff.

The third calculation then was the real test. The wind direction was again the 260° while the Kalman filter used the "measurements" created in the 270° wind direction calculation. The result can be seen in Figure 1. When the puff gets close enough to the detector points the *H*-matrix, which holds the derivatives of the detector point gamma rates with respect to the puff centre coordinates, gets different from zero, and the Kalman update makes the puff

deviate from its wind given course and more or less follow the path of the puff that has created the "measurements". Simultaneously the error covariances decrease. When the puff again gets further from the detector points, then $H = 0$, the error covariances increase, and the puff again follows the wind.

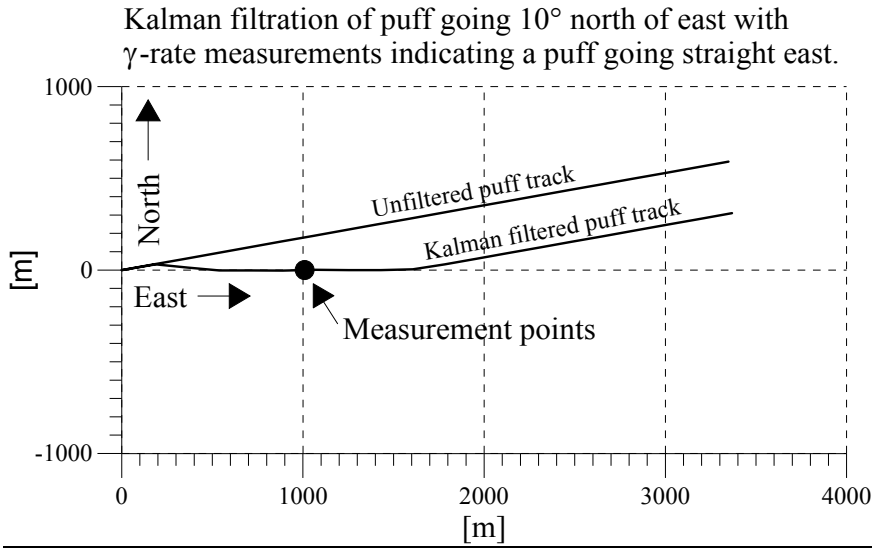

Figure 1: Track of puffs following a wind going 10° north of east, one unfiltered and one Kalman filtered with measurements indicating a puff going straight east.

Cases with internally generated "measurements"

All other reported test cases have been performed with the final RODOS integrated RIMPUFF/Kalman system, and all but one with "measurements" generated by the code itself in an initial no-Kalman run. For these cases the release point has been Risø, Denmark, and there have been 8 detector points surrounding Risø at a distance of 2 km and 15 other detector points in a 5*3 array, the 5 midpoints being 10, 20, 30, 40 and 50 km right east of Risø, the other points 5 km right north and south of the midpoints, all in all 23 detector points. The 15 points of the array are shown in Figure 2 but the 8 points surrounding Risø are not, as they should just clutter the figure. The resolution of the computation grid is 2 km.

The "measurements" at the 23 detector points have been created in a "base" run with 2 hours release of pure ^{137}Cs, release rate 10^{18} Bq/h, release height 60 m above ground, no heat in the release. The meteorological situation was strict westerly wind, 7 m/s at 60 m above ground at Risø, neutral stability, no rain. Figure 2 shows the gamma dose field (time integrated gamma dose rates) of this calculation on the background of the land cover map.

Cases with change in release rate

Some cases have been run with change just in the release rate, and with different uncertainties "*a*" specified for this rate. Figure 3 shows results for

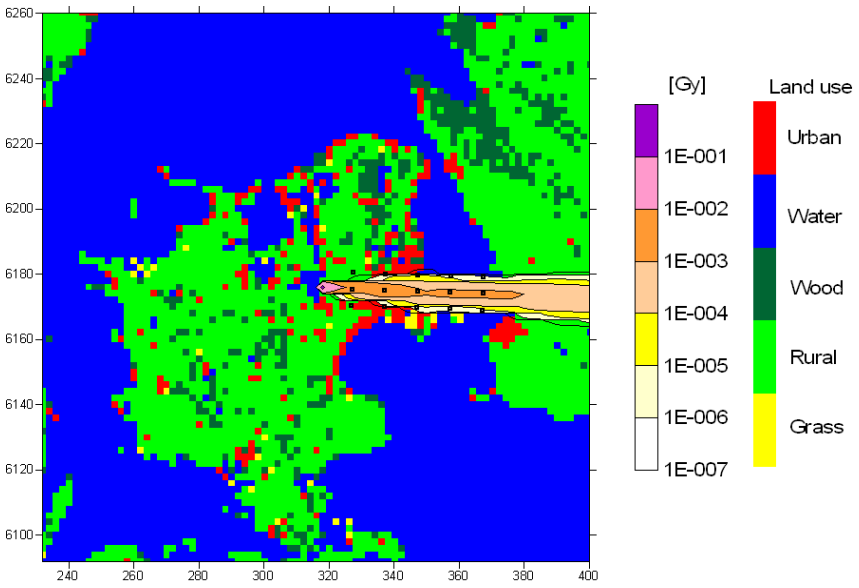

Figure 2: Gamma dose field from puffs in measurement generating run. The 15 detector points 10 to 50 km east of the release point are seen as black squares, the 8 points surrounding the release point are not marked. The background picture is the land use map.

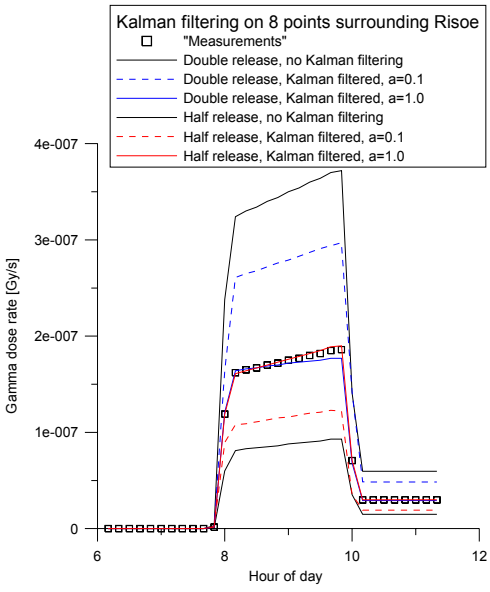

Figure 3: Gamma dose rates 50 km from the release point, right below the plume. Kalman filtering applied in runs with the release doubled and halved relative to that having generated the "measurements", and with different release rate uncertainties "a".

half and double release rate and Kalman filtering just based on the 8 detectors surrounding Risø, while in figure 4 the rates have been 10 times and 1/10th the base rate and Kalman filtering have been based on all 23 detector points. In all cases the results shown are for the detector point 50 km right east of Risø. Figures 5 and 6 show the fields of gamma doses for these cases. It is clear that the specification of the release uncertainty is of importance and that in these cases the higher tried values prove the better. It is also clear that the 1/10th release case requires a larger release uncertainty that the 10-fold release case.

Cases with change in wind direction

With the release rate as in the base run but the wind shifted 5° south, runs with the Kalman filtering based on 8, 11 or all 23 detector points have been performed. The 8 points are those surrounding Risø, the 11 the same plus the easternmost column of the array points. Again calculations have been made for different assumed release rate uncertainties. Figure 7 shows the resulting gamma dose rates for the 11 and 23 points Kalman filtering at the point 50 km straight east of Risø. In this case with "correct" release rate it is not surprising, that the low value of the release uncertainty proves best, a result further highlighted by figures 8 and 9, where the gamma dose fields calculated for the two Kalman filtering configurations are shown.

For the a = 0.1 calculations, figure 10 shows the influence of the number of detector points used for the Kalman filtering, or rather the influence of the density of these points. It is clear that the higher density, the better. The same can be seen from figures 8b and 9b.

Cases with change in both release rate and wind direction

With the wind 5° south of west, i.e. 5° off the base wind, and with the release rate 10 and 1/10 the base release rate a number of cases have been run with different release rate uncertainties. Figures 11 and 12 show the results. As for the cases with only release rate changes, the results get better with the higher release rate uncertainties.

Also for wind 10° off and 1/10th release rate, the higher release rate uncertainty, a=5, proves best, figure 13. Not shown but also tested here is a=10. This made however no enhancement as compared to a=5.

Cases with externally generated "measurements"

In order to test the system against data not generated by itself, we got help from Rijksinstitut voor Volksgezondheid en Milieu (RIVM) in the Netherlands. Dr. Yvo Kok, Yvo Kok (2003), provided us with gamma dose rate "measurements" for the real operational Dutch detector points, as calculated with the dispersion code of RIVM, simulating a 4-hour release from the Borssele nuclear power station, starting 25th September 2003, 0600 UTC. The driving meteorology was field data of the HIRLAM numerical weather prediction model of Koninklijk Nederlands Meteorologisch Instituut (KNMI). The HIRLAM model, Sass (1994), is being developed by a cooperation of European meteorological institutes including the Danish Meteorological Institute and the KNMI. An extract of the used meteorological field data, i.e. data representative for a point near the point of release, plus source terms were also provided. This is believed to be the most

realistic simulation we can make of a real case where a plant fails, the released material is dispersed by the atmosphere, and the best meteorological data available are those measured close to the failing plant.

After a first test we added 12 virtual detector points surrounding the Borssele plant at a distance of 1 km.

Figure 14 shows - on the background of the land use map - the field of gamma doses as calculated and interpolated from the provided gamma dose rates for the irradiated detector points within the computation area. The surrounding but not irradiated points are not used for this plot. The points numbered on the plot are the real detector points, the three irradiated virtual points are not shown. Figure 15 presents the equivalent RIMPUFF calculation based on the one point meteorology and with no Kalman filtering applied. The two plumes cover almost the same area, but it is quite clear, that the RIMPUFF results are rather different from those of RIVM, although only the values at the detector points and not the fields as such should be compared.

With the RIVM calculated detector point values used as measurements, Kalman filtering of the RIMPUFF calculation has been carried out in five different ways, based 1) on the values of the real detector points only, 2) on the values of the 12 virtual detector points only, and 3) on the values of both sets of detector points, all for release rate uncertainty a=0.1. Further, for release uncertainty a=1.0 and Kalman filtering on all detector points, with 4) specified release rate and 5) double of specified release rate. The resulting gamma dose rates for 8 of the detector points are shown in figure 16 together with results for no Kalman filtering and with the RIVM data. Comparing RIVM and RIMPUFF without Kalman filtering the difference in maximum rates but especially the difference in irradiation times at the different points is striking, RIVM giving far the longest times. The only exception to this is at point 140, which is very close to the release point. The "RIMPUFF without Kalman" curve cannot be seen in this "point 140" plot as it collapses with the "Kalman on real points" curve. It is clear, that the two models, RIVM and RIMPUFF, cannot both be close to being correct, was this a real case. The RIVM model exposes most points for a much longer time than does RIMPUFF and with a comparable dose rate, so it produces a rather much higher dose at these points.

The effect of the different Kalman filterings is better seen from dose plots than from dose rate plots, and figure 17 shows the figure 16 equivalent doses. It can be seen that with a release rate as specified by RIVM and the release rate uncertainty a=0.1, the Kalman filtering on only the real points leads to an enhanced prediction for only three of the 8 points plotted, and only marginally for two of these, while inclusion of the 12 virtual detector points around the release point makes the Kalman filter enhance the results at all 8 points except at point 140, the point close to the release point, although again only marginally for most of the points. Setting the release rate uncertainty to 1.0 instead of 0.1 increases the gamma doses at all points except point 143, the results at most points getting better. Combining a=1.0 with double release doesn't help here.

For some combinations of parameters, this Borssele release case also causes the Kalman filter to move a single puff far away from a reasonable position,

figure 18. The tendency for such behaviour has, however, been greatly reduced by limiting the detector points actually used for Kalman filtering of a given puff to only those having gamma rate derivatives with respect to the puff inventory exceeding 10% of the maximum found for all the points, with other words by excluding detector points which do not really see the puff.

All in all the Kalman filtering does generally enhance the calculated gamma doses in this most realistic case, especially for a=1. And it is the impression that it is the huge difference between the RIVM and the basic RIMPUFF predictions plus the sparsity of the detector points that prevent a better result.

ToDeMM

The results of the RIMPUFF/Kalman modules, are used as input to other early-phase RODOS modules, e.g. the dose module and the arrival time module, and to later phase modules of RODOS, especially to the Deposition Monitoring Module (DeMM), Gering et al. (2000), which requires fields of time integrated air concentrations at ground level and the amounts of wet deposited material for each of the actual nuclides. And in order to apply Kalman filtering in DeMM, this module also needs an estimate of the uncertainty of the provided fields.

DeMM itself makes this estimate, and what is presented here is the so far last method in a series of more or less similar methods for providing data for this estimation. It still awaits testing with DeMM.

Ensemble of results

DeMM applies a so-called Ensemble Kalman filter, so the information to base the uncertainty estimate on is provided as an ensemble of 100 sets of normal RODOS fields of time integrated concentrations and wet depositions, each set being a kind of possible RIMPUFF outcome, the actual RIMPUFF calculated results forming one of the sets.

Running RIMPUFF one hundred times with perturbed wind and release rates is not feasible. Instead we take advantage of the error covariance matrix, the *P*-matrix used in the Kalman module and updated in the RIMPUFF prediction steps as well as in the Kalman filtering steps.

Generation of ensemble results

At each time step, an ensemble of 100 state vectors are created by perturbing the actual Kalman state vector, i.e. position and content *(x,y,z,q)* of all puffs, into 99 other possible state vectors. The perturbations are based on the actual error covariance matrix plus 99*4 numbers, $Z_{1,1}$,$Z_{1,2}$,...,$Z_{99,4}$, stochastically drawn from a unit variance Gaussian distribution. To make perturbed ensemble member N, $1 \le N \le 99$, simulate a possible RIMPUFF answer, the same four Gaussian numbers, ($Z_{N,1}$, $Z_{N,2}$, $Z_{N,3}$, $Z_{N,4}$), are used for the perturbation of all the state vector variable parts *(x,y,z,q)*, i.e. for all the puffs. At each time step we thus calculate:

$$PC = Cholesky(P)$$
$$X_1 = X + PC \cdot (Z_{1,1}, Z_{1,2}, Z_{1,3}, Z_{1,4}, Z_{1,1}, Z_{1,2}, Z_{1,3}, Z_{1,4}, ..., Z_{1,1}, Z_{1,2}, Z_{1,3}, Z_{1,4})$$
$$X_2 = X + PC \cdot (Z_{2,1}, Z_{2,2}, Z_{2,3}, Z_{2,4}, Z_{2,1}, Z_{2,2}, Z_{2,3}, Z_{2,4}, ..., Z_{2,1}, Z_{2,2}, Z_{2,3}, Z_{2,4})$$
.....
$$X_{99} = X + PC \cdot (Z_{99,1}, Z_{99,2}, Z_{99,3}, Z_{99,4}, Z_{99,1}, Z_{99,2}, Z_{99,3}, Z_{99,4}, ..., Z_{99,1}, Z_{99,2}, Z_{99,3}, Z_{99,4})$$

where X is the actual state vector and PC is the Cholesky decomposition of the actual error covariance matrix P. In this way all puffs in an ensemble, are displaced in coherent directions, and the inventory is perturbed in a way that may simulate a coherent perturbation in wet deposition. For each ensemble member the corresponding fields of ground level time integrated concentration and wet deposition are calculated using the formulas and models from RIMPUFF. Figure 19 shows for a case of southerly wind the mean of the concentration fields of the 100 ensemble members compared to the field of unperturbed RIMPUFF alone.

To save disk space, data of the final fields are only saved for grid points where the data are different from 0, typically reducing the needed space from around 30 to around 2 Mbyte.

Figures and their captions

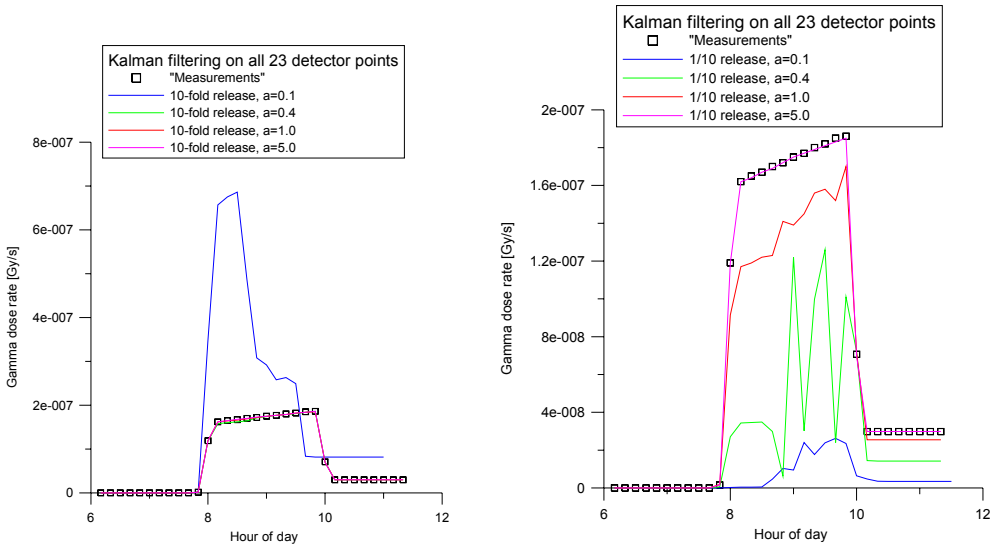

Figure 4: Gamma dose rates 50 km from the release point, right below the plume. Kalman filtering applied in runs with the 10 fold and 1/10th release of that having generated the "measurements", and with different release rate uncertainties "a".

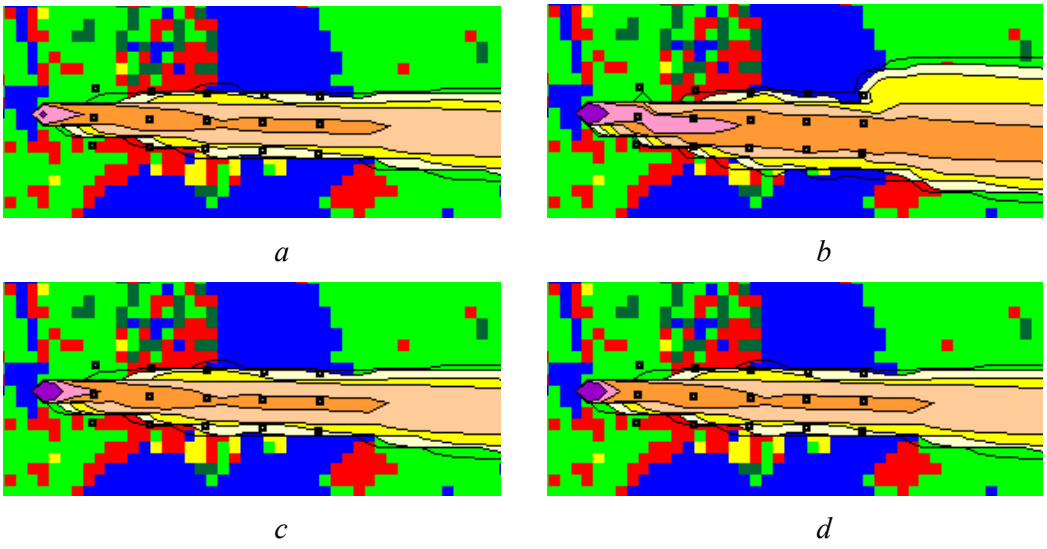

Figure 5: Kalman filtering applied in runs with 10 fold the release having generated the "measurements", and with different release uncertainties "a". a) Measurement run. Relative release rate uncertainties: b) a=0.1, c) a=0.4, d) a=1.0.

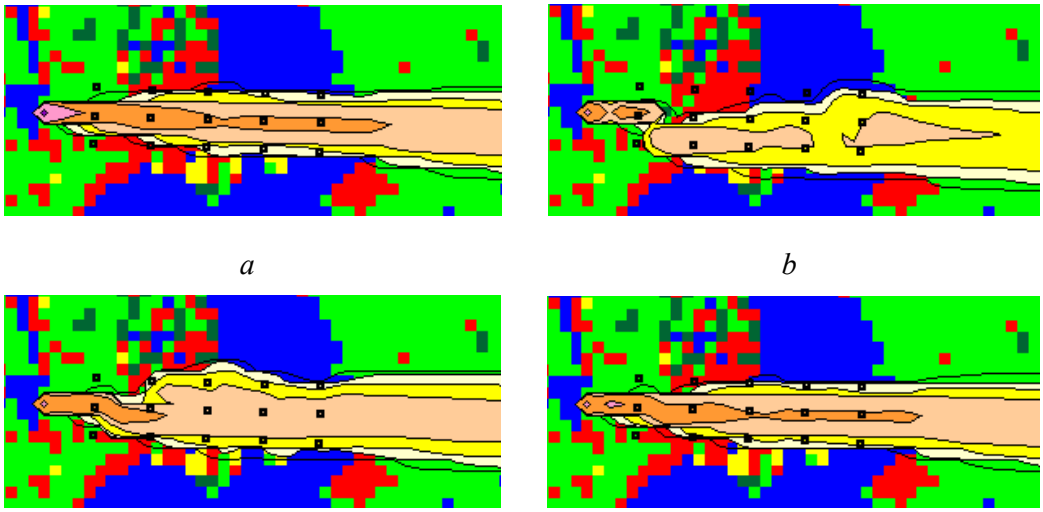

a *b*

c *d*

Figure 6: Kalman filtering applied in runs with 1/10th the release having generated the "measurements", and with different release uncertainties "a". a) Measurement run. Relative release rate uncertainties: b) a=0.1, c) a=0.4, d) a=1.0.

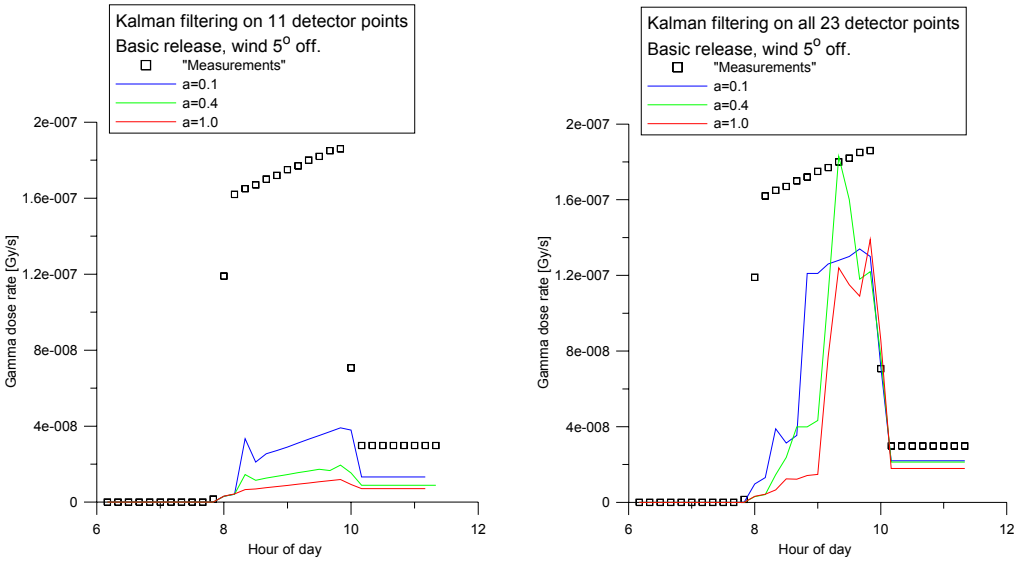

a *b*

Figure 7: Gamma dose rates 50 km right east of the release point with wind 5° south of west. Kalman filtering on the 8 detector points surrounding the release point plus: a) the 3 eastern most detector points and, b) all 15 array detector points. All for different release rate uncertainties "a".

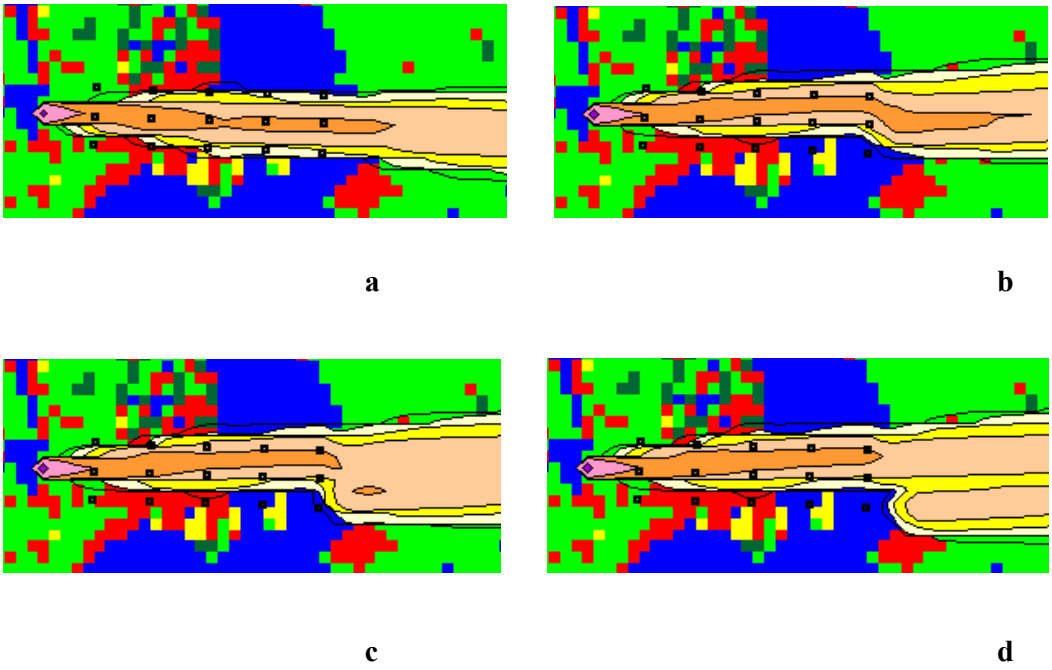

a **b**

c **d**

Figure 8: Gamma dose rates fields with wind 5° south of west. Kalman filtering on the 8 detector points surrounding the release point plus the 3 eastern most detector points.

a) Measurement run. Relative release uncertainties: b) a=0.1, c) a=0.4, d) a=1.0.

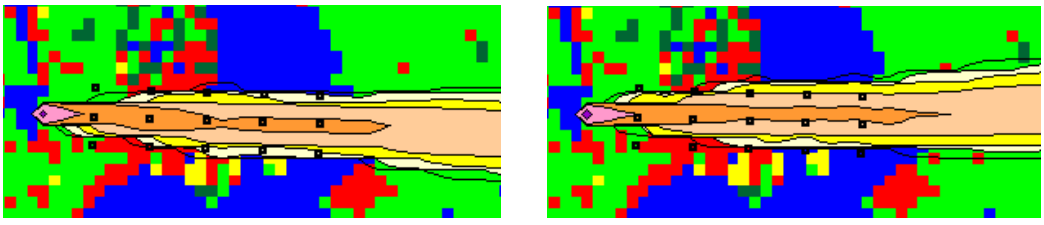

a **b**

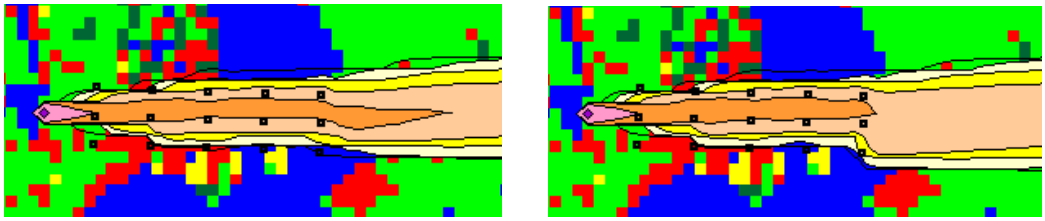

c **d**

Figure 9: Gamma dose rates fields with wind 5° south of west. Kalman filtering on the 8 detector points surrounding the release point plus all 15 array detector points.

a) Measurement run. Relative release uncertainties: b) a=0.1, c) a=0.4, d) a=1.0.

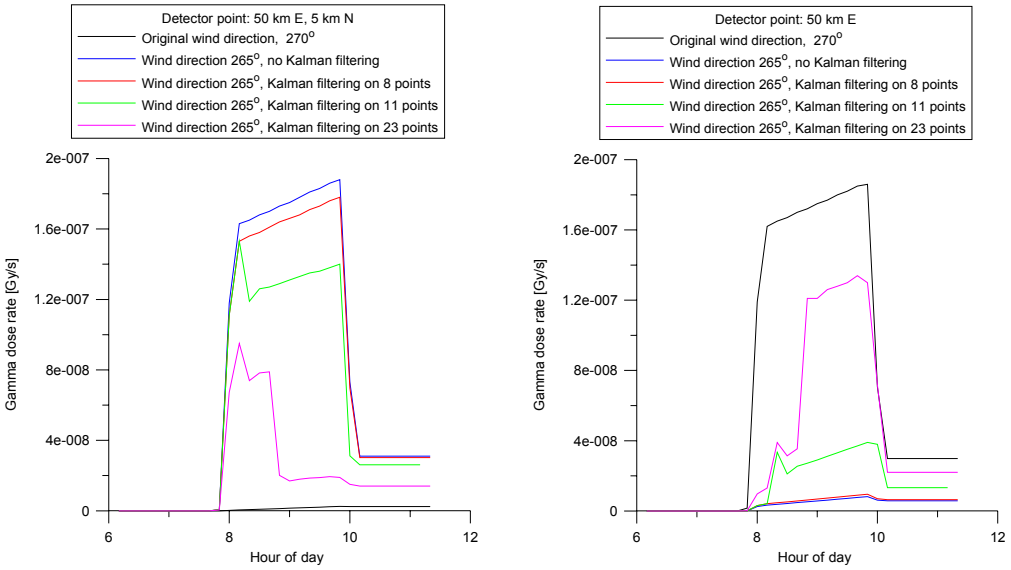

Figure 10: Gamma dose rates at northernmost and central detector point 50 km east of release point. Wind 5° south of west. Kalman filtering on different amounts of detector points. Relative release unvertainty a=0.1.

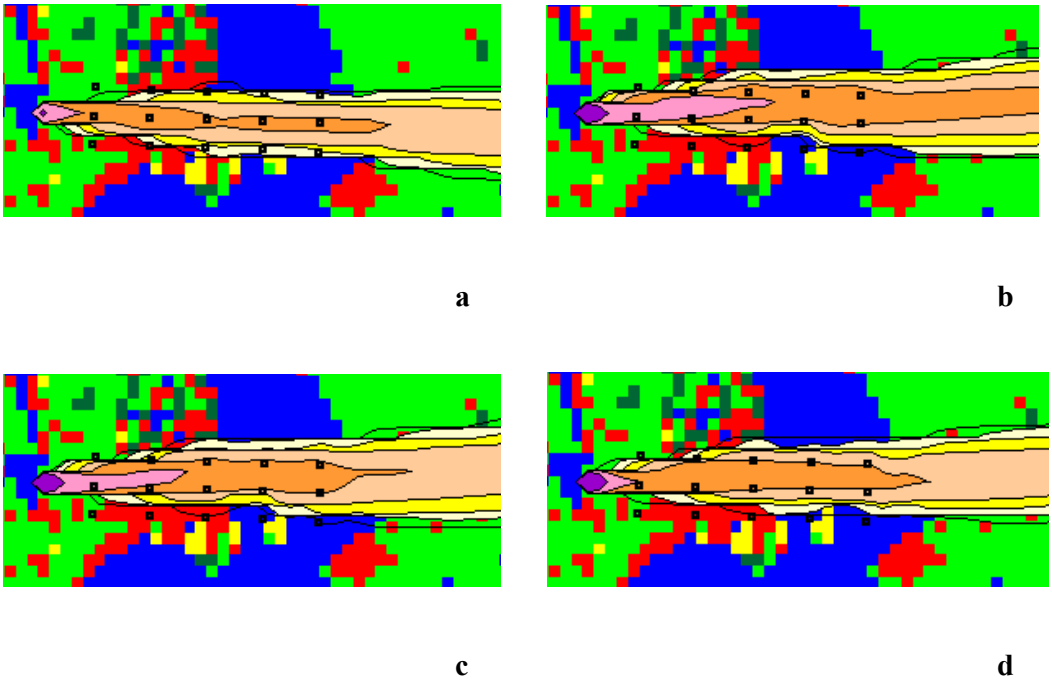

Figure 11: Gamma dose rates fields with wind 5° south of west and 10 fold release rate. Kalman filtering on all 23 detector points.

a) Measurement run. Relative release uncertainties: b) a=0.4, c) a=1.0, d) a=5.0.

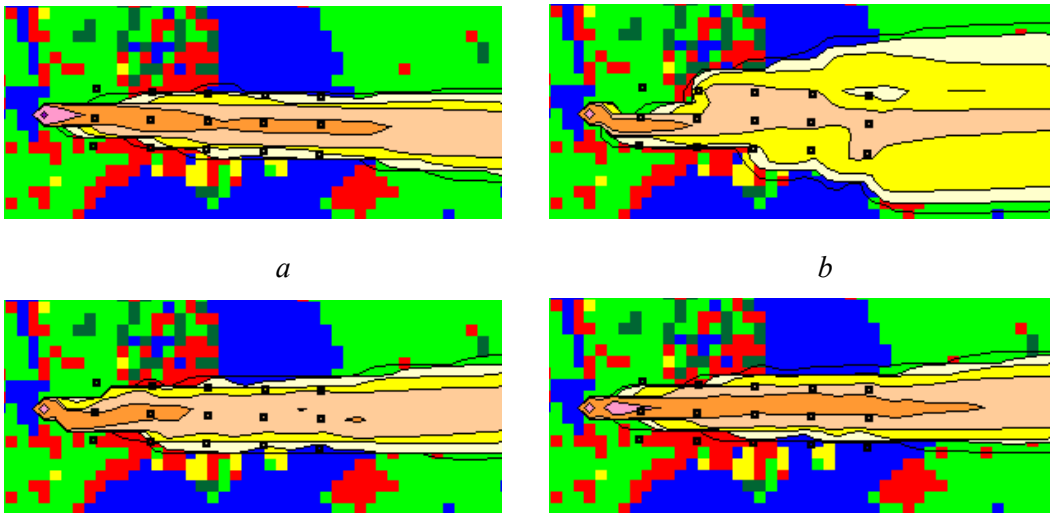

a *b*

c *d*

Figure 12: Gamma dose rates fields with wind 5° south of west and 1/10th release rate. Kalman filtering on all 23 detector points.

a) Measurement run. Relative release uncertainties: b) a=0.4, c) a=1.0, d) a=0.5

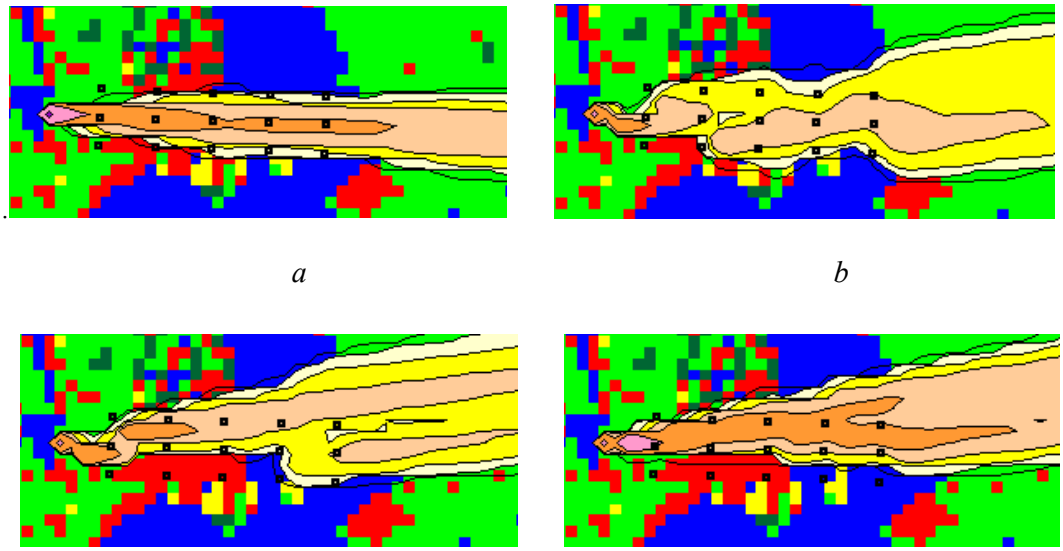

a *b*

c *d*

Figure 13: Gamma dose rate fields with wind 10° south of west and 1/10th release rate. Kalman filtering on all 23 detector points.

a) Measurement run. Relative release uncertainties: b) a=0.4, c) a=1.0, d) a=5.0.

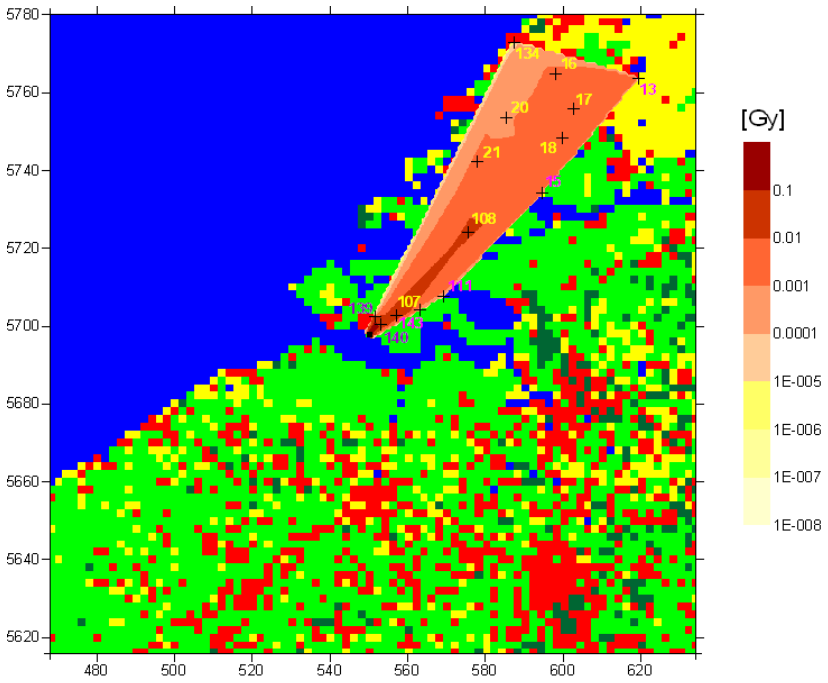

Figure 14: Plot based on time integrated gamma dose rates as calculated by RIVM. The numbered detector points (crosses) are the real Dutch detector points having received gamma doses in the RIVM calculation.

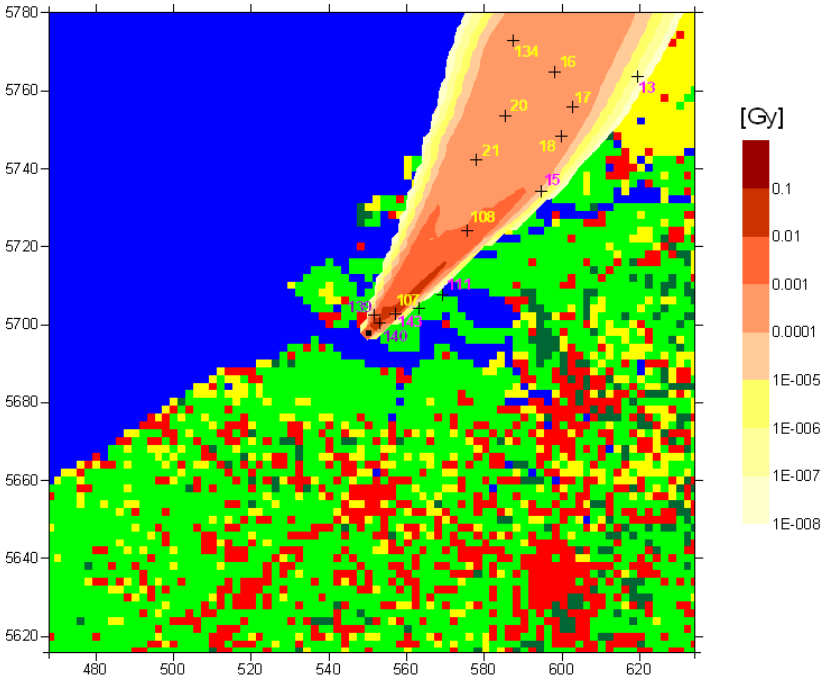

Figure 15: Time integrated dose rates as calculated by RIMPUFF based on one point meteorological data from RIVM (KNMI). No Kalman filtering.

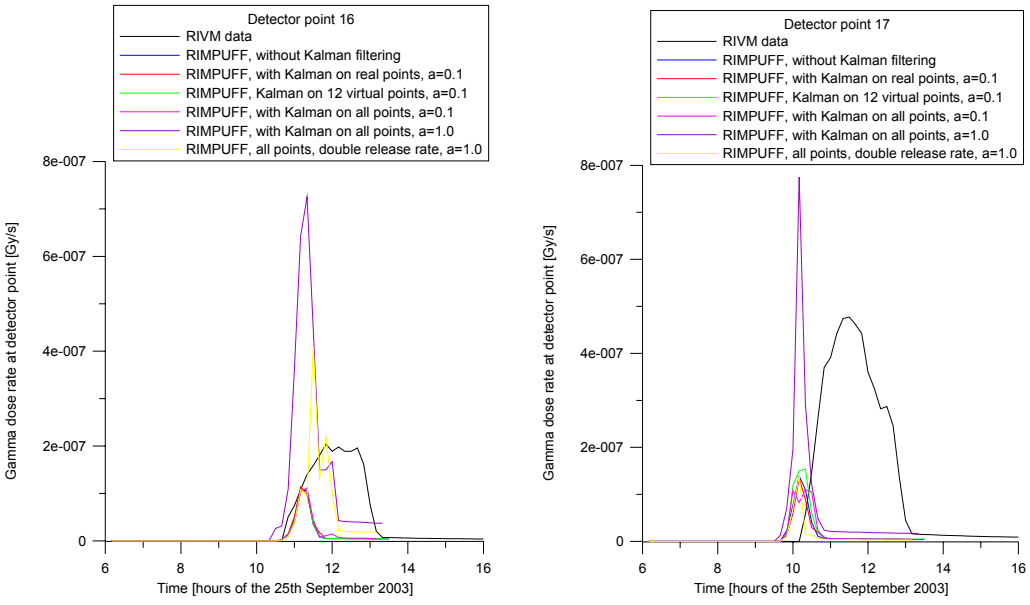

a **b**

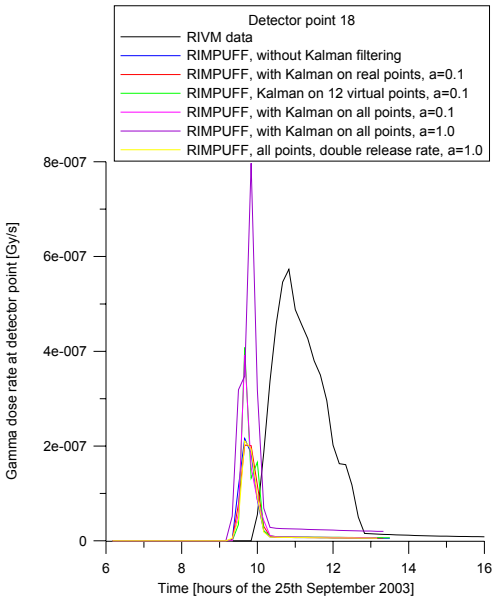
Detector point 18
RIVM data
RIMPUFF, without Kalman filtering
RIMPUFF, with Kalman on real points, a=0.1
RIMPUFF, Kalman on 12 virtual points, a=0.1
RIMPUFF, with Kalman on all points, a=0.1
RIMPUFF, with Kalman on all points, a=1.0
RIMPUFF, all points, double release rate, a=1.0
Gamma dose rate at detector point [Gy/s]
8e-007
6e-007
4e-007
2e-007
0
6
8
10
12
14
16
Time [hours of the 25th September 2003]

c

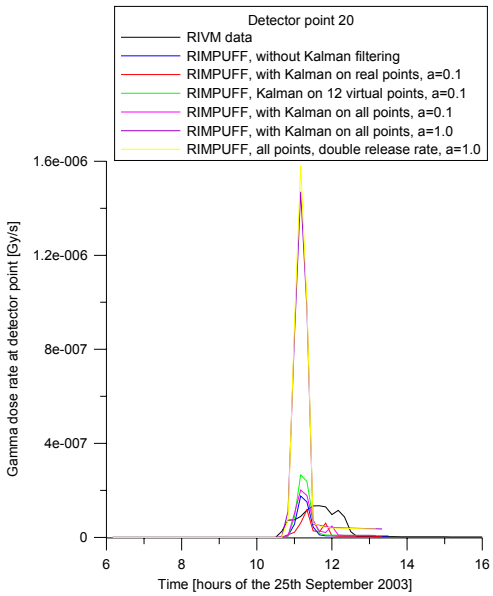
Detector point 20
RIVM data
RIMPUFF, without Kalman filtering
RIMPUFF, with Kalman on real points, a=0.1
RIMPUFF, Kalman on 12 virtual points, a=0.1
RIMPUFF, with Kalman on all points, a=0.1
RIMPUFF, with Kalman on all points, a=1.0
RIMPUFF, all points, double release rate, a=1.0
Gamma dose rate at detector point [Gy/s]
1.6e-006
1.2e-006
8e-007
4e-007
0
6
8
10
12
14
16
Time [hours of the 25th September 2003]

d

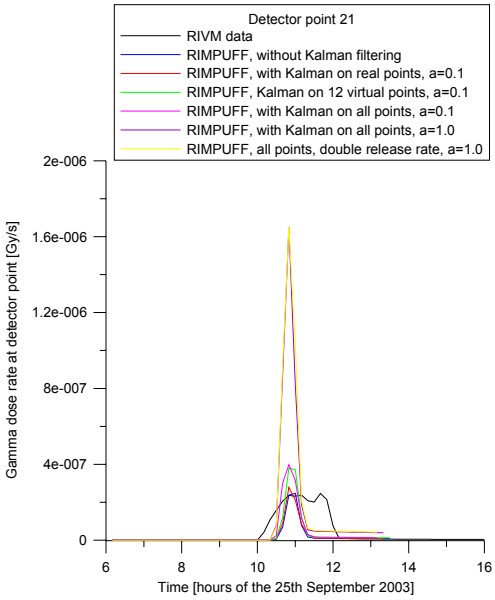
Detector point 21
RIVM data
RIMPUFF, without Kalman filtering
RIMPUFF, with Kalman on real points, a=0.1
RIMPUFF, Kalman on 12 virtual points, a=0.1
RIMPUFF, with Kalman on all points, a=0.1
RIMPUFF, with Kalman on all points, a=1.0
RIMPUFF, all points, double release rate, a=1.0
Gamma dose rate at detector point [Gy/s]
2e-006
1.6e-006
1.2e-006
8e-007
4e-007
0
6
8
10
12
14
16
Time [hours of the 25th September 2003]

e

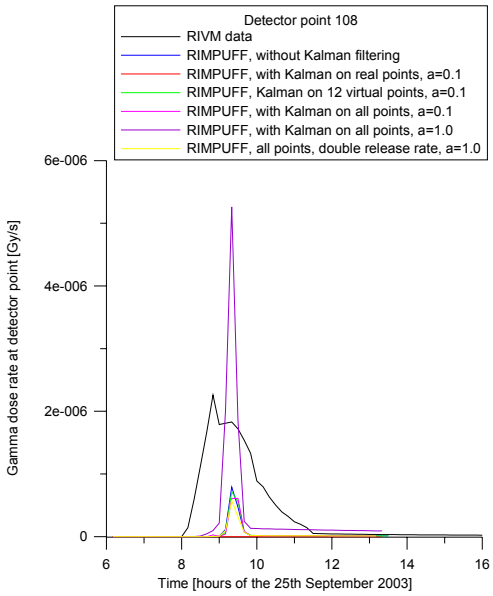
Detector point 108
RIVM data
RIMPUFF, without Kalman filtering
RIMPUFF, with Kalman on real points, a=0.1
RIMPUFF, Kalman on 12 virtual points, a=0.1
RIMPUFF, with Kalman on all points, a=0.1
RIMPUFF, with Kalman on all points, a=1.0
RIMPUFF, all points, double release rate, a=1.0
Gamma dose rate at detector point [Gy/s]
6e-006
4e-006
2e-006
0
6
8
10
12
14
16
Time [hours of the 25th September 2003]

f

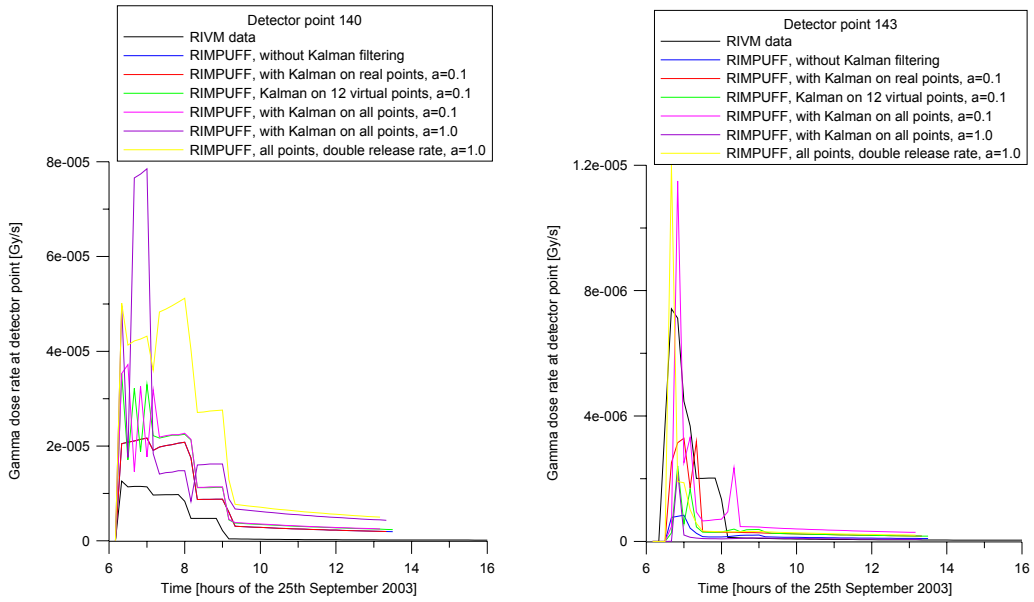

g **h**

Figure 16: Gamma dose rates at 8 detector points as calculated by RIVM, by RIMPUFF, and by RIMPUFF with Kalman filtering on different extracts of RIVM data. Release as specified. Release rate uncertainty a=0.1.

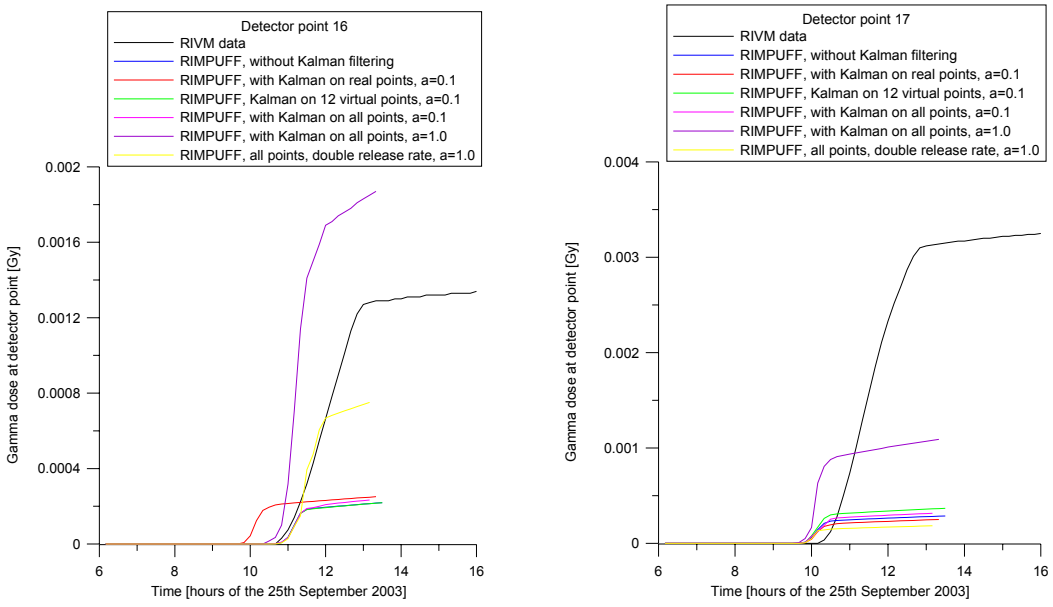

a **b**

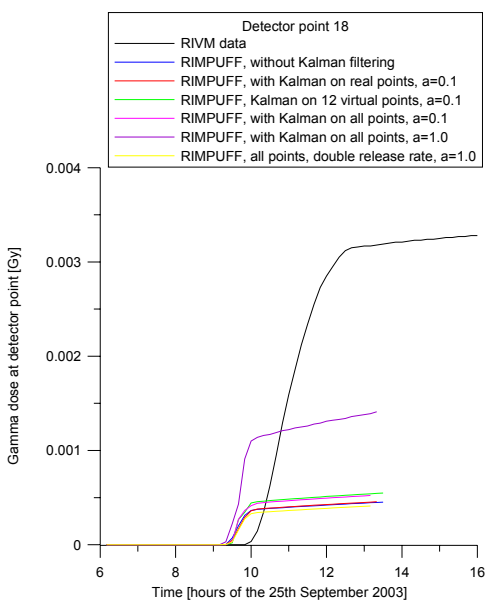
Detector point 18
RIVM data
RIMPUFF, without Kalman filtering
RIMPUFF, with Kalman on real points, a=0.1
RIMPUFF, Kalman on 12 virtual points, a=0.1
RIMPUFF, with Kalman on all points, a=0.1
RIMPUFF, with Kalman on all points, a=1.0
RIMPUFF, all points, double release rate, a=1.0
Gamma dose at detector point [Gy]
0.004
0.003
0.002
0.001
0
6
8
10
12
14
16
Time [hours of the 25th September 2003]

c

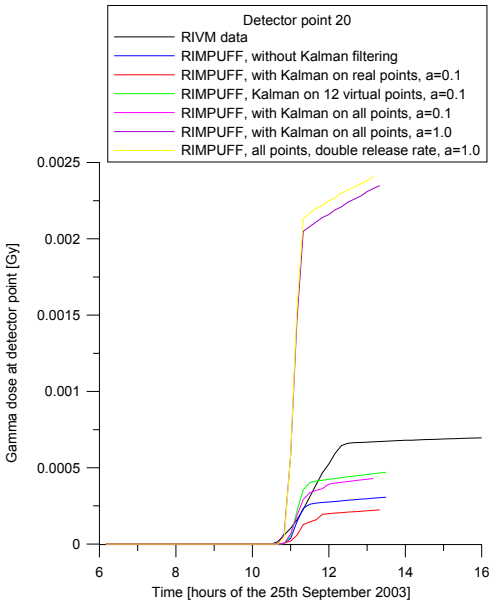
Detector point 20
RIVM data
RIMPUFF, without Kalman filtering
RIMPUFF, with Kalman on real points, a=0.1
RIMPUFF, Kalman on 12 virtual points, a=0.1
RIMPUFF, with Kalman on all points, a=0.1
RIMPUFF, with Kalman on all points, a=1.0
RIMPUFF, all points, double release rate, a=1.0
Gamma dose at detector point [Gy]
0.0025
0.002
0.0015
0.001
0.0005
0
6
8
10
12
14
16
Time [hours of the 25th September 2003]

d

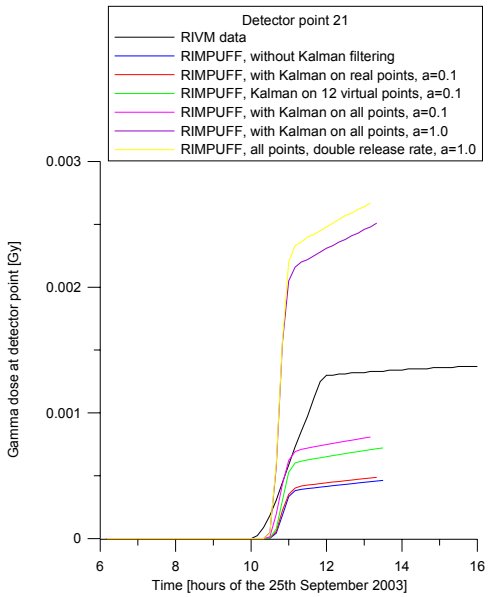
Detector point 21
RIVM data
RIMPUFF, without Kalman filtering
RIMPUFF, with Kalman on real points, a=0.1
RIMPUFF, Kalman on 12 virtual points, a=0.1
RIMPUFF, with Kalman on all points, a=0.1
RIMPUFF, with Kalman on all points, a=1.0
RIMPUFF, all points, double release rate, a=1.0
Gamma dose at detector point [Gy]
0.003
0.002
0.001
0
6
8
10
12
14
16
Time [hours of the 25th September 2003]

e

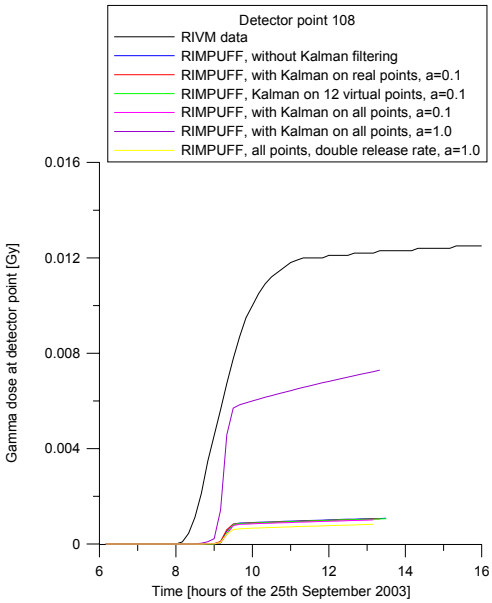
Detector point 108
RIVM data
RIMPUFF, without Kalman filtering
RIMPUFF, with Kalman on real points, a=0.1
RIMPUFF, Kalman on 12 virtual points, a=0.1
RIMPUFF, with Kalman on all points, a=0.1
RIMPUFF, with Kalman on all points, a=1.0
RIMPUFF, all points, double release rate, a=1.0
Gamma dose at detector point [Gy]
0.016
0.012
0.008
0.004
0
6
8
10
12
14
16
Time [hours of the 25th September 2003]

f

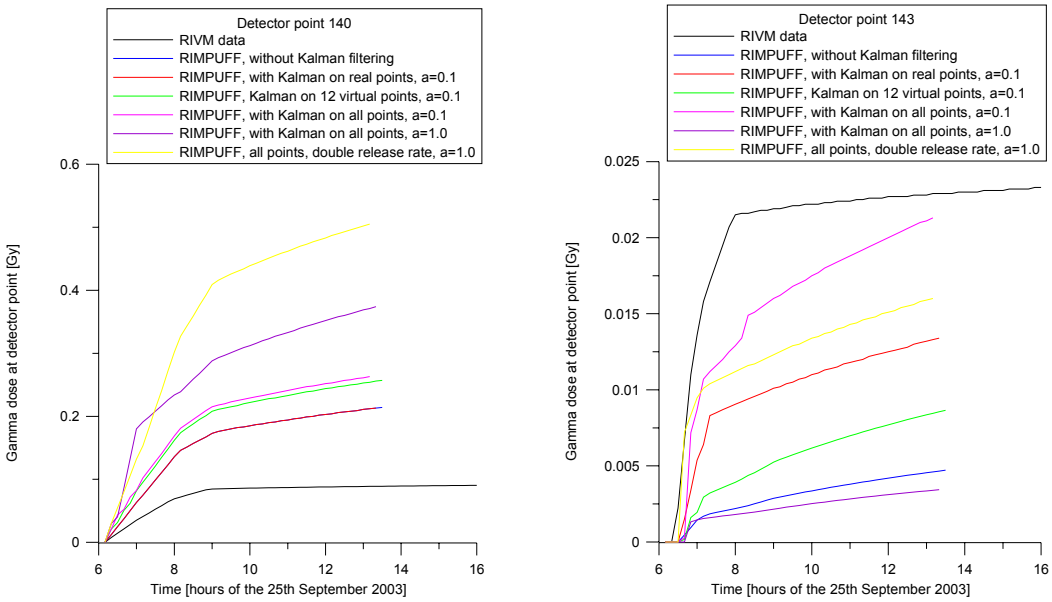

g **h**

Figure 17: Gamma doses (time integrated dose rates) at 8 detector points as calculated by RIVM, by RIMPUFF, and by RIMPUFF with Kalman filtering on different extracts of RIVM data. Different releases: as specified, and doubled, and different release uncertainties: a=0.1 and a=1.0.

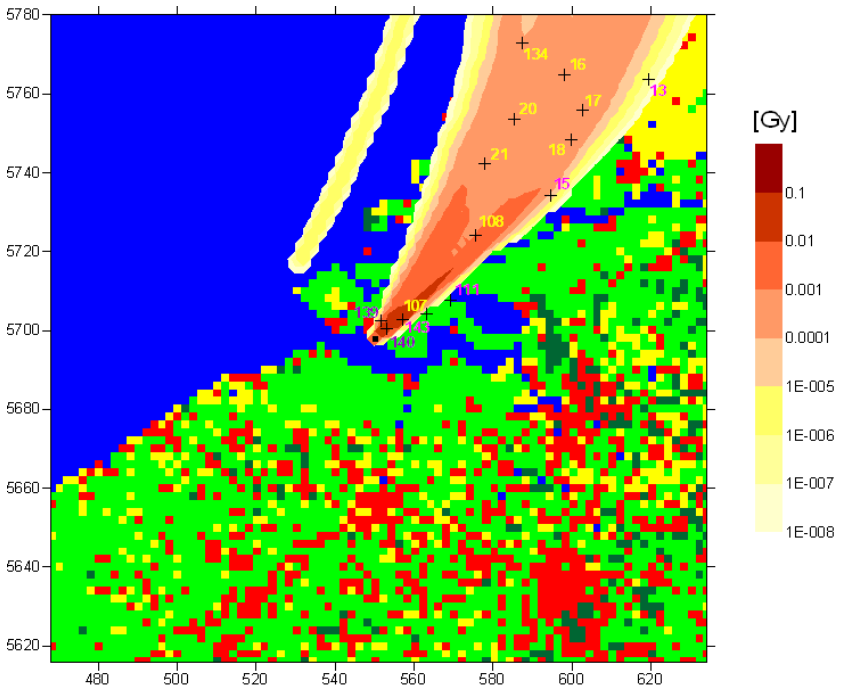

Figure 18: Time integrated dose rates as calculated by RIMPUFF based on one point meteorological data from RIVM (KNMI). Kalman filtering on all detector points, release uncertainty a=0.1.

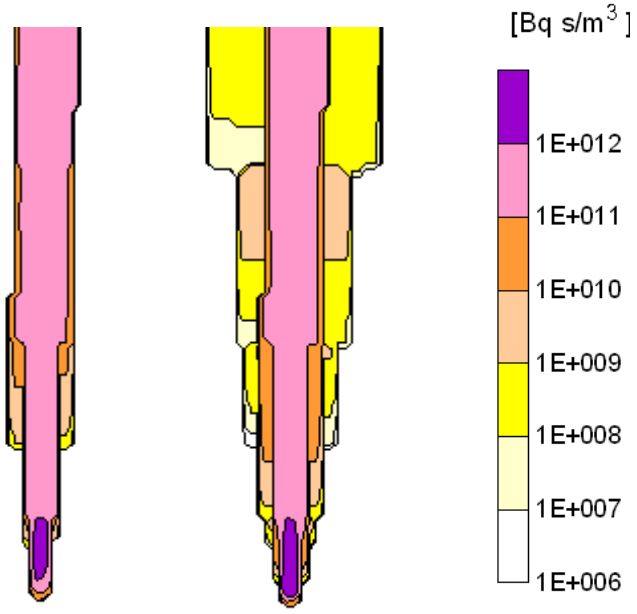

Figure 19: Time integrated air concentration at ground level. Case with 15° uncertainty in the southerly wind direction. a) RIMPUFF, b) mean of 100 ensemble results.

Data assimilation in the late phase (WP3)

The work packages WP3.1 to WP3.5 of the DAONEM project aimed at data assimilation in the late phase. "Late phase" in this context means that time period after an accidental release of radioactive material when the transport in the atmosphere and subsequently the deposition of radionuclides has finished. The reason for distinguishing this phase from the early phase is that dose rate measurements can be used to derive information on the present and future radiological situation with much less uncertainty than in the early phase because in the early phase the dose rate is caused by both radionuclides in the air and those deposited on ground. The main objective in the late phase field was to improve existing and incorporate new data assimilation tools in the deposition and the food chain modelling, and to validate these tools by testing them against measured and simulated data sets.

In the following, first a general description of the progress achieved with respect to optimisation of data assimilation strategies for late phase application is given. Specific results of data assimilation in deposition modelling are described and also those in food chain modelling. A synopsis of experiences with data assimilation in the late phase modules of RODOS is given in the section assessment of results.

Optimization of data assimilation strategies

Work on data assimilation capabilities for the late phase models started already in the 4th framework programme. A standard Kalman filter was chosen as data assimilation methodology for a prototype for data assimilation in the deposition model. This approach proved to be not suitable for a real-time, online decision support system like RODOS, mainly due to unfeasible runtime and storage requirements. Therefore, a key goal of the DAONEM project was to investigate alternative data assimilation strategies suitable for large-scale real-time problems.

The concept of the Kalman filter (KF) was introduced by Kalman in the sixties [Kalman, 1960] for application in linear systems. For non-linear systems some generalisations have been proposed. Methods based on local linear approximations include: the extended Kalman filter [Gelb, 1974], Gaussian sum filters [Anderson, 1979] and iterated Kalman filters [Jazwinsky, 1970]. Methods based on sequential Monte Carlo techniques are described by Liu and Chen [Liu, 1998].

The recursive algorithm of the KF consists of two steps, a prediction and a correction step: first the numerical model gives a prediction of the modelled system at a given time, for which measurements are available; then this prediction is corrected using the new measurements. The corrected prediction is then used as a new input for the next model prediction step. This recursive nature is one of main advantages of the KF, since it allows to incorporate new data without having to start from the beginning again.

Basis for the KF methodology is a state-space formulation of the numerical model and the measurement process with stochastic extensions, which includes the following components:

- the state vector representing the state of the modelled system at given time,
- the model operator representing the numerical scheme of the model,
- the forcing of the system (i.e. all external influences on the model state),
- a stochastic element representing the uncertainty of the system,
- the measurement vector representing all available measurements for a given time period
- the observation operator which defines the relation between system state and measurements
- a stochastic element representing the uncertainty of the measurements.

Central to the concept of data assimilation with the Kalman filter is the concept of uncertainties, uncertainty estimation and uncertainty modelling. Uncertainties in the model are captured by assigning probability distributions to key model parameters and to input data. The uncertainty of the state of the system can then be assessed by propagating these probability distributions through the system according to the model dynamics described by the model operator. Uncertainties are propagated in a model chain by forcing downstream models by the uncertainties in the upstream models according to the model interfaces. Describing all the uncertain quantities in the modelling

system by probability distributions would result in a huge number of statistical parameters and variables and hence make the uncertainty assessment computationally infeasible. Instead, uncertainties in the model predictions are captured by assigning probability distributions to key parameters and variables only. In addition, due to the high-dimensional state of many system or a non-linearity in the modelling equations, mathematical approximations are needed for describing the propagation of uncertainties.

The main challenge for the operational use of the Kalman filter is the realisation of the uncertainty propagation, i.e. the propagation of the error covariance matrix of the system state. But it is not only this more technical constraint which makes a brute-force implementation of the Kalman filter unfeasible, it is also the lack of knowledge of all required statistical input data (see for example [Dee, 1991], [Todling, 1994], [Fukumori, 1995], [Cane, 1996]). In the case of non-linear model dynamics more advanced Kalman filter schemes are required, since the original Kalman filter provides a correct solution only for linear models. One example is the extended Kalman filter (EKF, see e.g. [Gelb, 1974]), in which the uncertainty propagation is based on a statistical linearisation of the model equation. For all these reasons many approximations of the Kalman filter - often called sub-optimal schemes - have been developed in the last decade. According to Todling and Cohn [Todling, 1994] the following categories of sub-optimal KF schemes can be distinguished:

1) Covariance modelling
2) Limiting filtering
3) Dynamic simplification
4) Reduced resolution
5) Local approximation
6) Monte Carlo methods
7) Combination of methods

Comprehensive tests were performed with a variety of these advanced KF schemes approaches, results of the tests were documented in a report. The tests of the different approaches were based on twin experiment scenarios, see section 3.3.1. The Ensemble Kalman filter (EnKF) was identified as the most promising approach for data assimilation in the later phase. The advantages of the EnKF compared with other filter approaches are:

- relatively easy implementation in an existing model
- relatively easy consideration of model error, forcing error and measurement error
- suitability for non-linear problems
- suitability for large-scale problems
- applicable in all later phase models, i.e. allowing a consistent data assimilation approach in the late phase

The Ensemble Kalman filter (EnKF) was introduced by Evensen [Evensen, 1994] and has been used in many applications since then. The approach has proven to be especially useful for systems with many degrees of freedom and for non-linear system dynamics. In the EnKF, the error covariance's have ensemble representations. The EnKF algorithm starts with an initial ensemble

whose mean is the initial system state estimate and whose sample statistics represent the error covariance, i.e. the initial system uncertainty. Then, the full (possibly non-linear) model is applied to each ensemble member to obtain a forecast ensemble. The forecast ensemble mean and covariance are then used to assimilate measurements into each ensemble member. Such, an analysis ensemble is created which can be fed into a new cycle of the EnKF.

Currently two main categories of EnKF schemes exist, which differ in the generation of the analysis ensemble. The first category is based on the concept of perturbed observations, it is also referenced as stochastic analysis ensemble update [Tippett, 2003]. The idea is to assimilate different sets of observations to each ensemble member, which is realised by adding random (stochastic) noise to the observations. Burgers et al. [Burgers, 1998] extended the first approach of Evensen with the concept of perturbed observations to maintain sufficient ensemble spread and avoid filter divergence. The consequences of perturbing observations were explored recently [Anderson, 2001]. Houtekamer and Mitchell [Houtekamer, 1998] presented a version of the EnKF which works with two parallel ensembles ("double EnKF") to avoid filter divergence and which also uses perturbed observations. An efficient implementation of this version was demonstrated by the same authors recently [Houtekamer, 2001]. This approach employs a distance-dependent attenuation to the error covariances and works sequentially with batches of observations. The benefits of distance-dependent attenuation of covariance's (i.e. limiting the impact of observations to a short range) were further investigated by Hamill and Whitaker [Hamill, 2001]. Distance-dependent attenuation can reduce the computational costs and can avoid spurious long-range correlation's resulting from the limited ensemble size. Recently Mitchell et al. found that a severe attenuation (i.e. a small impact radius) can cause imbalance in the data assimilation [Mitchell, 2002]. Mitchell and Houtekamer also proposed an adaptive EnKF, in which the model error is estimated from both the innovations and the ensemble [Mitchell, 2000].

In the second main category of EnKF schemes a deterministic algorithm is used for transforming the forecast ensemble into an analysis ensemble with consistent statistics. First the analysis is done once to obtain the updated mean of the ensemble. Then perturbations for the updated mean are generated and added to the mean to produce the analysis ensemble (i.e. an updated ensemble). Recently three EnKF's with deterministic analysis ensemble have been proposed: the Ensemble Adjustment Kalman Filter [Anderson, 2001], the Ensemble Transform Kalman filter [Bishop, 2001] and the Ensemble Square-Root Filter [Whitaker, 2002], which is related to the class of RRSQRT-filters. These approaches differ in the method how the analysis perturbation ensemble is generated. A localised version of the Ensemble Square-Root Filter was presented by Ott et al. [Ott, 2003]. Very recently it was demonstrated that filters from both EnKF categories belong to the family of square-root filters, and those with deterministic analysis ensemble update are implementations of Kalman square-root filters [Tippett, 2003].

The two steps of the Kalman filter, the forecast step and the analysis step are described in the following for the EnKF, according to [Evensen, 1994; Burgers, 1998; Houtekamer, 1998; Madsen, 1999]. The EnKF is especially

suitable for high dimensional, non-linear systems. The basic idea of the EnKF is that the statistical information's about state vector x and covariance matrix P is represented by an ensemble of possible state vectors. The mean of the ensemble members is identified as approximation of the state vector, and the deviations of the ensemble members from their mean are identified as approximation of the square root matrix S of the covariance matrix. As only a limited number (typically q=100) of ensemble members are used, the approximation for S is reduced in rank, thus making the EnKF to an sub-optimal scheme for the Kalman filter. In the EnKF approach the full covariance matrix P is never calculated, instead the Kalman gain is directly calculated from S. Thus the forecast step reduces to the application of the model operator M to each of the ensemble members, which is a dramatic reduction of computational effort (model M applied q=100 times, while in the full Kalman filter model M is applied 2*n times; n is the dimension of the state vector, here about 10^5-10^6).

In the forecast step of the EnKF each of the initial state vectors is propagated through the deposition model one time step ahead:

forecast step:

state forecast $$x_{t|t-1,i} = M_t\left(x_{t-1|t-1,i}, u_{t,i}, \eta_{t,i}\right) \quad (2.1)$$

mean of state vectors $$\overline{x}_{t|t-1} = \frac{1}{q}\sum_{i=1}^{q} x_{t|t-1,i} \quad (2.2)$$

covariance forecast

$$P_{t|t-1} = S_{t|t-1}\left(S_{t|t-1}\right)^T,\ S_{t|t-1} = \left[s_{t|t-1,1},\ldots,s_{t|t-1,q}\right],\ s_{tt-1,i} = \frac{1}{\sqrt{q-1}}\left(x_{t|t-1,i} - \overline{x}_{t|t-1}\right) \quad (2.3)$$

where

i	= 1,2,...,q index of state vector in ensemble (q = number of ensembles),
n	is the size of the state vector,
$x_{t-1\|t-1,i}$	is the analysed ensemble of possible state vectors at time t-1,
$x_{t\|t-1,i}$	is the forecasted ensemble of possible state vectors at time t,
$\eta_{t,i}$	is the ensemble of error terms describing the uncertainty of a model forecast, here resulting from errors in model forcing and model parameters,
$s_{t\|t-1,i}$	is the i-th column of matrix $S_{t\|t-1}$,
$S_{t\|t-1}$	is the matrix approximating the square root matrix of matrix $P_{t\|t-1}$,
$P_{t\|t-1}$	is the forecast covariance matrix at time t (representing the uncertainty of forecasted state of the system).

This means running the deposition model as many times as the number of possible state vectors in the ensemble (typically about 100 [Burgers, 1998; Houtekamer, 1998]). For complex models this step is the bottleneck of the data assimilation process in terms of computational burden. Applying the full deposition model a hundred times would also make the data assimilation process to slow for an operational real-time system like RODOS. Thus, a simplified deposition model is used, in which a constant atmospheric resistance is assumed (i.e. no dependence of the resistance on wind speed and surface roughness). This allows to calculate global deposition velocities applicable for the whole RODOS grid instead of localised deposition velocities. The improvement in the computational burden is nearly a factor of 100, thus reducing the computation time for applying the simplified model to the full ensemble to about the same time as applying the full model one time.
Model errors are considered in this step by applying an ensemble of possible sets of model parameters according to their uncertainty distributions. With

other words, each possible state vector is propagated with the model with a different set of model parameters. As a result, the initial spread of the ensemble will be enlarged by the model error resulting from uncertain parameters.

The forecast of the system state can be represented by the first two statistical moments, the mean value and the covariance. In the EnKF the mean value of the system state is defined as the mean of all state vectors in the ensemble (equation 2.2), and the covariance can be approximated from the deviation of each possible state vector from the mean (equation 2.3).

In the analysis step of the EnKF, each state vector of the ensemble is updated separately using a common weighting matrix, the Kalman gain. The formulation of the weighting matrix is the most essential part of the data assimilation scheme. The update is a linear combination of the forecast and the so-called innovation, which is the difference between the measurements and the forecast of the measured data from the system state. A major advantage of the EnKF is that it is not necessary to calculate the full covariance matrix P, since the Kalman gain can directly be calculated from the much smaller matrix S:

<u>analysis step:</u>

perturbed measurements $$y_{t,i} = y_t + \varepsilon_{t,i} \quad (2.4)$$

innovation vector $$d_{t,i} = y_{t,i} - H(x_{t|t-1,i}, 0) \quad (2.5)$$

innovation covariance $$\Gamma_t = \left(H_t S_{t|t-1}\right)\left(H_t S_{t|t-1}\right)^T + R_t \quad (2.6)$$

Kalman gain $$K_t = S_{t|t-1}\left(H_t S_{t|t-1}\right)^T \Gamma_t^{-1} \quad (2.7)$$

state analysis $$x_{t|t,i} = x_{t|t-1,i} + K_t d_{t,i} \quad (2.8)$$

mean of state vectors $$\overline{x}_{t|t} = \frac{1}{q}\sum_{i=1}^{q} x_{t|t,i} \quad (2.9)$$

covariance analysis $$P_{t|t} = S_{t|t}\left(S_{t|t}\right)^T, \quad S_{t|t} = \left[s_{t|t,1},\ldots,s_{t|t,q}\right],$$
$$s_{t|t,i} = \frac{1}{\sqrt{q-1}}\left(x_{t|t,i} - \overline{x}_{t|t}\right) \quad (2.10)$$

where

m is the number of measurements,

$d_{t,i}$ is the ensemble of possible innovation vectors at time t,

Γ_t is the innovation covariance matrix,

K_t is the Kalman-Gain,

R_t is the measurement error covariance matrix,

y_t is the measurement vector, which contains all measurements at time t,

$y_{t,i}$ is the ensemble of possible measurements, which is distributed around the measurement vector y_t according to the measurement error ε_t.

Measurement errors are considered by replacing the measured values through an ensemble of possible measurements generated from the measurement error covariance matrix, see equation 2.5 [Burgers, 1998]. The resulting ensemble of updated state vectors provides an estimate of the updated system state and the updated covariance matrix (equations 2.9 and 2.10):

Data assimilation in deposition modelling

One key issue of the late phase part of DAONEM has been to evaluate and improve the prototype of the deposition monitoring module DeMM. The deposition monitoring module DeMM is designed to update the predicted total (dry + wet) deposition on the ground and on all kind of plant surfaces. The predicted deposition data is calculated with a deposition model using results from atmospheric dispersion modelling. The update is based on measurements of net gamma dose rates after the deposition process has ended. For the future it is planned to incorporate also measurements of nuclide-specific dose rates (i.e. from in situ gamma-spectrometry).

One key part of DeMM is the deposition model for radionuclides in RODOS. The deposition model for radionuclides in RODOS bases on the radioecological model ECOSYS-87 [Müller, 1993], which has been extended by a resistance model for dry deposition to account for the influence of atmospheric properties. Input data are mainly results of atmospheric dispersion models, e.g. concentration of radionuclides in air and rain water and atmospheric resistances. From this data the deposition model calculates the activity deposited on soil, lawn and up to 22 plant types. The deposition process is modelled with two components, dry deposition and wet deposition. Total wet deposition is calculated in atmospheric dispersion models through modelling of wash-out and rain-out and provided as input data to the deposition model. Wet deposition onto a plant surface consists of that fraction of wet deposited radionuclides, which is hold back on the plant (interception fraction). The calculation of the interception fraction considers the water storage capacity of the plant's leaves, and the actual leaf area index. Dry deposition onto plant and soil is calculated from the time-integrated concentration of activity in air (near ground) using a deposition velocity which depends on the surface type. In the original version of ECOSYS-87 generic values are used for the deposition velocities for fully developed plant canopies. In the improved deposition model in RODOS the influence of atmospheric properties like wind speed and turbulence is considered by modifying the generic values through a resistance approach (e.g. [Wesely, 2000; Baklanov, 2001]). The flow of radionuclides from the contaminated cloud to the vegetated soil is determined by a series of resistances (see Figure 20). The deposition process consists of two parts, an atmospheric part and a surface part, which act as a series of resistances. The surface part itself includes two surfaces, soil and plant, which act as parallel resistance's.

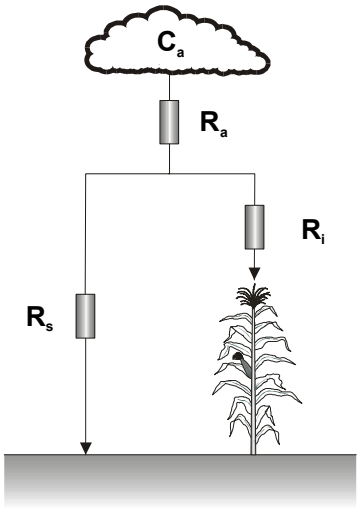

Figure 20: Deposition model with a resistance approach.

Results of the deposition model are always afflicted with some uncertainty, which can be attributed to uncertain model parameters, the uncertainty of the input data, and the general imperfection of the numerical model in describing physical processes. The first two sources of uncertainty can be described by assigning probability distributions to the uncertain quantities. The uncertainty of model results can then be assessed by propagating these probability distributions through the deposition model. Probability distributions for model parameters have been derived based on earlier studies [Müller, 1993; Goossens, 2000; Smith, 2002].

The Deposition Monitoring Module DeMM in RODOS

The prototype DEMM v6.0 of the Deposition Monitoring Module DeMM has been implemented into the actual RODOS PV6.0 version.

DeMM starts from a contamination of air and precipitation above agricultural production areas and living areas. Input to DeMM is essentially the output of the atmospheric dispersion modules or the atmospheric dispersion updating module ADUM. Main input data are:

- concentration of radionuclides in the air near ground (including uncertainty information in terms of a covariance matrix)
- wet deposited activity (including uncertainty information in terms of a covariance matrix)
- amount of rainfall
- atmospheric resistance
- measurement data of net gamma dose rates
- model parameters (including uncertainty information in terms of probability distributions)

The endpoints of DeMM are essentially the total (i.e. dry + wet) deposition onto ground and a variety of crops. This data is input to the Food Chain Module FDMT and also the Food Monitoring Module FoMM. Moreover, DeMM provides information about uncertainty of this data in form of a covariance matrix, this information is required from FoMM and also the data assimilation tools of the hydrological model chain. Some standard outputs are generated by DeMM and are displayed by the graphical system of RODOS as maps:

- Deposition to pasture grass (interface data for FDMT)
- Deposition to lawn (incuding soil, interface data for FDMT)
- Deposition to soil (covered by pasture, interface data for FDMT)
- Integrated air concentration (interface data for FDMT)
- Wet deposition (interface data for FDMT)
- Deterministic prediction of deposition to lawn (without data assimilation)
- Stochastic prediction of deposition to lawn (without data assimilation)
- Corrected prediction of deposition to lawn (with data assimilation)
- GDR measurements
- Three ensembles of stochastic prediction of deposition to lawn (without data assimilation)
- Three ensembles of corrected prediction of deposition to lawn (with data assimilation)

The position of DeMM within the RODOS model chain and also the according data flow can be seen in Figure 21.

Within RODOS many modules can run in two different modes: the automatic mode, where a set of standard results is calculated, and the interactive mode, where specifications made by the user are allowed and thus determine the type of the results. At the moment it is only foreseen to run the Deposition

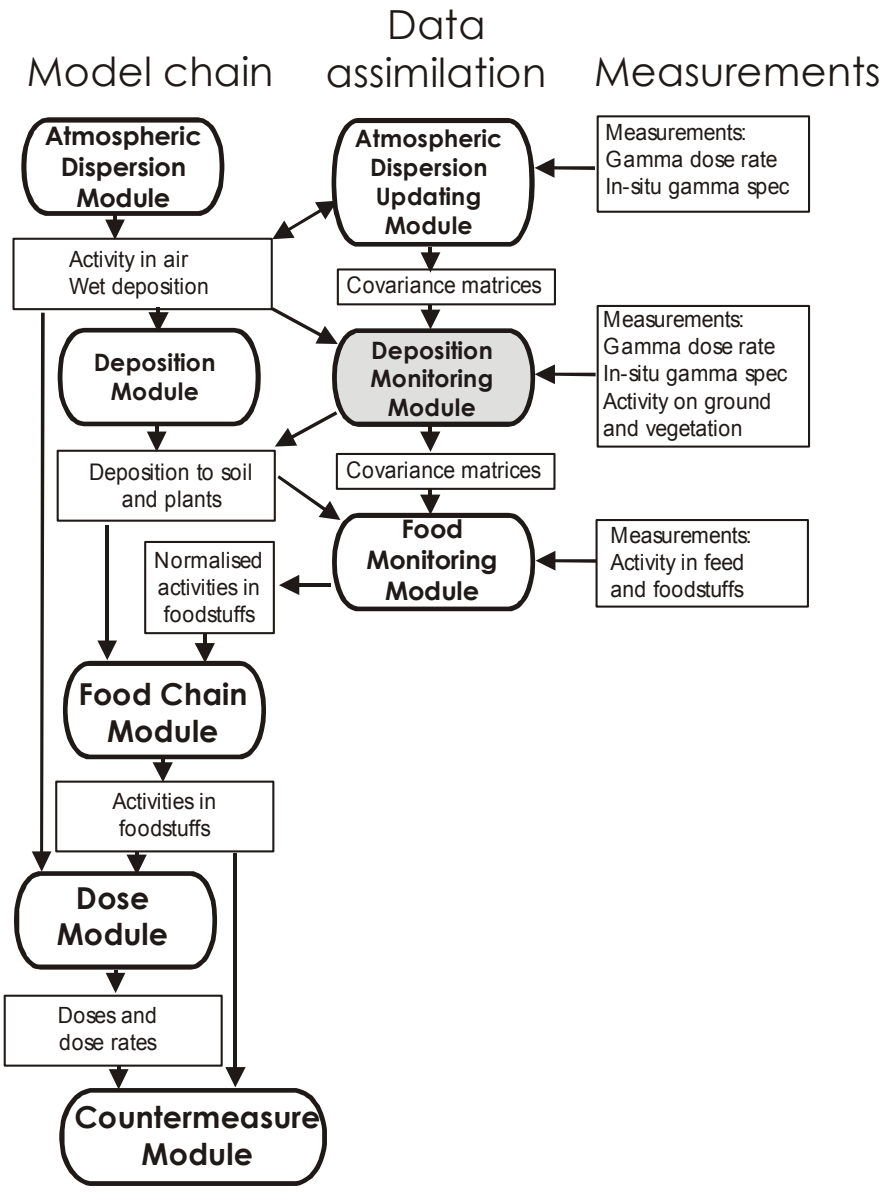

Figure 21: Structure and data flow in RODOS. The grey shaded module is the Deposition Monitoring Module DeMM which is described in this section.

Monitoring Module DeMM in the interactive mode. In this mode DeMM can be configured via a graphical user interface. The main aim of the graphical user interface of DeMM in the latest version 6.0 is to give the user the choice between three different application modes of DeMM:

- input from ADUM (atmospheric dispersion updating module) with uncertainty information about dispersion results + measurement data
- input from ADM (atmospheric dispersion module), uncertainty information about dispersion results is simulated within DeMM + measurement data

- only measurement data as input, DeMM runs without data assimilation, DeMM results only based on measurements.

Application of the Kalman filter in DeMM

Data assimilation in DeMM bases on the Ensemble Kalman Filter (EnKF), which has been optimised for operational use (i.e. batch-wise assimilation of measurements). The state vector of the EnKF includes the following system variables: the total deposited activity onto lawn (as reference surface), the wet deposited activity, both variables for up to 10 radionuclides and for each cell of the RODOS grid. Additionally, the state vector includes the deposited activity onto soil and all plants considered in the food chain model for those grid cells, for which measurements of food or feed contamination exists (this data is required as input for the data assimilation in the food chain model). The dimension of this state vector is in the order of 10^5-10^6. Since typically the probability distribution of deposited activity follows a log-normal distribution, all variables of the state vector in DeMM are log-transformed. The EnKF in DeMM works with an ensemble of 100 members, each member being a possible realisation of the system state. In principle the full deposition model has to be applied to each ensemble member separately. To reduce the computational burden, the full deposition model is only applied to the mean of the ensemble members, while a simplified model is applied to each of the 100 members. The simplified model does not consider the influence of the atmospheric resistance on the deposition velocity, thus allowing the use of a single set of deposition velocities for all grid cells. The ensemble of state vectors in DeMM is initialised by an ensemble of 100 possible results of the atmospheric dispersion calculation, which represent the uncertainty of the dispersion modelling. Uncertainties of the deposition model are considered by applying an ensemble of possible sets of model parameters according to pre-defined uncertainty distributions. With other words, each possible state vector is propagated with the model with a different set of model parameters. As a result, the initial spread of the ensemble will be enlarged by the model error resulting from uncertain parameters. Each ensemble member is the corrected separately in the EnKF using the measurement data for total gamma dose rate and nuclide-specific ground contamination.

Test and validation studies of DeMM

Twin experiments

The standard Kalman filter approach proved to be not fully suitable for a real-time, online decision support system like RODOS, mainly due to unfeasible runtime and storage requirements. Therefore, alternative data assimilation strategies suitable for large-scale real-time problems had to be found. Several advanced filter approaches were investigated and tested in a simplified test environment using twin experiments. Some results of these test are documented in this section.

The layout of the twin experiment is as following:

1. One model run is chosen to be the reference "true" data set (Figure 22a).

2. Simulated "measurements" are generated from the true data, the mean value (of the probability distribution) of each measurement is derived from the corresponding true value and measurement errors are realised as perturbations around the mean (Figure 22b).

3. A second model run is generated with some modifications to the input data and/or the model parameters to provide a false model "forecast" (Figure 22c).

4. In the "update" part the forecast data is assimilated with the measurements using the chosen data assimilation approach. This assimilation results in updated data, which can be compared against the true data. The better the updated data matches the true data, the better the chosen data assimilation approach is working (Figure 22d).

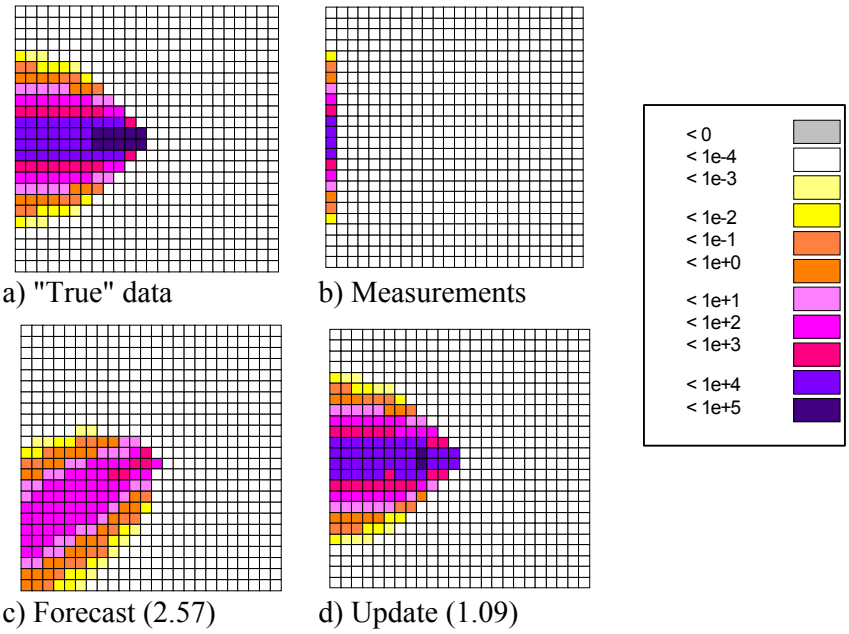

Figure 22: Twin experiment for data assimilation in the simplified dispersion and deposition model. Figures (a), (c) and (d) represent the deposition footprint as deposited activity of ^{137}Cs (in Bq/m^2), Figure (b) shows net dose rates (in pGy/h) arising from the deposited activity.

The performance of the data assimilation approach is assessed based on two criteria:

- qualitative comparison: the graphic representation of the update is compared visually against that of the true data;

- quantitative comparison: the overall differences are quantified with the geometric average error (GAE)

One example result for a twin experiment using the Ensemble Kalman filter is shown in Figure 22. All data is displayed for a grid of 24 x 24 cells with a grid spacing of 1 km. This grid covers the most inner part of the calculational grid in RODOS, which typically covers 168 x 168 km with grid spacing increasing in four steps with increasing distance from the centre. A simulated release of 10^{15} Bq of ^{137}Cs occurred in the centre of the grid (only one radionuclide is considered here for simplification). The release lasted for 30 minutes, during and after the release the wind was constantly blowing from east to west (right to left). The data represents ground deposition for ^{137}Cs in Figure 22a, c and d, and the net dose rates resulting from the true deposition is given in Figure 22b (all data displayed in a logarithmic scaling). Measuring sites are defined as a line of 24 points about 12 km downwind from the release point. Measured values are generated from the ground deposition of the grid cell closest to each measuring site using the appropriate dose rate conversion factor. The original measurements are disturbed with some noise, these measurement errors are chosen to be 1 % of the uncertainty of the false prediction at each site. Measurements below 1 nGy/h are not indicated. The "false" model prediction in Figure 22c is generated based on a modified scenario, where the wind direction is turned by 30° to NE and the released activity is 2 magnitudes smaller compared to the "true" scenario in Figure 22a.

Uncertainty of the false prediction is modelled as follows: first, each member of the ensemble of the false prediction is scaled by a random factor drawn from a log-normal distribution (with mean 1 and standard deviation of 100). Then, each member is rotated by a random angle drawn from a normal distribution (with mean 0 and standard deviation of 30°).

It can be seen from Figure 22d, that the Ensemble Kalman filter can quite successfully correct the deviations in wind direction and source term. Nevertheless, the shape of the plume close to the release point cannot be fully reconstructed. The GAE improves from 2.57 for the false prediction to 1.09 for the updated prediction (a value of 1.0 represents a perfect update). With other words, false and true prediction differ on average by a factor of 2.57, while updated and true prediction only differ on average by 9 %.

EnKF in normal space

In the twin experiment shown in Figure 23 the EnKF is applied with the state vector being in normal space, i.e. the state vector contains the calculated deposition. In the forecast the true source term is underestimated by a factor of 0.01, while the true wind direction is used. The true data and the corresponding measurements are the same as before in Figure 22, which is the case for all following tests if not mentioned differently. Grey shaded cells in the update indicate negative values. The update is unsatisfying, especially because of the unrealistic negative values for the deposition.

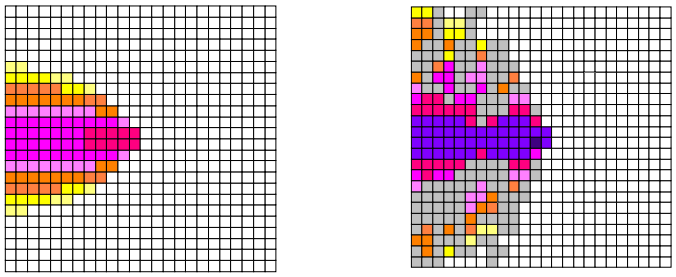

a) Forecast b) Update

Figure 23: EnKF in normal space

EnKF in log-space

In this experiment the EnKF is applied with the state vector now being transformed into log-space, i.e. the state vector contains the logarithms of the deposition data. In the twin experiment shown in Figure 24 the forecast underestimates the true source term by a factor of 0.01, and the wind direction used in the forecast differs by 30° from the true wind direction. The EnKF works very well in this case, i.e. both the error in the source term and the deviation in the wind direction can be corrected in the filter step. Only the increased deposition close to the release point can not be fully reconstructed. Due to the convincing effect of the log-transformation most following applications of data assimilation approaches are applied to a log-transformed state vector (if not stated differently).

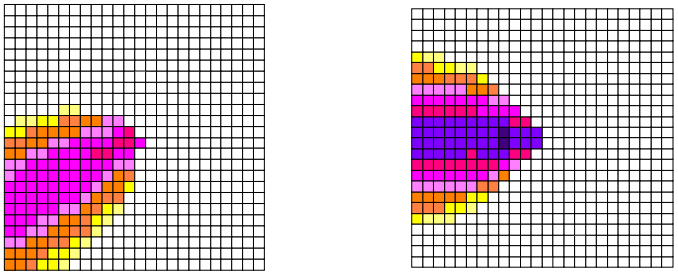

a) Forecast (2.57) b) Update (1.09)

Figure 24: EnKF in log-space

In Figure 25 the EnKF is compared for different ensemble sizes (500, 100, 20 and 10 ensemble members). The quality of the update decreases with decreasing ensemble size, as it is expected. Only exception is the update with 500 ensemble members, which is worse than that with 100 members, contrary to what one would expect. This effect could be due to the stochastic background of the EnKF, so that e.g. the initialisation of the random number generator could influence the result for large ensembles. The update with 100 ensemble members works very well and is a reasonable compromise between update quality and computational speed.

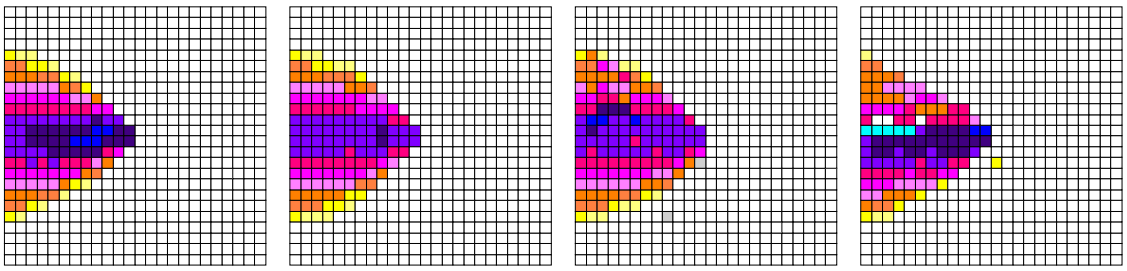

a) q=500 (1.17) b) q=100 (1.09) c) q=20 (1.19) d) q=10 (1.53)

Figure 25: Update for EnKF for different ensemble sizes (q)

Reduced Rank Square Root Kalman filter (RRSQRT-KF)

In the twin experiment shown in Figure 26 the reduced rank square root Kalman filter (with 100 eigenvectors) is used for data assimilation. The forecast underestimates the true source term by a factor of 0.01, and the wind direction used in the forecast differs by 30° from the true wind direction. The RRSQRT-KF does work reasonably well in this case, the result is comparable to that of the EnKF.

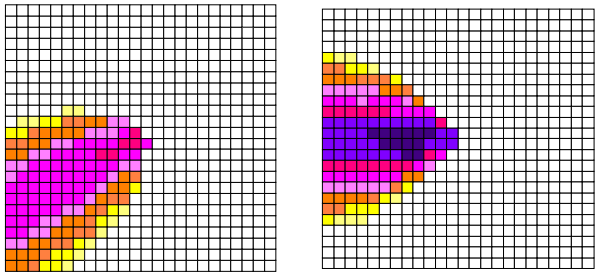

a) Forecast (2.57) b) Update (1.12)

Figure 26: RRSQRT-KF with 100 eigenvectors

Particle Filter

The particle filter is tested in the twin experiment shown in Figure 27. The update here is the superposition of 100 particles, their weights are determined from the difference between the forecasted data and the measurements. The forecast underestimates the true source term by a factor of 0.01, and the wind direction used in the forecast differs by 30° from the true wind direction. The particle filter works very well in this case, the performance is comparable to that of the standard EnKF. The runtime of the particle filter is comparable or even superior to the EnKF. A general problem of the particle filter is that the covariance is not well described any more after the updating step, since typically only a few particles have non-zero weights given the initial uncertainty was large. In this case only 5 particles remain after the updating and thus the covariance cannot be reasonably estimated any more from their spread (as it is done in the EnKF).

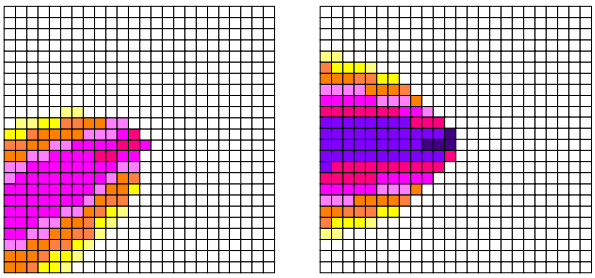

a) Forecast b) Update

Figure 27: Particle Filter with 100 particles

Realistic test scenario

Finally, the data assimilation method for the deposition model - the EnKF as described before - is tested with a realistic test scenario. Contrary to the twin experiments as described above, here the reference solution is derived from the results of a fully independent atmospheric dispersion and deposition model. Results from this model are gamma dose rate measurements, which are directly applied in the data assimilation. The dispersion model and the resulting reference solution is described in the following. In the next step the full model chain in RODOS is run to predict atmospheric dispersion and deposition. The model forcing (i.e. mainly underlying wind fields and source term) is perturbed for the RODOS model run. Finally, the RODOS model predictions are corrected with the EnKF using the measurements of the reference solution, results are presented later in this section.

In the test scenario an accident is assumed for the nuclear power plant Borssele in the west of the Netherlands (3.72088° east, 51.4286° north). The NPP is a pressurised water reactor with 450 MW electric power. The accident is assumed to occur on November 25, 2003, the release starts at 06:00 (UTC) and lasts until 10:00 with constant release rates. The total released activity is about 3E+18 Bq for noble gases, about 2E+18 Bq for iodines and about 1E+17 Bq for aerosols. The release height is 30 m, and zero thermal energy is assumed for the release.

The monitoring stations used in the test scenario are shown in Figure 28, which covers the western part of the Netherlands with the NPP Borssele in the centre. The map represents the RODOS calculation area, which covers 168 x 168 km^2 and is centred around the release point. All stations shown in the map belong to the Dutch national radioactivity monitoring network NMR. The Dutch monitoring network NMR consists of 163 monitoring stations in total, and 47 out of them are inside the RODOS calculation area. Five out of these 47 stations are used as reference stations to assess the performance of the data assimilation, i.e. the reference data is compared against the RODOS prediction before and after data assimilation at these stations. The reference stations are indicated by the red circle in Figure 28. Measurements from all other 42 stations are used in the data assimilation approach.

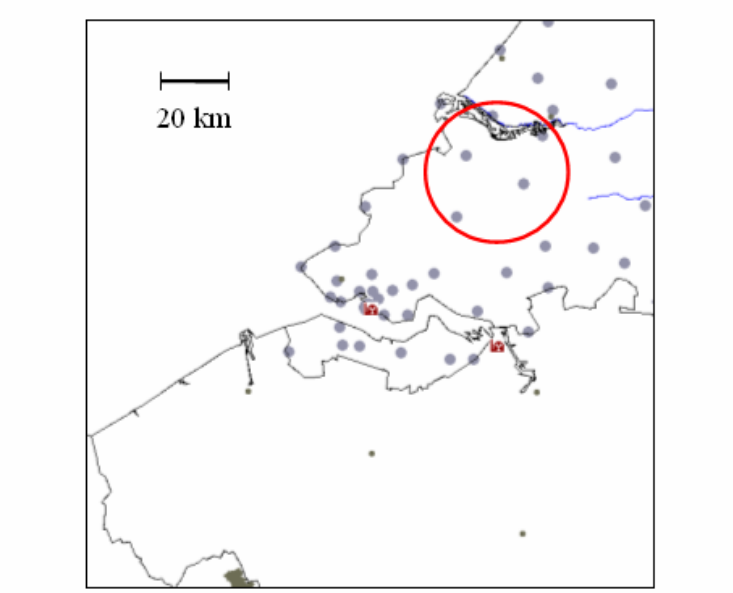

Figure 28: Monitoring stations considered in the test scenario. The NPP Borssele is indicated by a symbol in the centre of the map. The red circle indicates the reference stations which are not considered for data assimilation, but are used to assess the performance of the data assimilation approach.

Reference data set

The reference data is calculated with the NPK-PUFF dispersion model of RIVM (National Institute of Public Health and the Environment, the Netherlands). NPK-PUFF is a version of the Dutch operational dispersion model for emergency management. Originally it has been designed for long range calculations, but now it also covers typical meso-scale distances. The NPK-PUFF model uses KNMI-HIRLAM meteorological fields for the day of the accident. These HIRLAM fields are available for the full area of the Netherlands with a resolution of about 55 km. The dispersion calculation is followed by a deposition and dose modelling. Final results are net gamma dose rates at those 163 detector positions described above. Figure 29 shows such calculated gamma dose rates for several times after the begin of the release.

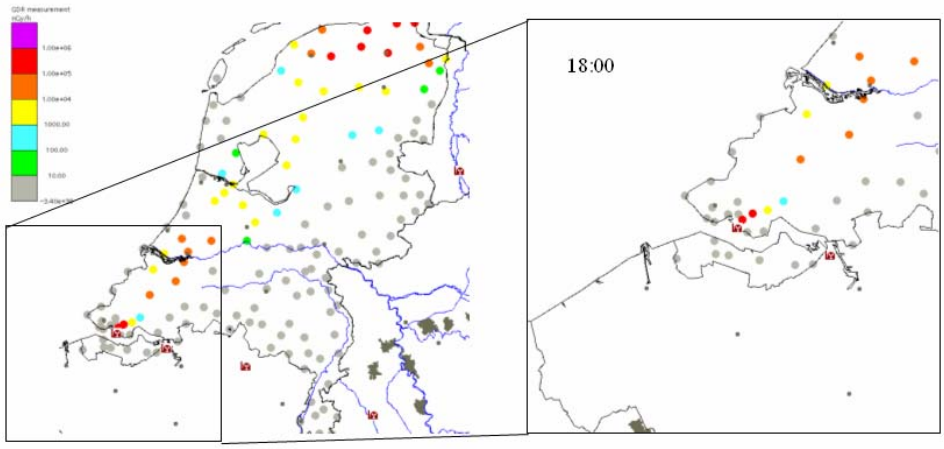

Figure 29: Net gamma dose rate predicted with the Dutch NPK-PUFF model for the all NMR monitoring stations (left) and those stations inside the RODOS calculation area (right). Grey coloured stations indicate zero readings.

RODOS model predictions

RODOS model predictions are calculated with ALSMC and the deposition model as being integrated in RODOS (version 5). ALSMC consists of a meteorological pre-processor and the atmospheric dispersion model ATSTEP, which is an elongated Gaussian puff model [Päsler-Sauer, 1997]. The deposition model has been described above, results as shown in the following are nuclide-specific activity deposited to the ground. The release stopped at 10:00 and the contaminated plume has completely left the RODOS calculation area at about 14:00. After that time the deposition has ended and activity on the ground only changes through radioactive decay. Prediction for ^{137}Cs deposition after plume passage (at 18:00) calculated with the deposition model is shown in Figure 30 (this data is called scenario 1 in the following).

Additionally, two more RODOS predictions were prepared:

- scenario 2: the same meteorological data as in scenario 1 was used, but the source term was scaled down by a factor of 0.01 for all radionuclides (i.e. only 1% of the emission in scenario 1); see Figure 31a.
- scenario 3: a wind direction turned by 30° compared to scenario 1 was used, additionally the source term was scaled down by a factor of 0.01 for all radionuclides; see Figure 31b.

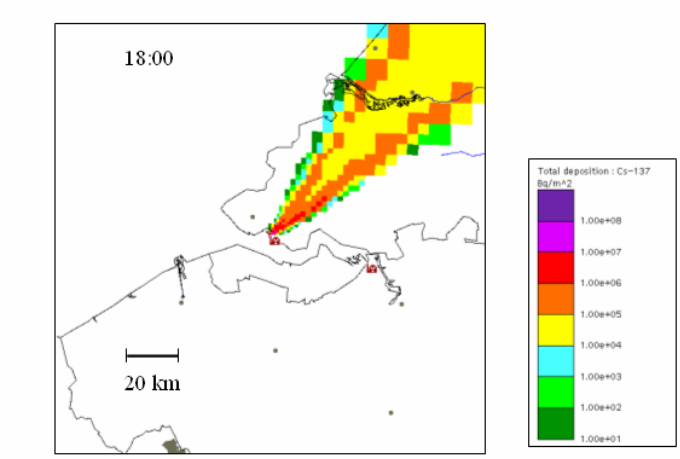

Figure 30: Deposition of ^{137}Cs onto the ground predicted with the deposition model in RODOS for scenario 1.

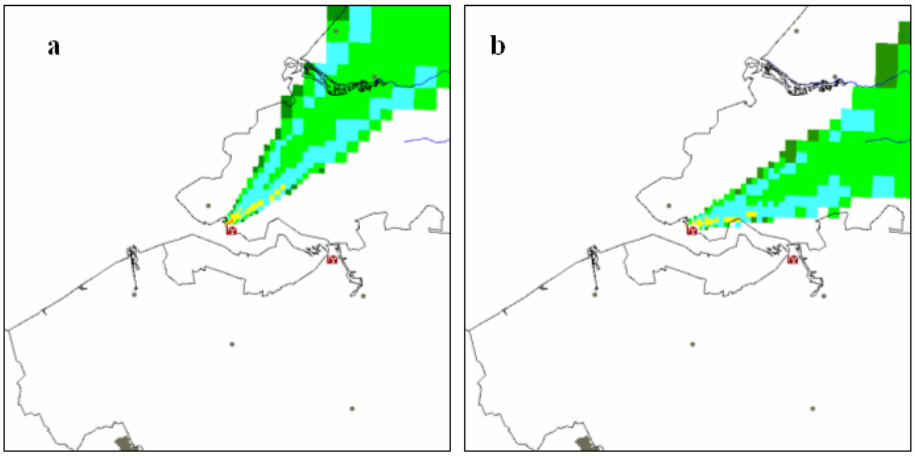

Figure 31: Deposition of ^{137}Cs onto the ground predicted with the deposition model in RODOS for scenario 2 (a) and scenario 3 (b); same legend as Figure 30.

Data assimilation results

Predictions for ^{137}Cs and all other considered radionuclides are updated in the data assimilation process with the EnKF using the gamma dose rate measurements calculated with the NPK-Puff model (reference data set). Results for scenario 1 are shown in Figure 32, for scenario2 in Figure 33a and for scenario 3 in Figure 33b.

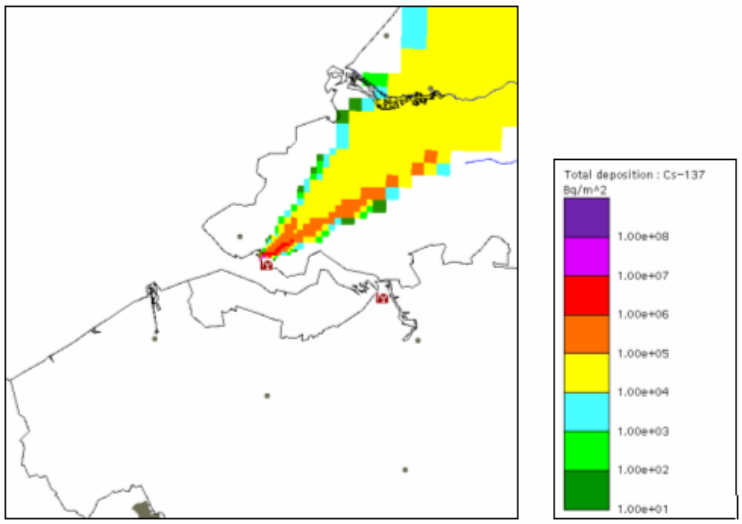

Figure 32: Deposition of ^{137}Cs onto the ground updated by data assimilation (EnKF) of GDR measurements from reference data set for scenario 1.

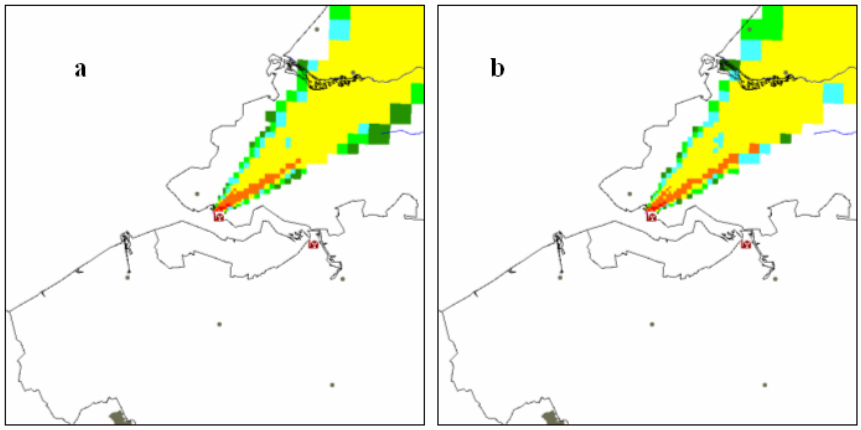

Figure 33: Deposition of ^{137}Cs onto the ground updated by data assimilation (EnKF) of GDR measurements from reference data set for scenario 2 (a) and scenario 3 (b) ; same legend as figure 32.

It can be seen, that the data assimilation with the EnKF leads to quite similar results for all scenarios. When the updated depositions are used to recalculate resulting gamma dose rates at those reference stations which were not used for DA and these results are compared against the reference data set, a significant improvement of the updated RODOS predictions compared to the original RODOS predictions can be noted in all three cases.

Data assimilation in food chain modelling

Another main development aim of the late phase part of DAONEM has been to implement data assimilation into the radioecological modelling of RODOS in order to combine model predictions of feed and food contamination and measured data. The software package FoMM (Food Monitoring Module) has been developed for improving model predictions of radioactive contamination of feed and foodstuffs by assimilation of corresponding

measurements [Richter 2002, RODOS reports 2003]. The food chain model, which is part of FoMM, bases on the ECOSYS model [Müller 1993a]. In a first step, it predicts the radioactive contamination in feed and foodstuffs assuming unit deposition [1 Bq m^{-2}] to soil and to plant. By multiplying these normalised activities with deposition data, the activity concentration of plant products are calculated. Furthermore, by modelling feeding habits and inhalation of radionuclides by animals, activity concentrations of animal products are calculated. FoMM is part of the RODOS module chain [Rojas-Palma 2002, Rojas-Palma 2003].

The Food Monitoring Module FoMM in RODOS

The prototype PV6.1 of the Food Monitoring Module FoMM was implemented into the actual RODOS PV6.0 version.

Input to FoMM is the output of the Deposition Monitoring Module DeMM (see chapter 3) which describes the deposition of nuclides onto agricultural areas. Data provided by DeMM are e.g.

- contamination (Bq/m²) (immediately after deposition) of foliage of plants used as feed and/or foodstuffs,
- contamination (Bq/m²) of vegetated soil (which is considered as representative for agricultural areas) immediately after deposition,
- activity concentration in air (Bq s/m^3) integrated over the time period of the plume passage.

Further input is the measured data of activity concentrations of feed and/or foodstuffs. In the prototype version of FoMM the measured data (activities of feedstuffs and foodstuffs) are read from a data file. In later versions, this data may be provided by the online data base of RODOS.

The endpoints of FoMM are updated values of the food chain model parameters, updated deposited activities and updated activity concentrations in air. These data are used by FDMT for calculating feed and food contaminations as well as ingestion doses. Moreover, FoMM uses these data to calculate the activities of those feedstuffs and foodstuffs, which have been selected by the user and to display them graphically as maps and time-plots.

The main flow of data between the modules around FoMM is shown schematically in Figure 34. The data transfer via files and shared memory is shown in Figure 35.

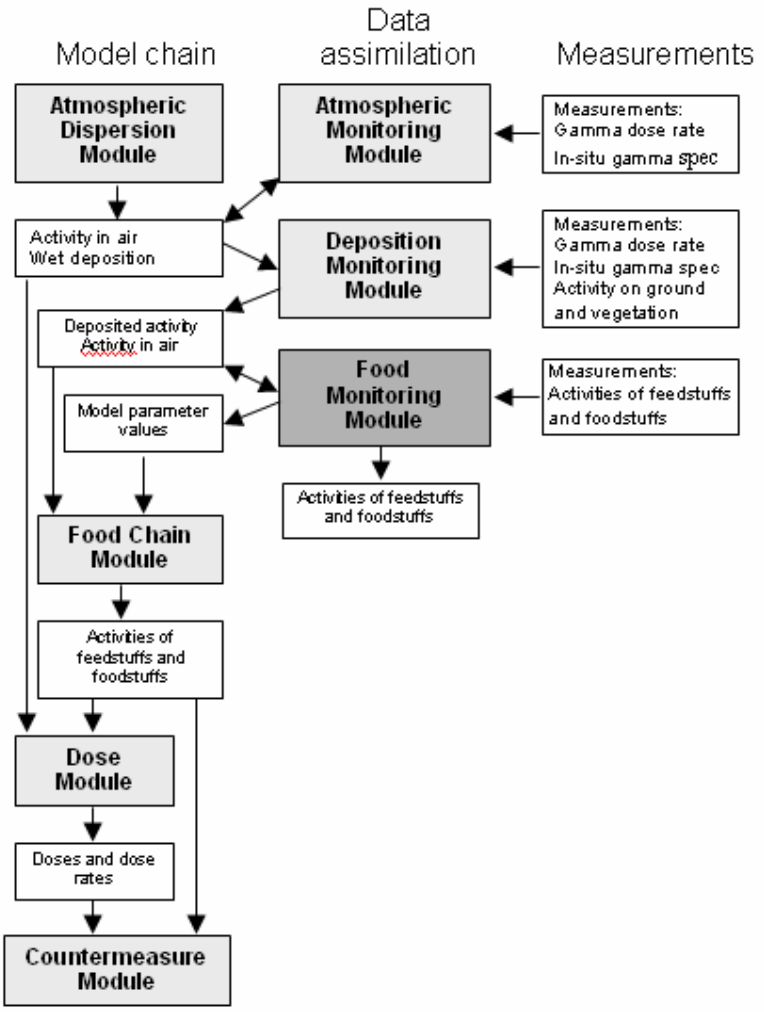

Figure 34: Data flow between modules of the RODOS emergency management system. The Food Monitoring Module is highlighted.

The user of FoMM PV6.1 can select in program windows among different products (feedstuffs and foodstuffs). Furthermore, he can define characteristics of the deposition data. Time courses of model predictions and data assimilated activity concentrations can be displayed. The data assimilated model parameter values are written to files for further use by other RODOS modules. Figure 36 shows an example of a graphical output as it is displayed by RODOS.

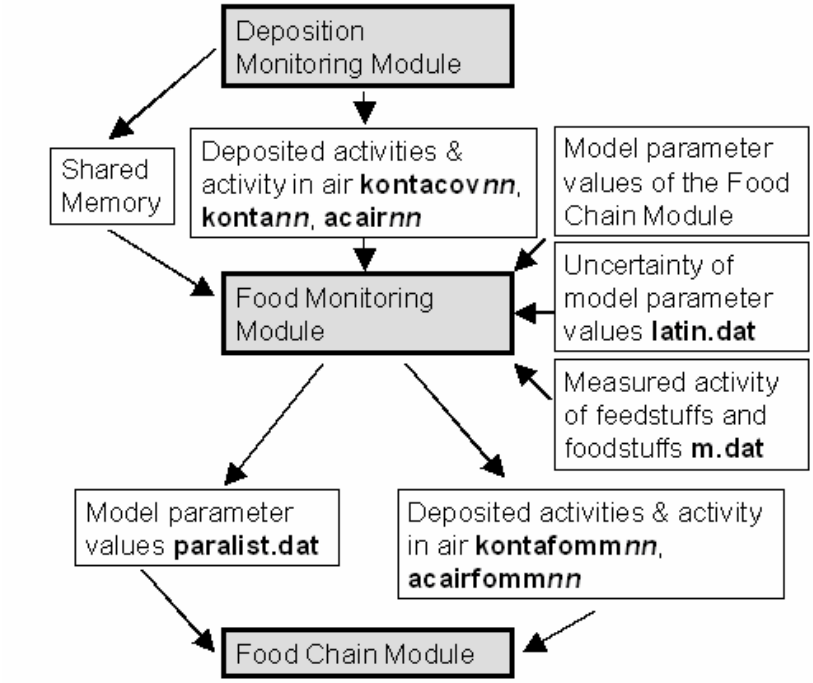

*Figure 35. Data transfer via files (**bold**) and Shared Memory for the Food Monitoring Module.*

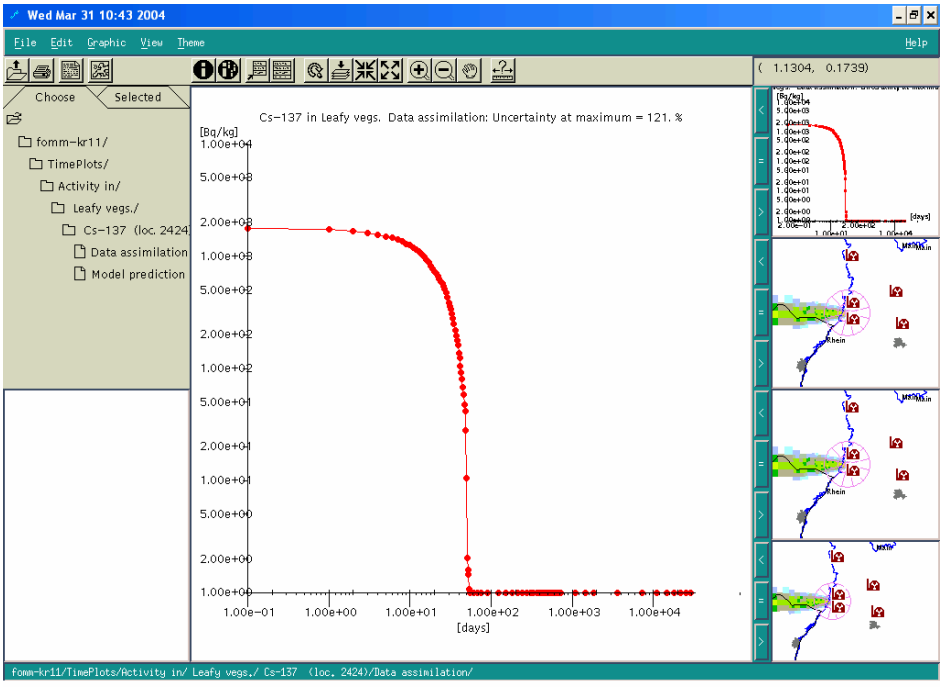

Figure 36. Graphical output of the Food Monitoring Module FoMM PV6.1. The figure shows an example of time-dependent data assimilated activity concentrations of leafy vegetables (logarithmic scale).

Application of the Kalman filter in FoMM

As stated earlier, the Food Monitoring Module uses the Kalman filter as data assimilation tool. Tests with different possible state vector definitions in FoMM have been made. The best results could be achieved with using the values of the model parameters as the elements of the state vector. Therefore, this state vector definition has been implemented in the final version of FoMM. Additionally, FoMM offers the (default) option to augment the state vector with deposited activities and activity concentrations in air. In this case the deposited activities and activity concentrations in air are not only updated by ADUM and DeMM but additionally with food measurements by FoMM.

The number of model parameters in the food chain model is rather high. Therefore, it was necessary to reduce the number of model parameters in the state vector in order to keep the calculation effort reasonably small for an application in a real-time system like RODOS. This has been achieved by determining the key model parameters which contribute most to the uncertainty of the resulting feed/food contaminations. Only these key parameters are used in the state vector.

Identification of key model parameters with sensitivity analysis

For the calculation of activities in feed/foodstuffs a lot of model parameters are needed, such as the weathering rate describing the decrease of radionuclides on plant surfaces due to wind or rain, factors describing the transfer of nuclides from soil to plant, feeding rates and biological half-lives of radionuclides in animals' metabolism. The values of the model parameters are subject to natural variability and thus have always some uncertainty. This causes uncertainties of the values of the normalised activities.

Estimations of the uncertainty of the model parameters have been made in order to estimate the uncertainty of the FoMM results as good as possible. Using the results of earlier studies [Brown 1997, Goossens 2000, Luczak-Urlik 1997, Smith 2002] the uncertainty characteristics of the food chain model parameters were derived. A probability density function (uniform, triangular, normal, log-uniform, log-triangular or log-normal) was assigned to each model parameter. By applying Latin Hypercube Sampling (LHS) and using the probability density functions random values of the model parameters were generated. LHS optimises the choice of the randomly generated parameter values, so that the number of random values can be kept small [McKay 1979]. The resulting ensembles of possible parameter values represent the uncertainty of the model parameters. Furthermore, the ensembles allow to take into account correlations among model parameters [Iman 1982, Owen 1994]. Sensitivity analysis with Monte Carlo methods was carried out in order to identify those model parameters, on which the output of the food chain model is most sensitive. For this analysis routines of the program package PRISM [Gardner 1983] have been used [Müller 1993b]. The routines perform statistical analysis of input and output values and assess the contribution of input data to the uncertainty of output data.

By using the results of the sensitivity analysis, the key model parameters and a description of their uncertainty characteristics have been derived. This serves as input for the Food Monitoring Module.

The Kalman filter in FoMM

With a sub-optimal type of the Kalman filter, the Ensemble Kalman filter [Evensen 1994] high-dimensional nonlinear models, such as the food chain model, can be handled. In the Ensemble Kalman filter the uncertainty of the state vector is described by an ensemble of N state vectors, where each state vector is a possible representation of the system. As in the sensitivity analysis, the initial values of the state vector elements are created with Latin Hypercube Sampling and correlations between model parameters are taken into account. The update equation of a state vector (which contains n vector elements) in the Ensemble Kalman filter can be written as follows:

$$x_k^{(i)} = x_{k-1}^{(i)} + K_k \cdot \left[y_k^{(i)} - M\left(x_{k-1}^{(i)} \right) \right]$$

i:	index of ensemble member; i = 1,…, N
k:	number of Kalman filter application
$x_{k-1}^{(i)}$, $x_k^{(i)}$:	i*th* ensemble state vector before and after Kalman update
K_k:	Kalman gain, n x m matrix
$y_k^{(i)}$:	i*th* ensemble vector with m measured activity concentrations
$M(x_{k-1}^{(i)})$:	vector containing m activity concentrations calculated by using the values of the i*th* state vector

The update of the state vector is achieved by adding a weighted difference between measurement and model prediction to the initial state vector. The weighting factor is the Kalman gain which contains the covariance matrices of the model predictions and the measurements:

$$K_k = \frac{S_k F_k^T}{F_k F_k^T + R_k}$$

K_k:	Kalman gain, n x m matrix
S_k:	n x N ensemble matrix of the state vector
F_k:	m x N ensemble matrix of the model prediction vector
R_k:	m x m measurement error covariance matrix

The numerator of the Kalman gain represents the correlation of the state vector with those model predictions for which corresponding measured values are available. The multiplication of the ensemble matrix F_k with its transpose yields the model error covariance matrix.

For carrying out the Ensemble Kalman filter an ensemble of measurement vectors has to be created [Burgers 1998]. The m diagonal elements of the measurement error matrix R_k contain the variances of the measured values. The uncertainty of the measurements can be given through the experimental set-up or calculated as statistical quantity deduced from several measurements as described below.

The improved predictions are carried out with the Food Monitoring Module for different times beginning with the day of deposition up to 100 years later. Furthermore, FoMM results can be used to display the food contamination on a spatial grid. FoMM calculates ensemble values of activity concentrations, from which percentile values, in particular median values, can be derived. FoMM is able to calculate activity concentrations

- for up to 22 feedstuffs and up to 35 foodstuffs
- for up to 10 radionuclides
- for radioactive deposition on up to 6 deposition days. If there are more than 6 deposition days, interpolation routines are applied. The interpolation routines are able to cover a deposition period of up to 48 deposition days.

In summary, it can be stated, that by considering on the one hand the uncertainty of the model parameters and input data and, on the other hand, the uncertainty of the measurements, updated values for the model prediction are computed. The applied method of data assimilation enhances the quality of food contamination predictions, since the information from the model inter- and extrapolates the information coming from the measurements in several respects:

- at any time, the measurements lead to an update of the predictions of past and future contaminations,
- measurements at individual locations can improve the predictions at the whole calculation grid,
- measurements of certain foodstuffs allow an update also of other products, if their model approaches are correlated,
- measurements at individual locations can improve the predictions at the whole calculation grid,
- measurement of activity concentrations of one nuclide updates the predictions for other radionuclides.

Furthermore, the results of FoMM are associated with less uncertainty than the uncertainty of model prediction and measurements.

The prototype PV6.1 of the Food Monitoring Module FoMM was implemented into the actual RODOS version 6.0. The user of FoMM PV6.1 can select in program windows among different products (feedstuffs and foodstuffs) for which time dependent model predictions and data assimilated activity concentrations be displayed. Furthermore, the user can define

characteristics of the deposition data. The data assimilated model parameter values are written to files for further use by other RODOS modules.

Estimation of the uncertainty of food measurements

The Food Monitoring Module processes measured values of the activity concentration of feed and foodstuff. As shown above, the uncertainty of these measured data is considered in this process. This uncertainty results on the one hand from the pure measurement errors, on the other hand also from a lack of reliability of the measurements. If there are several measurements within the area of a grid cell and within pre-defined time periods, a statistical analysis can be carried out in order to calculate an updated error for the measurements. For FoMM a sub-module has been developed with the aim to determine an uncertainty which takes into account the instrumental uncertainty and the uncertainty due to lack of reliability. The methodology bases on an approach described in [Bevington 1969] and is described in the report RODOS(RA5)-TN(04)-01.

Test and validation studies of FoMM

The Food Monitoring Module FoMM has been tested and validated by using different sets of input data and measurement data. The tests and validation studies include so-called twin experiments with intentionally modified input data, the use of grass and milk measurements which were taken in Bavaria after the Chernobyl accident as well the performance of FoMM with measurements only the very first days after a deposition of radionuclides. Furthermore extreme cases were studied, in which model predictions and measurements provide inconsistent data for data assimilation.

Twin experiments

Calculations have been carried out by using artificial measurements and artificial input data in order to test the Food Monitoring Module. The artificial data are intended as estimations of deposited activities and activity concentrations. The chosen values should demonstrate the capability of data assimilation in the Food Monitoring Module.

In order to test data assimilation so-called twin experiments were carried out. In a twin experiment first a reference data set is created by applying the model to certain input data. This reference data set represents the “true” scenario, e.g. the time course of milk contamination. Some selected values from these “true” data are now considered as measurements. Then a “false” data set of model predictions is created by modifying the input data of the model. By carrying out the Kalman Filter with the “false” model predictions and with the values taken as measurements data assimilated results are calculated. The better the results agree with the “true” data set the better data assimilation is working.

Figure 37 shows an example of a twin experiment. There is a good agreement between the “true” and the median of the data assimilated time course. Figure 38 shows how some elements of the state vector have been changed during the data assimilation process: due to the changes of the state

vector elements an agreement of the "true" time course with the data assimilated time course could be achieved. The updated values of the model parameters can be used later for improved model predictions at other locations.

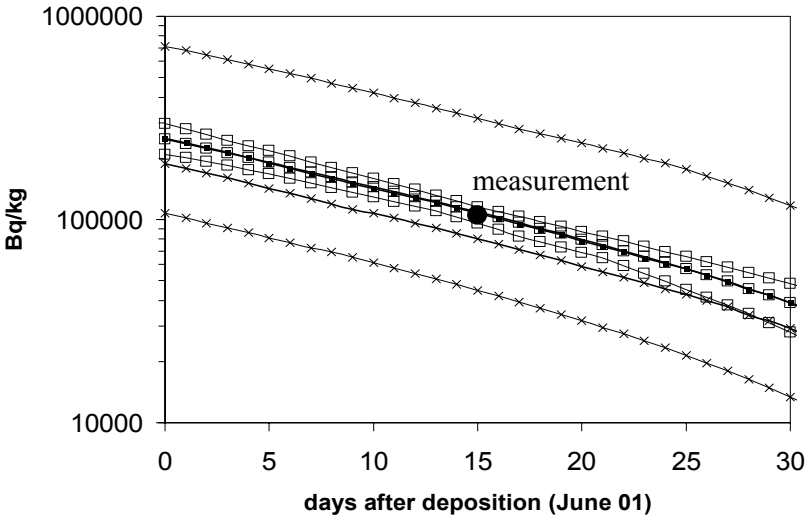

Figure 36: Twin experiment with model prediction and measurement of activity concentration in leafy vegetables. The "true" time course (black squares) has to be compared with the data assimilated time course (empty squares). The data assimilated time course is calculated by data assimilation of the "false" time course and the measurement. The 5% percentile median and 95% percentile time course is shown.

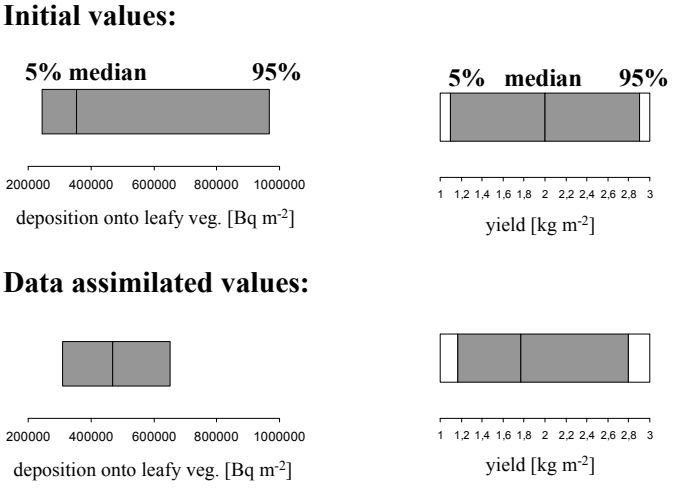

Figure 38: Values of state vector elements before and after data assimilation in case of the twin experiment shown.

Validation studies with Chernobyl data

After the Chernobyl accident in 1986 radionuclides were deposited in many European countries. At Arnhofen, Bavaria, 50 km East of Munich, the contamination of grass and milk was measured. At Neuherberg, near Munich, deposited activities and activity concentrations in air were measured [Hötzl 1987]; this has been used as input data of deposited activities.

The following example (Figure 39) of the validation studies shows the results where the measurements of the whole time course were used for data assimilation. Figure 40 illustrates how the values of the model parameters have been changed during the data assimilation process.

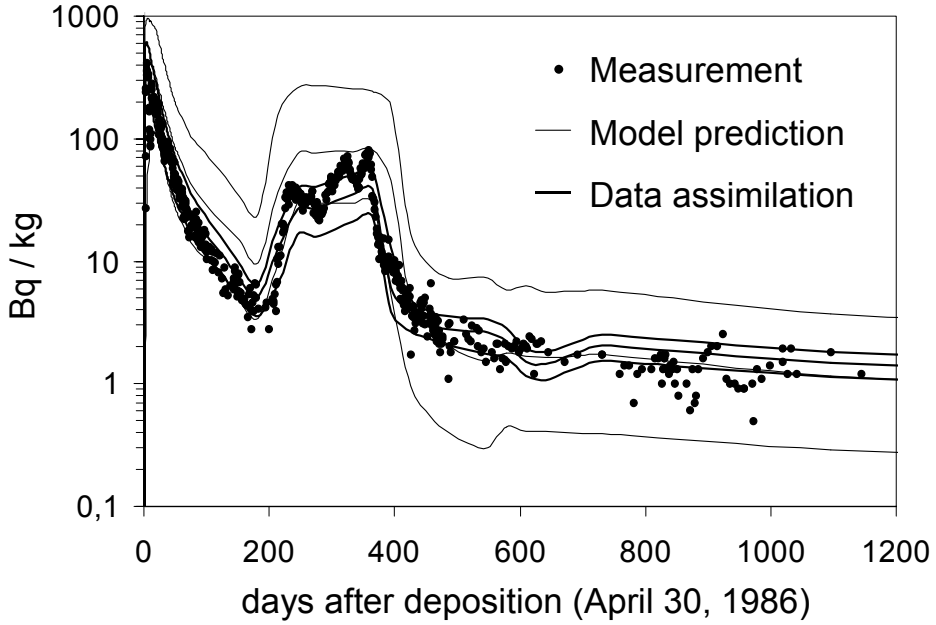

Figure 39: ^{137}Cs activity concentration of milk (5% percentile, median and 95% percentile values). As input data deposited activities measured at Neuherberg, were used. The model prediction of the contamination of grass already agrees well with the measurements. By data assimilation, the uncertainty is reduced.

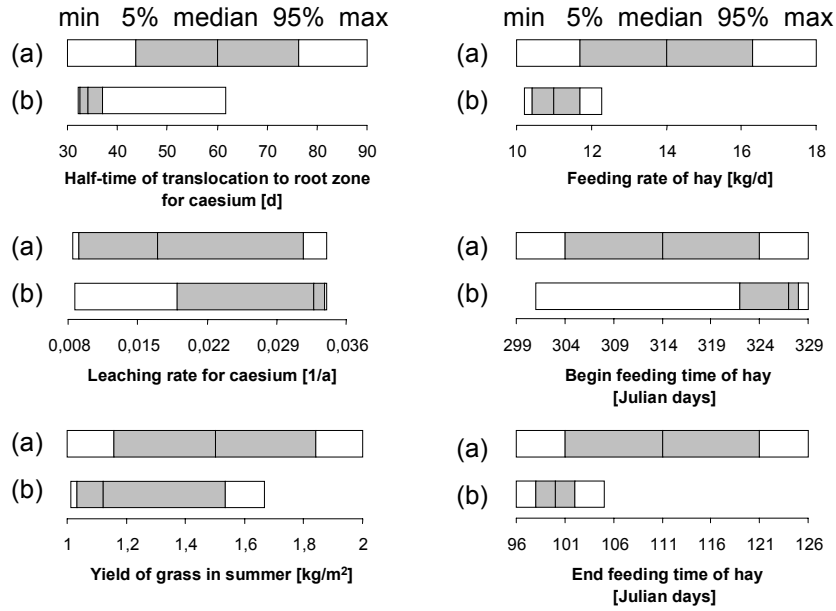

Figure 40: Changes of selected state vector elements due to data assimilation of the predictions of the food chain model with measured values of milk contamination.

The Food Monitoring Module is part of an emergency management system, so the test calculations should reflect the applicability in a real emergency. Therefore, data assimilation runs have been made in which only the measurements of the first days after deposition have been used. Figure 41 shows the result of data assimilation where the milk measurements of the first two days after deposition were used for data assimilation. The result can be compared with the data assimilation results where the milk measurements of the first two years were used. Data assimilation with measurements of the first 2 days (up to the first dotted line) is able to correct the time course considerably. Measurements of 2 years after deposition (up to the second dotted line) lead to a data assimilated time course which matches the observed time course even better, since now the measurements provide more information about long-term processes.

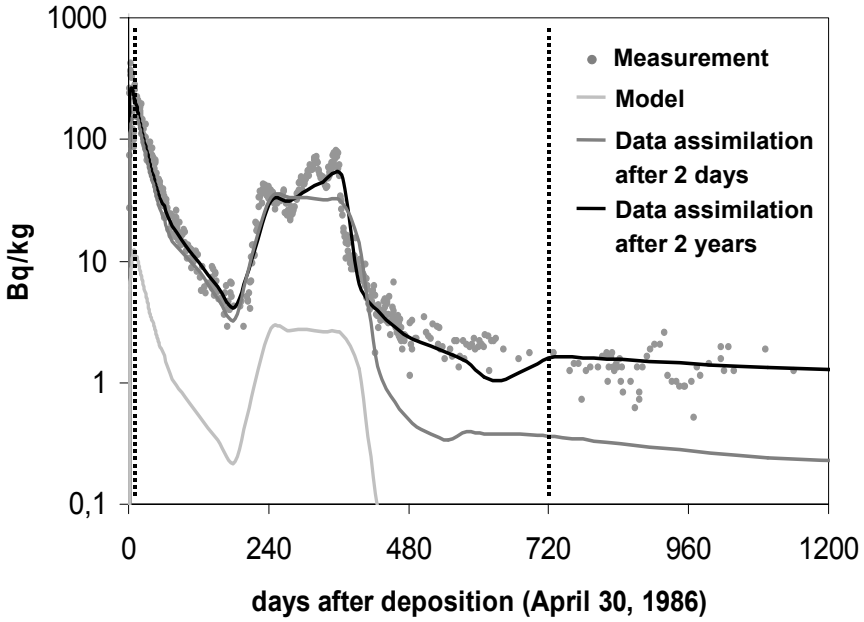

Figure 41: ^{137}Cs activity concentration of milk after the deposition of radionuclides from the Chernobyl accident. The samples were taken at Arnhofen (near Munich, Germany). In order to demonstrate the capability of data assimilation, the prediction of the food chain model is calculated with wrong (underestimated) input data.

Case studies

The data assimilation process in FoMM has been checked with respect to its performance in special cases where problems were anticipated. An example is shown in Figures 42 and 43, where it was assumed that the initial model prediction of maize contamination is zero because of a wrong assumption o f the time of harvest in he model. The measurement of contamination shows a value greater than zero since harvest has occurred in "reality" already. In Figure 42 the time of measurement was within the assumed uncertainty range of the harvest; in this case the result is shifted towards an earlier harvest by data assimilation. In Figure 43 the uncertainty range of the harvest time was estimated too small. In this case the model prognosis remains unchanged, the contradiction between measured value and model prognosis persists, the uncertainty of the state vector elements is not reduced. This shows that an appropriate estimation of the uncertainty ranges of model parameters (like time of harvest) is essential for a successful data assimilation.

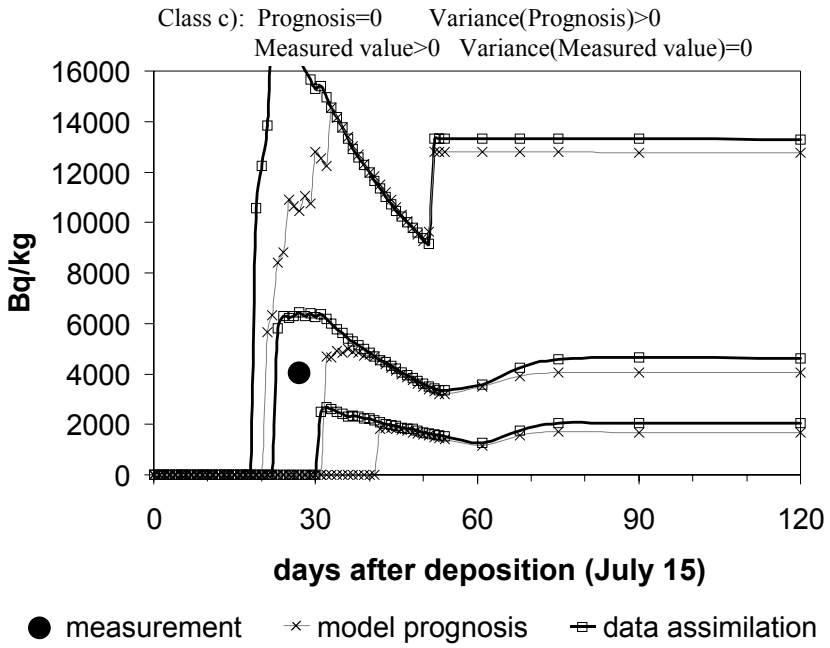

Figure 42:Cs-137 activity concentration of maize; measurement: August, 10. The ensemble members are shifted due to the measurement. Explanation see text.

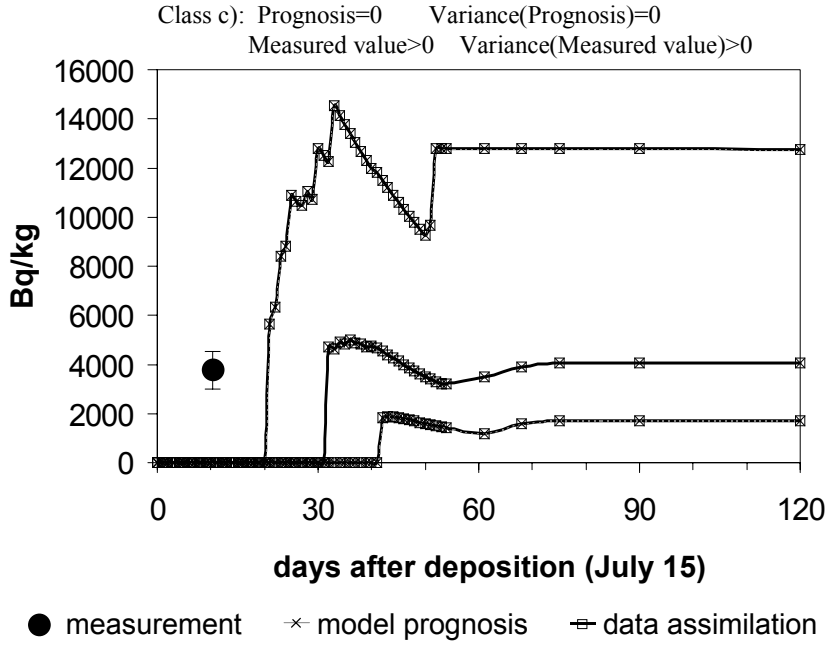

Figure 43: Cs-137 activity concentration of maize; measurement: July, 25. No change of data assimilated time course. Explanation see text.

Data assimilation in the hydrological model chain (WP4)

The objective of workpackages WP4.1 – WP4.4 was to develop and implement data assimilation and uncertainty assessment procedures in the hydrological model chain of the Hydrological Dispersion Module (HDM) of RODOS. The models in HDM simulate the transport and dispersion of radionuclides in the aquatic environment. This includes wash-off from watersheds following an atmospheric deposition and transport and sedimentation in rivers, lakes, reservoirs and coastal areas. The output from the hydrological model chain is used by the aquatic food and dose module in RODOS for calculating the transfer of radionuclides to man and the resulting radiation exposure.

In this project data assimilation and uncertainty assessment procedures have been developed and implemented into the different models in HDM. This includes the basic hydrological model chain that combines a watershed model (RETRACE) for simulation of runoff of radionuclides, following an atmospheric deposition, and a 1D-model for describing radionuclide transport and sedimentation in river systems (RIVTOX). Extended modelling components include 2D (COASTOX) and 3D (THREETOX) models for simulation of radionuclide transport and sedimentation in lakes, reservoirs and coastal areas.

RIVTOX, COASTOX and THREETOX use as input the was-off of radionuclides from RETRACE and can also handle direct releases into the water bodies. If deposition occurs directly on water bodies, surface concentrations from the Atmospheric Dispersion Module (ADM) of RODOS are used as input in COASTOX and THREETOX.

Data assimilation in the basic hydrological model chain

The data assimilation developments in the basic hydrological model chain included development of an uncertainty assessment procedure for the watershed model RETRACE and Kalman filter based data assimilation procedures for the 1D river model RIVTOX. The data assimilation algorithm utilises measurements of concentrations of different radionuclides in solute and on suspended sediments. Direct observations for the watershed wash-off modelling will usually not be available, and hence no updating procedure has been included in RETRACE. In addition to the direct updating of RIVTOX, the basic hydrological model chain is also updated via the updating of the radionuclide depositions in the Deposition Monitoring Module (DeMM).

The main uncertainties in the basic hydrological model chain are caused by errors in the forcing terms and key model parameters. This includes errors in atmospheric deposition, precipitation, source terms (in case of direct releases into the water bodies), and wash-off coefficients that determine the rate of wash-off of radionuclides from watersheds. An outline of the implemented uncertainty propagation and data assimilation procedure is shown in Figure 44.

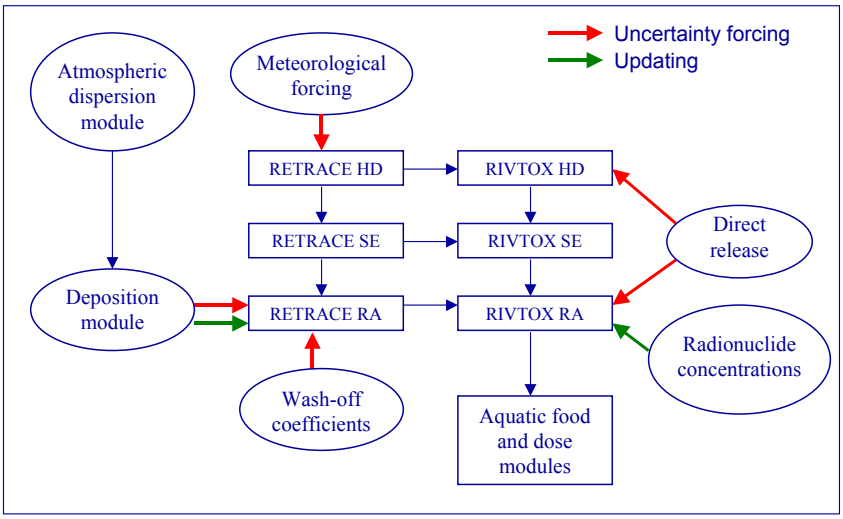

Figure 44 Outline of uncertainty propagation and data assimilation procedure for the basic hydrological model chain. Red arrows indicate the forcing of the model with uncertainties. Green arrows indicate the data flow in the data assimilation update.

Uncertainty assessment in RETRACE

The simulation of radionuclide wash-off from watersheds based on RETRACE is influenced by a number of uncertain quantities. Of these, the uncertainty of the radionuclide depositions, precipitation and the wash-off coefficients are the most important ones. The different uncertainty sources are described as follows.

Radionuclide depositions

The uncertainty of the radionuclide depositions are provided from the Deposition Monitoring Module (DeMM). The data contains an ensemble approximation of the covariance matrix for the time-integrated deposition to the ground (soil covered with lawn) for each day. The deposition is the sum of dry and wet deposition. Data are given for a number of radionuclides at each cell of the model grid in RODOS.

Precipitation

The uncertainty in the precipitation field is described by a relative error that is multi-normal distributed with an exponential correlation structure.

Wash-off coefficients

For each radionuclide the variance of the wash-off coefficient for overland runoff and baseflow are specified. A uniform distribution is applied for the uncertainty propagation. It is assumed that the uncertainties of the individual coefficients are uncorrelated.

To calculate the uncertainty of the output a Monte Carlo approach is adopted. In this case a number of independent RETRACE runs are made using the ensemble realisations of the radionuclide depositions and randomly generated precipitation fields and wash-off coefficients

according to the specified statistics. The output from RETRACE includes an ensemble of water and radionuclide wash-off to each river cell. In addition, the mean of the ensemble is calculated and stored. The ensemble output from RETRACE is used as input in the data assimilation and uncertainty assessment module in RIVTOX.

To test the RETRACE uncertainty assessment module and analyse the relative importance of the different uncertainty sources on the output a sensitivity analysis has been performed. For this analysis data for the Ilia river in 1988 published in Nikitin et al. (1992) were used. The density of ^{137}Cs depositions on the Ilia catchment after the Chernobyl accident is shown in Figure 45. This is used as initial conditions for the radionuclide wash-off simulations by RETRACE. The wash-off coefficients for ^{137}Cs for the surface runoff and baseflow components were, respectively, 0.0085 m^{-1} and 0.004 m^{-1}. Uniform precipitation over the catchment was assumed. See Kolomeev and Madsen (2002) for a more detailed description of the model setup.

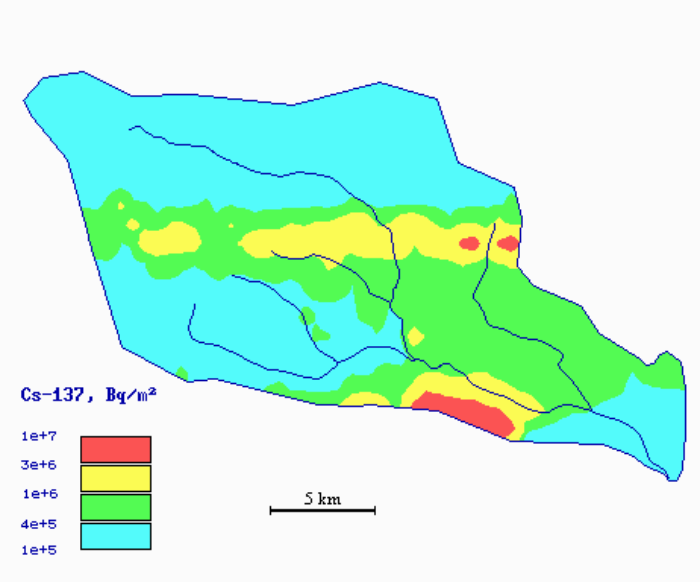

Figure 45 Density of ^{137}Cs depositions on the Ilia catchment after the Chernobyl accident.

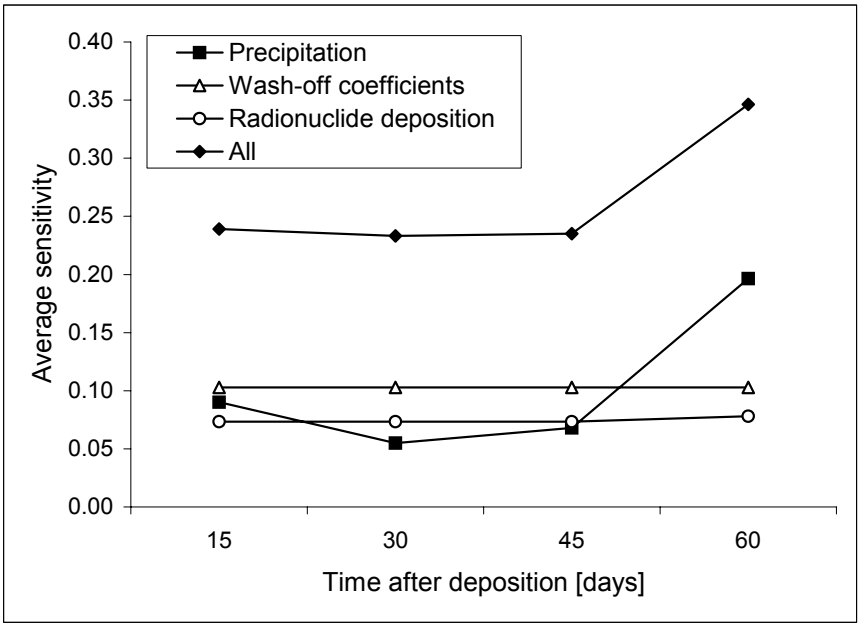

Figure 46 Average relative uncertainty of radionuclide wash-off to river cells.

The uncertainty of the wash-off was simulated by considering each of the three uncertainty sources (precipitation, radionuclide deposition and wash-off coefficients) individually as well as jointly. For each source a 10% relative uncertainty was assumed. The average relative uncertainty for all river cells is shown as a function of time in Figure 46. For both radionuclide deposition and wash-off coefficients the sensitivity on the wash-off is almost constant during the simulation period, whereas the sensitivity to precipitation varies during the simulation. In general, the uncertainty in the wash-off coefficients is the most dominating uncertainty source. The sensitivity with respect to precipitation is highly dependent on the precipitation rate.

Data assimilation in RIVTOX

Within the project several sub-optimal variants of the Kalman filter algorithm (Todling and Cohn, 1994) have been analysed. Two of these were further advanced and implemented in the 1D radionuclide transport model RIVTOX, the Ensemble Kalman filter (EnKF) (Evensen, 1994) and the reduced rank square root (RRSQRT) filter (Verlaan and Heemink, 1997).

The EnKF provides a robust filtering procedure but suffers from a low rate of convergence of the covariance matrix, which generally requires high computational demands. Additionally, being a Monte Carlo procedure it possesses a *statistical noise* problem. In this project a modified version of the EnKF has been developed and implemented in RIVTOX, which reduces the impact of statistical noise caused by

applying a finite ensemble size. The main features of the new algorithm are:

- A more accurate random number generator, the Mersenne Twister algorithm (Matsumoto and Nishimura, 1998).
- A square-root implementation of the update step whereby the perturbation of the observations is avoided (Whitaker and Hamill, 2002).
- A new sampling scheme in which the statistical properties of the generated ensemble are set equal to the population values (Evensen, 2004).

Details of the algorithm are reported in Treebushnyy et al. (2004).

The RRSQRT filter provides a relatively fast and stable scheme, which can be seen as a deterministic ensemble approach, but opposed to the EnKF no noise is introduced by the finite low rank approximation. On the other hand, the RRSQRT filter includes truncation of the covariance matrix, which causes difficulties in case the state vector is formed of physical variables of different orders of magnitude. This is the case with a multi-phase modelling system such as RIVTOX that includes three phases of the modelled radionuclide; in solute phase, in suspended sediments, and in bottom depositions, respectively.

The extension of the RRSQRT filter, denoted Subspace Parsing Enhanced Reduced Rank Square Root (SUPERR SQRT) filter, is described in detail in Treebushny and Madsen (2003, 2004). The algorithm provides a more efficient truncation step of the RRSQRT. The main advantages are:

- It utilises explicitly the block structure of the state vector that naturally appears in a multiphase system.
- It gives the modeller an additional degree of freedom by specifying independently the number of modes used to represent each sub-space (or phase in a multi-phase system).
- No normalisation of the square-root matrix is needed. When applying the classical RRSQRT, normalisation is used to deal with a state vector with variables of different orders of magnitude. However, no optimal normalisation as such exists and hence important covariance information can be lost in the truncation step using normalisation.
- It includes a precision coefficient that can be tuned for specific applications depending on the trade-off between precision and computational load. The classical RRSQRT cannot be tuned.
- It uses less computational time than the classical RRSQRT algorithm, which is extremely important for real-time application in the RODOS system.

In addition to the data assimilation development, improvements of the numerical engine of RIVTOX have been carried out. The major positive impact on the stability of the data assimilation is implementation of a

fully implicit numerical scheme that solves the advection-dispersion part of the pollutant transport. The implicit scheme is known to be very robust, and hence unphysical corrections produced by the filter will not cause any instability that will eventually lead to a blow-up, which is often encountered with a pure explicit scheme.

The developed data assimilation procedures have been applied for simulation of ^{90}Sr propagation in the Dnieper river. A comprehensive set of river contamination data exists for the Dnieper river after the Chernobyl accident. The last event of propagation of a significant amount of radionuclides through this river system was measured in 1999 during the high spring flood in the Pripyat river basin (Voitsekhovich et al., 2002). Due to inundation of the contaminated floodplains in the Chernobyl zone ^{90}Sr was discharged into the Pripyat river and further discharged into the Kiev reservoir during the flood event. The propagation of this wave of contamination was measured in the entire Dnieper river reservoir cascade.

The model consists of 6 reservoirs in series from Kiev reservoir to the Black Sea (Figure 47), which includes a total river length of about 840 km. For 1999 measurements of ^{90}Sr in the solute phase are available in 5 of the reservoirs for every 10 days. In the data assimilation tests measurements were assimilated at the upstream Kiev reservoir, whereas the downstream measurements were kept for validation. Thus, the test showed how the simulation of radionuclides is affected at downstream points by updating at an upstream point. For the EnKF an ensemble size of 50 was used and for the SUPERR SQRT filter a low rank subspace approximation in each of the three components equal to 25 was applied.

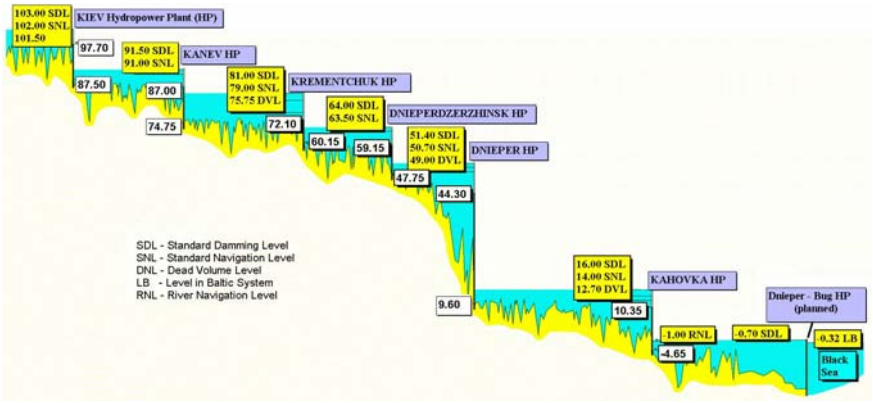

Figure 47 The cascade of reservoirs in the Dnieper river.

Results of the data assimilation applications are shown in Figure 48-Figure 50. The figures compare the EnKF and SUPERR SQRT with a simulation without assimilation at the measurement point in Kiev reservoir (Figure 48) and in two downstream validation points in Kanev reservoir (Figure 49) and in Kakhovka reservoir (Figure 50). Both filters produce comparable results that in general are closer to the measurements at both the measurement location and at the downstream validation points. When using the filter, one should define measurement

and model error statistics according to prior knowledge about the uncertainties. If unrealistic statistics are used, one may adapt closely to a noise measurement, which is not supported by the downstream validation points. For instance, the observed concentration peak in Kiev reservoir is highly uncertain and probably overestimated. The filtering procedure provides a balanced update between the model forecast and the measurement, which is consistent with the observed peak at the downstream reservoirs.

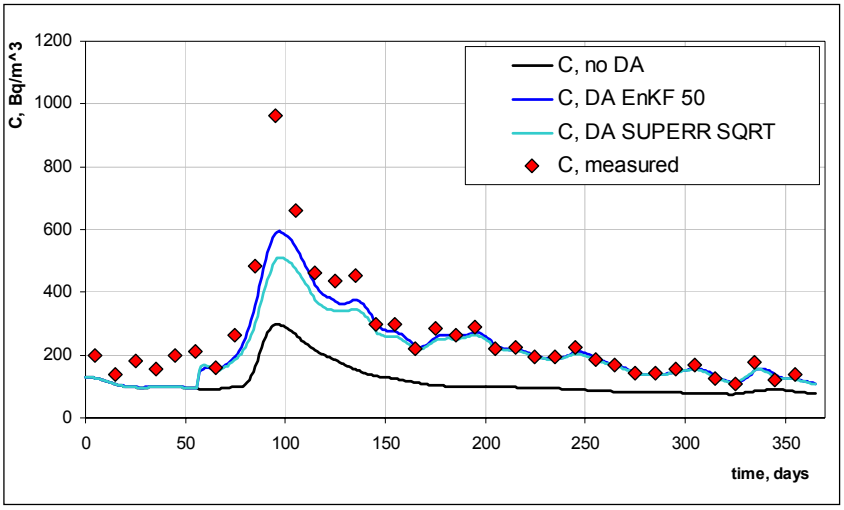

Figure 48 Simulated concentration of ^{90}Sr in solute phase in Kiev reservoir (measurement location).

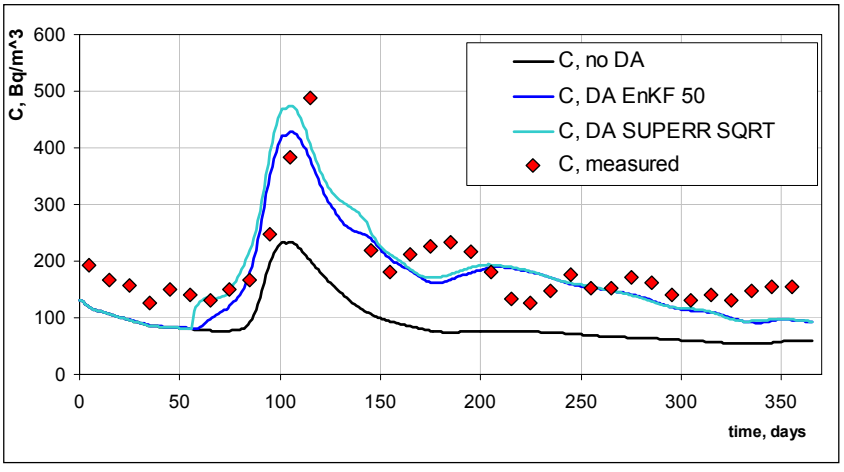

Figure 49 Simulated concentration of ^{90}Sr in solute phase in Kanev reservoir (validation).

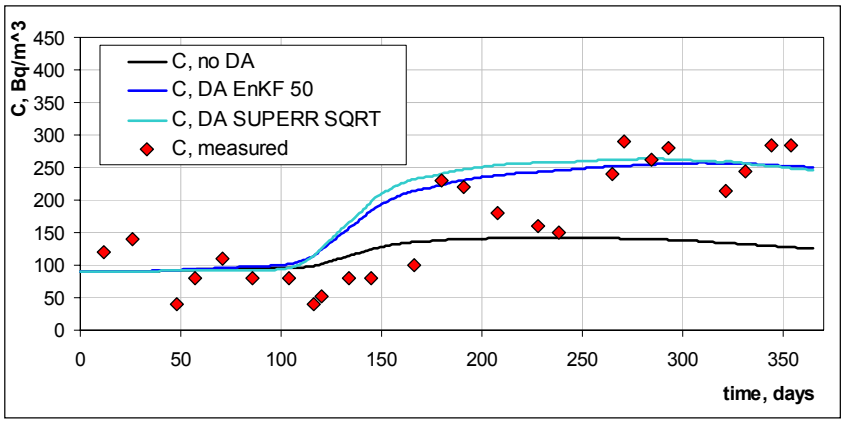

Figure 50 Simulated concentration of ^{90}Sr in solute phase in Kakhovka reservoir (validation).

In conclusion, the test showed that both filters are suitable tools for improving the prediction skills in RIVTOX, and, importantly, they provide an estimate of the prediction uncertainty. The improved EnKF has been chosen as the default assimilation scheme when using RIVTOX in combination with RETRACE since this allows a transparent and consistent transfer of the ensemble approximation of the uncertainty in the output from RETRACE as forcing of the RIVTOX model. For a stand-alone application of RIVTOX both filters can be used. In the test, an ensemble size of 50 was shown to be sufficient to produce reliable results. An ensemble size of 50 will in most applications be feasible for real-time applications of RIVTOX in the RODOS system.

Data assimilation in the extended hydrological model chain

The data assimilation developments in the extended hydrological model chain included development of Kalman filter based data assimilation procedures for the 2D model COASTOX and the 3D model THREETOX. The implemented data assimilation algorithms utilise measurements of concentrations of different radionuclides in solute and on suspended sediments.

For the data assimilation in COASTOX and THREETOX the EnKF and RRSQRT filter cannot be directly applied due to the high computational load of these models. Instead more cost-effective procedures have been developed and tested. These include different sub-optimal variants of the Kalman filter that assume constant, time-independent uncertainty in the model forecast and the measurements, and hence do not require propagation of the full covariance matrix (or rather its ensemble approximation) between measurement updates. These techniques are only slightly more expensive than a normal model run and therefore highly suitable for operational applications in the RODOS system.

Data assimilation in COASTOX

In COASTOX a data assimilation procedure based on optimal interpolation has been developed and implemented. Optimal

interpolation is a particular sub-optimal Kalman filter in which the forecast error covariance matrix is replaced by an approximation that is computed as the product of a time-independent correlation matrix and a diagonal variance matrix (Cohn et al., 1981; Ghil et al., 1982; Marshall, 1985). The correlation matrix is based on the assumption that the mass field errors are homogeneous, isotropic, and that their correlations have a Gaussian dependence on distance. The evolution of the forecast error variance matrix between update times is prescribed as the sum of the updated variance matrix at the last update time step and an empirically determined variance matrix that approximates the mean forecast error integrated over a model time step. The procedure is described in more detail in Kivva et al. (2004).

Available data of measurements of ^{90}Sr concentrations at the inflow and outflow of the Kiev reservoir for the period March - April 1999 (Voitsekhovich at al., 2002) were used for setting up a hypothetical twin test experiment for testing the optimal interpolation method. The observed concentrations of ^{90}Sr were taken as boundary conditions for a numerical simulation of ^{90}Sr transport in the Kiev reservoir. The results of this simulation were used for generation of "measurement data" of ^{90}Sr in the solute phase at 9 locations in the reservoir. These measurements where then used for updating a simulation where the inflow boundary conditions for ^{90}Sr were changed. The model setup and the location of the "measurement points" are shown in Figure 51.

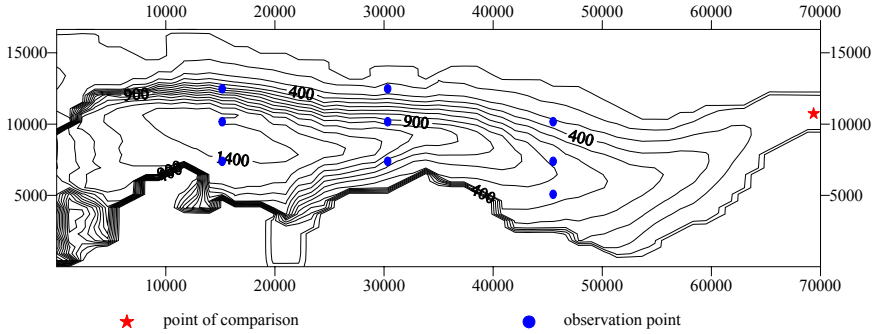

Figure 51 Concentration of ^{90}Sr (Bq/m^3) in solute phase 25 days after start of the simulation. Location of "measurement points" and point of comparison.

In Figure 52 comparison of results for observed and changed boundary conditions, with and without data assimilation is provided at a point located at the outlet of the Kiev reservoir (see Figure 51). The test showed that the optimal interpolation procedure improves the predictive capabilities of the COASTOX model. In addition, for operational applications in the RODOS system the procedure has several important advantages:

- It is rather simple to setup and apply. The user only needs to specify two algorithmic parameters: (i) the correlation length of the Gaussian correlation model, and (ii) the mean forecast variance integrated over a time step.

- It is a robust procedure that provides physically consistent and smooth updates of the concentration fields.
- It is a computationally cheap method, which is only slightly more expensive than a normal model run.

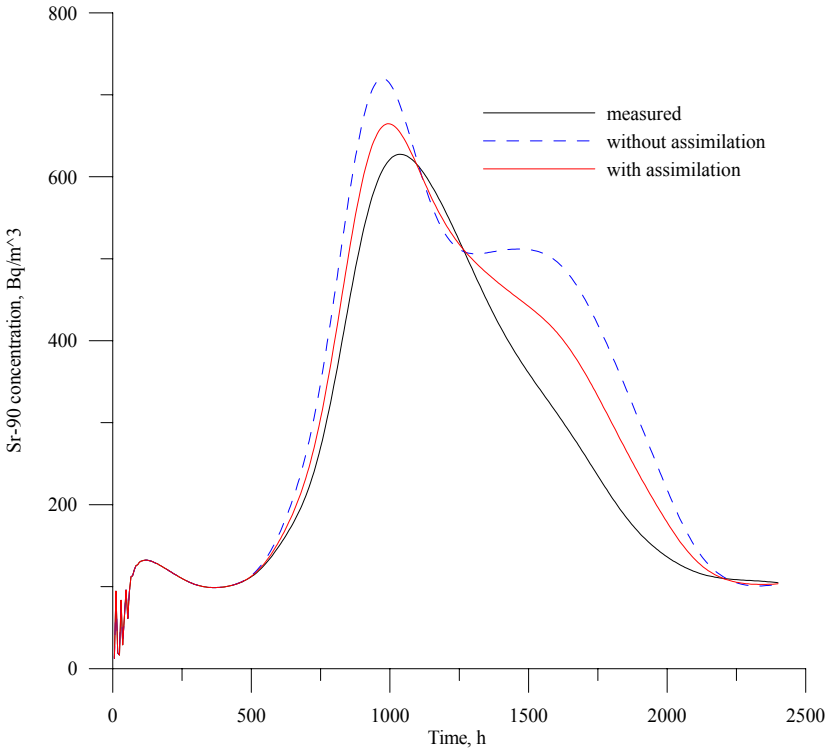

Figure 52 Comparison of ^{90}Sr concentrations in solute phase at the outlet of the Kiev reservoir for different scenarios.

Data assimilation in THREETOX

Three different sub-optimal variants of the Kalman filter have been developed and implemented into the THREETOX model. These include:

- Variance evolution method.
- Steady state Kalman filter (Steady KF).
- Iterative optimal interpolation (OI).

The methods are based on different approximations of the covariance matrix. All methods assume that the covariance can be expressed as a product of a time-independent correlation matrix and a diagonal variance matrix. While the variance evolution method propagates the variance matrix according to the system dynamics between model updates, a constant variance matrix is assumed in the Steady KF and OI method. The procedures are described in more detail in Yuschenko et al. (2004).

The three data assimilation methods were applied to the observed data of ^{137}Cs concentrations for the period June 1986 to September 1990 in the Black Sea. Preliminary tests demonstrated that the variance evolution method has severe stability problems, and hence it was excluded from further analysis. Results of the other two data assimilation procedures at one of the update times are shown in *Figure*. In this figure red points indicate measurements used for the data assimilation and blue points validation points used for calculation of the root mean square error (RMSE). In general, the OI method modifies the radionuclide field more than the Steady KF. In addition, the structure of the radionuclide field obtained with OI is smoother than the radionuclide field obtained from the Steady KF. The Steady KF seems to push the corrected field too much towards the observations, and hence produces a very irregular field.

The calculated field of radionuclide concentration presented in Figure 53 shows a high maximum in the middle of the Black Sea when simulations are performed without data assimilation. This maximum is doubtful from a physical point of view and it is not consistent with the observed concentrations. When applying the OI data assimilation procedure, the maximum vanishes on the updated field.

The overall performance of the data assimilation procedures in terms of RMSE is shown in Figure 54 and compared with the RMSE for a simulation without data assimilation. The RMSE is decreasing with time, which is caused by a decrease of the average concentration. The rate of decrease is almost the same for the simulations with and without data assimilation. The RMSE values for the updated concentrations based on the Steady KF are only slightly smaller than the RMSE values obtained from the simulation without data assimilation. The reduction of RMSE is more significant when the OI method is applied, the reduction being in the order of 10 to 20 Bq/m^3 over the simulation period. The relative reduction in RMSE is increasing with time, indicating the strong effect of the data assimilation on the model predictions.

In addition to the Black Sea test example the OI method was applied in a twin-test experiment based on a model setup of the Kakhovka Reservoir. For this test case THREETOX was integrated with the Atmospheric Dispersion Module (ADM) in RODOS for calculation of the reservoir contamination after atmospheric fallout caused by a hypothetical release from the Zaporozhje NPP. Also in this test case an improvement of the radionuclide dispersion simulation was obtained when using the OI data assimilation procedure. More details on these tests are given in Yuschenko et al. (2004).

In conclusion, the tests showed that the OI method is preferable for data assimilation in the THREETOX model and significantly improves the predictive capability of the model. In addition, it has several important advantages for application in an operational setting. It is simple to setup and apply, robust, and computationally cheap.

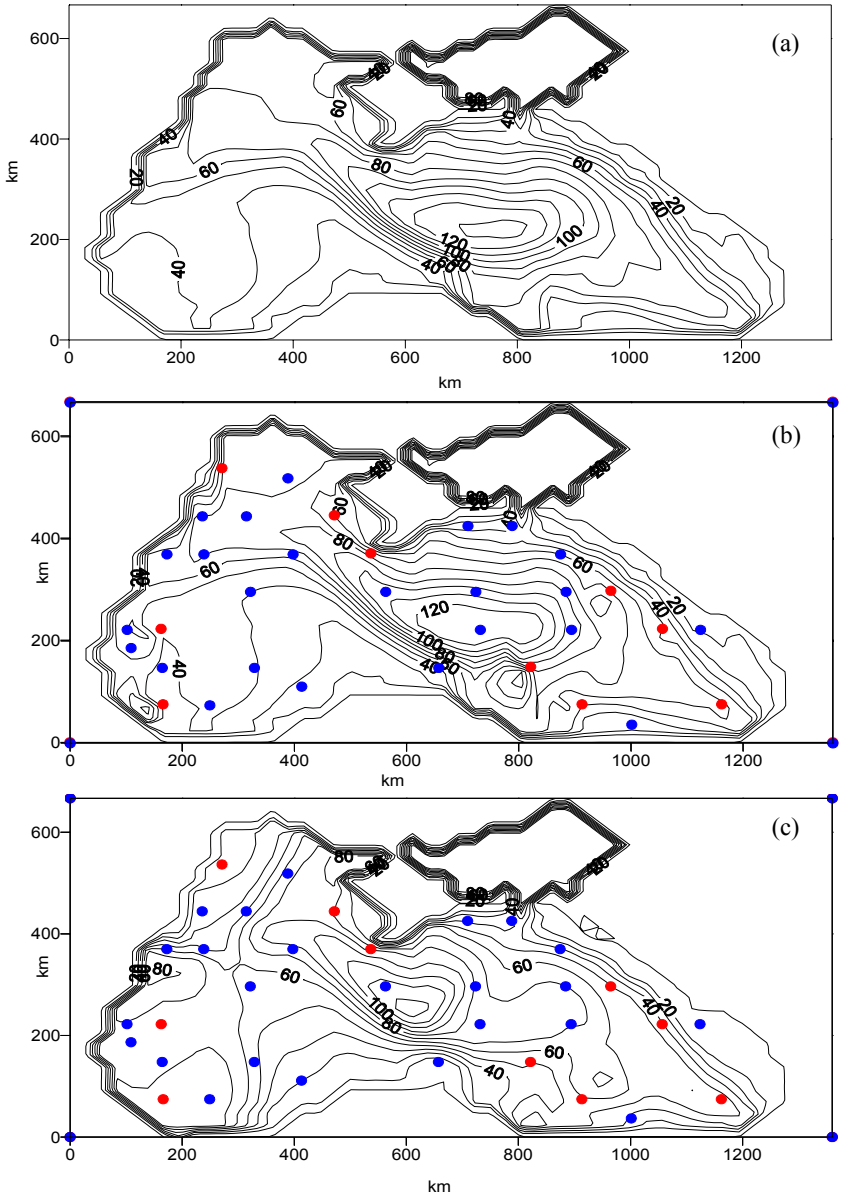

Figure 53 Concentration of ^{137}Cs in the surface layer, June 1987 (Bq/m^3): (a) without data assimilation, (b) Steady KF, (c) OI.

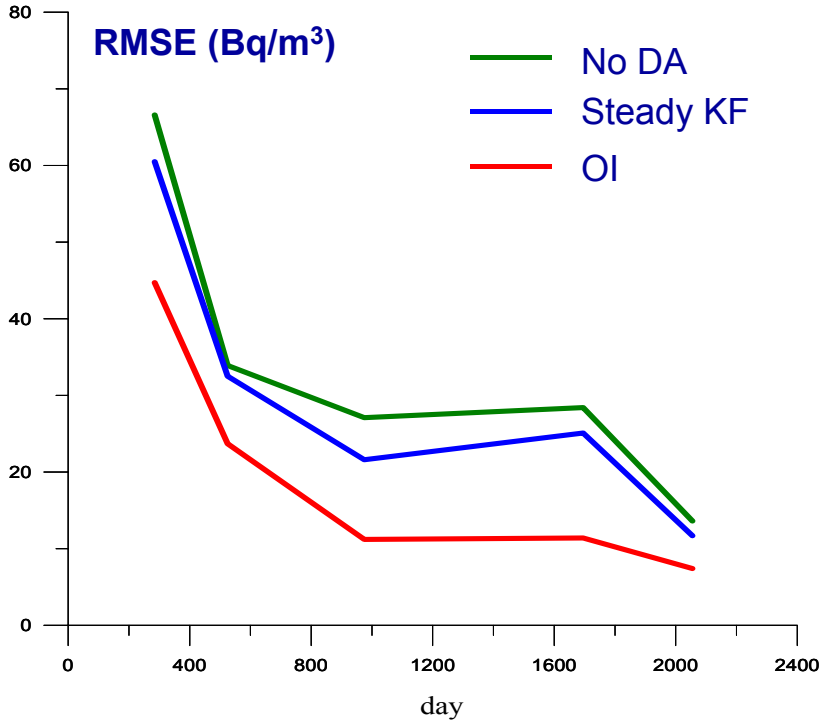

Figure 54 Root mean square error (RMSE) of predicted radionuclide concentrations in the surface layer in validation points. A THREETOX simulation without data assimilation (No DA) is compared with the steady Kalman filter (Steady KF) and the iterative optimal interpolation (OI).

Assessment of results and conclusions

Data assimilation in the early phase

A Kalman filtering module has been created for the Risø Mesoscale Puff dispersion model RIMPUFF built into RODOS. Based on predicted and measured 10-minute averaged gamma dose rates, it updates the state of the modelled puffs, i.e. their position and their content of radioactivity. And a separate but anyway connected module has been created to give uncertainty information for a following RODOS late phase deposition monitoring module, which implements an Ensemble Kalman filter.

Kalman filtering is intended for updating predictions with the help of measurements, keeping this difference small. The test cases indicate that, given reasonable circumstances, the developed Kalman filter enhances the predictive capability of the RIMPUFF model so that the gamma dose predictions get closer to those measured than what is found without applying Kalman filtering. "Reasonable circumstances" here means a reasonably tight net of detector points, a reasonably well specified wind field, and a reasonable accurate release rate.

The test cases also indicate that RIMPUFF as such, and the Kalman filtering of it, should benefit from a model that could limit the source specification error. Such a model might be based on a large amount of spatially distributed on site and near off site spectral gamma measurements, on site meteorology, and known plant status. It could be one that does not anticipate a certain form of the cloud but makes a kind of variational calculation on the 3D concentration distribution around the plant, or may be just a simpler iteratively optimized Gaussian plume model.

Another achivement with potential of enhancing the outcome of the presented model is data assimilation of the Numerical Weather Prediction model forecasts used as input to the RODOS meteorological pre-processor which delivers the needed meteorological fields for the dispersion calculation. Such work is under way, Kovalets et al. (2004).

Data assimilation in the late phase

The results of the twin experiments and the realistic test scenarios for data assimilation in the deposition model in RODOS show, that the Ensemble Kalman filter can be applied successfully to improve the model predictions of radioactive contamination on the ground by means of measured data. The improvement of model prediction is substantially determined by the uncertainty information about the prediction from the atmospheric dispersion models. Aside the improved prediction, the EnKF also delivers uncertainty information about the updated prediction. Such information can be highly relevant for decision makers in case of a nuclear emergency. The use of a generic data assimilation methodology in RODOS enables the propagation of uncertainties throughout the various models.

For the food chain model it can be stated, that the chosen sub-optimal type of the Kalman filter, the Ensemble Kalman filter, is a suitable data assimilation tool for improving model results by using the information coming from measurements. By considering on the one hand the uncertainty of the model parameters and input data and, on the other hand, the uncertainty of the measurements, updated values for the model prediction are computed. The applied method of data assimilation thus enhances the quality of food contamination for all point in times, locations, products and radionuclides which make use of the updated model parameters and input data. Furthermore, the results of FoMM are associated with less uncertainty than the uncertainty of model prediction and measurements. For this, FoMM helps to take measures aimed at minimizing health risks of population in the late phase after a nuclear emergency on a more reliable basis.

The current results for data assimilation in the late phase modules of RODOS are quite promising and allow the prognosis, that such tools have the potential to become operational in radiological decision support systems in future. This will facilitate the overview over all relevant information's in case of a nuclear emergency. Even with increasing information from measurements the prognosis of the radiological situation can be kept up-to-date. Nevertheless, considerable development work is still necessary to make data assimilation fully operational in all parts of the RODOS system.

Data assimilation in the hydrological model chain

Data assimilation and uncertainty assessment procedures have been developed and implemented into the different models in the Hydrological Dispersion Module (HDM) of RODOS. These include the watershed model RETRACE, the 1D river model ROVTOX, the 2D model COASTOX, and the 3D model THREETOX.

For the RETRACE model an uncertainty assessment module has been developed (RETRACE ASUN). The implementation is based on a Monte Carlo simulation approach that propagates the main uncertainty sources, including the radionuclide depositions, wash-off coefficients and precipitation. For the radionuclide depositions the uncertainty given by the ensemble approximation in the Deposition Monitoring Module (DeMM) is used. The output from RETRACE ASUN includes uncertainties in the runoff and radionuclide wash-off to the river model RIVTOX in terms of ensemble approximations.

For the RIVTOX model two different sub-optimal variants of the Kalman filter, the EnKF and the reduced rank square root (RRSQRT) filter, have been further developed. In the EnKF different enhancements have been made that reduces the impact of statistical noise caused by applying a finite ensemble size. For the RRSQRT filter a new algorithm has been developed that provides a more efficient truncation of the low-rank approximation of the covariance matrix. This new filter, denoted Subspace Parsing Enhanced RRSQRT, is especially tailored for use in a multi-phase system such as RIVTOX. The implemented data assimilation methods have been tested on a

setup of the Dnieper river for simulation of the transport and dispersion of ^{90}Sr caused by inundation of the contaminated floodplains in the Chernobyl zone in 1999. The test showed that both filters are suitable tools for improving the prediction skills in RIVTOX, and, importantly, provide an estimate of the prediction uncertainty.

For data assimilation in COASTOX and THREETOX the EnKF and RRSQRT filter cannot be directly applied due to the high computational load of these models. Instead more cost-effective procedures have been developed and tested. These include different sub-optimal variants of the Kalman filter that assume constant, time-independent uncertainty in the model forecast and the measurements, and hence do not require propagation of the covariance (or rather its ensemble approximation) between measurement updates. These techniques are only slightly more expensive than a normal model run. Twin-test experiments with simulated measurements based on model setups of the Kiev and Kakhovka reservoirs were applied for testing the methods. In addition, a test has been conducted based on ^{137}Cs dispersion in the Black Sea caused by Chernobyl fallout. These tests have shown that the implemented data assimilation procedures enhance the prediction capabilities of the models.

Testing the developed data assimilation tools has proven their ability to improve the quality and reliability of predictions. But it became also obvious that problems may occur in practical application due to imperfect uncertainty estimation, e.g. if measurement or prediction errors exceed the estimated uncertainty of measurements or models. For this reason, further testing and application of the developed data assimilation tools in realistic off-site emergency management situations is necessary in order to make the methodologies more robust in operational application.

Acknowledgements

This work has been possible thanks to EURATOM's 5th Framework Program funding through contract FIKR-CT-2000-00025. The editor in representation of the whole consortium wishes to thank the Lawrence Livermore National Laboratory operating the National Atmospheric Release Advisory Center (USA) and the Rijksinstitut voor Volksgezondheid en Milieu (NL) for their collaboration in the preparation of simulated monitoring data used to evaluate the methodologies developed in this project.

References

Bevington, P., *Data reduction and Error Analysis in the Physical Sciences*, McGraw-Hill Book Company, New York, 1969.

Brown, J., Goossens, L.H.J., Harper, F.T., Haskin, E.H., Kraan, B.C.P., Abbott, M.L., Cooke, R.M., Young, M.L., Jones, J.A., Hora, S.C. & Rood, A., *Probabilistic Accident Consequence Uncertainty Analysis: Food Chain Uncertainty Assessment*. Prepared for US Nuclear Regulatory Commission and Commission of European Communities, NUREG/CR-6523, EUR 16771 (Washington, USA and Brussels-Luxembourg), Volumes 1 and 2, 1997.

Burgers, G., van Leeuwen, P. J. & Evensen, G., *Analysis Scheme in the Ensemble Kalman Filter*, Monthly Weather Review, **126(6)**, pp. 1719 – 1724, 1998.

Cohn, S.E., Ghil, M., and Isaacson, E., 1981, Optimal interpolation and the Kalman filter. In: *Proceedings of the 5th Conference on Numerical Weather Prediction, Am. Meteorol. Soc*., Boston, Massachusetts, 36-42.

Evensen, G., 2004, Sampling strategies and square root analysis schemes for the EnKF. Available at

http://www.nersc.no/~geir/EnKF/Publications/eve04a.pdf

Evensen, G., *Sequential data assimilation with a non-linear quasi-geostrophic model using Monte Carlo methods to forecast error statistics*. J. Geophys. Res., **99**, pp. 10143 – 10162, 1994.

Gardner, R.H., B. Rojder, B. & Bergstrom, U., *PRISM: A systematic Method for Determining the Effect of Parameter Uncertainties on Model Predictions*. Tech. NW-83/555 (Nykoping, Sweden: Studsvik Energitek AB), 1983.

Gering, F.; Hübner, S.; Faria, A.E.; French, S.: *Model Description of the Deposition Monitoring Module (DEMM)*. RODOS(WG5)-TN(99)16, 2000

Ghil, M., Cohn, S.E., and Dalcher, A., 1982, Sequential estimation, data assimilation, and initialisation. In: *The Interaction Between Objective Analysis and Initialization, (D. Williamson, ed.),* Publ. Meteorol. 127 (Proc. 14th Stanstead Seminar), McGill University, Montreal, 83-97.

Goossens, L.H.J. & Kelly, G.N. (eds.), *Expert Judgement and Accident Consequence Uncertainty Analysis*, Radiation Protection Dosimetry - Special Issue, **90(3)**, 2000.

Hötzl, H., Rosner, G. & Winkler, R., *Ground Depositions and Air Concentrations of Chernobyl Fallout Radionuclides at Munich-Neuherberg*, Radiochimica Acta 41, 181-190, 1987.

Iman, R.L. & Conover, W.J., *A Distribution-Free Approach to Inducing Rank Correlation Among Input Variables*, Communications in Statistics, Part B – Simulation and Computation, **11(3)**, pp. 311 – 334, 1982.

Kalman, R.E.: *A new approach to linear filtering and prediction problems*. J. Basic Eng., 82D, 35-45, 1960

Kelly, G.N; Ehrhardt, J; Shershakov, V.M.: *Decision support for off-site emergency preparedness in Europe*. Radiation Protection Dosimetry, 64, 1/2, pp. 129-141, 1996.

Kivva, S.L., Zheleznyak, M., Madsen, H.*, Data assimilation algorithm implemented into the 2D radionuclide transport model COASTOX*, RODOS(RA5)-TN(04)-03, 2004

Kok, Yvo, Private communications, 2003

Kolomeev, M., Madsen, H., *Description of RETRACE: A new catchment model of the hydrological dispersion module in the RODOS system*, RODOS(RA5)-TN(01)-06. 2002

Kovalets, I.; Andronopoulos, S.; Bartzis, J.G.; Gounaris, N.; Kushchan, A. *Introduction of data assimilation procedures in the meteorological pre-processor of atmospheric dispersion models used in emergency responce systems.* Atmospheric Environment, 38, pp 457-467, 2004.

Luczak-Urlik, D., Bleher, M., Jacob, P., Müller, H., Hofer, E. & Krzykacz, B., *Unsicherheits- und Sensitivitätsanalyse von Anwendungen des Programmsystems PARK*, GSF – Forschungszentrum für Umwelt und Gesundheit, Institut für Strahlenschutz, GSF-Bericht 6/1997.

Marshall, J.L., 1985, Determining the ocean circulation and improving the geoid from satellite altimetry, *J. Phys. Oceanogr.*, 15, 330-349.

Matsumoto, M., Nishimura, T., 1998, Mersenne Twister: A 623-dimensionally equidistributed uniform pseudorandom number generator. *ACM Trans. Modeling and Computer Simulation*, 8, 3-30.

McKay, M.D., Conover, W.J. & Beckman, R.J., *A Comparison of Three Methods for Selecting Values of Input Variables in the Analysis of Output From a Computer Code*, Technometrics, **21**, pp. 239 – 245, 1979.

Mikkelsen, T.; Larsen, S.E.; Thykier-Nielsen, S.*Description of the Risø Puff Diffusion Model.* Nucl. Technol. 67, pp 56-65, 1984

Müller, H. & Pröhl, G., ECOSYS-87: *A Dynamic Model for Assessing Radiological Consequences of Nuclear Accidents*. Health Physics, **64(3)**, pp. 232 – 252, 1993a.

Müller, H., Friedland, W., Pröhl, G. & Gardner, R.H., *Uncertainty in the Ingestion Dose Calculation*. Radiation Protection Dosimetry, **50(2-4)**, pp. 353 – 357, 1993b.

Nikitin A.I., Bovkun L.A. et al., 1992, Investigation of ^{137}Cs and ^{90}Sr wash-off from a catchment contaminated as a result of the Chernobyl accident. *In: Ecological and Geophysical Aspects of Nuclear Accidents*, Moscow, 50-57 (in Russian).

Owen, A.B., *Controlling Correlations in Latin Hypercube Sampling*. Journal of the American Statistical Association – Theory and Methods, **89(428)**, pp. 1517 – 1522, 1994.

Puch, Roberto O.; Astrup, Poul, *An Extended Kalman Filter Methodology for the Plume Phase of a Nuclear Accident.* RODOS(RA5)-TN(01)-07, 2002

Richter, K., F. Gering, H. Müller, G.Pröhl, *Methodology for modelling the uncertainty of food model predictions in RODOS PV6.0*. Prepared at GSF-Forschungszentrum für Umwelt und Gesundheit, Neuherberg, within the EU program 'Data Assimilation for Off-Site Nuclear Emergency Management', Report No. RODOS(RA5)-TN(02)-06, 2003.

Richter, K., Gering, F. & Müller, H., *Data assimilation for assessing radioactive contamination of feed and foodstuffs*, in: C.A. Brebbia & P. Zannetti (Eds.), Development and Application of Computer Techniques to Environmental Studies. Proceedings of the Ninth International Conference on the Modeling, Monitoring and Management of Environmental Problems ENVIROSOFT 2002, pp. 393–402. Wessex Institute of Technology Press, Southampton, 2002.

Richter, K., Müller, H. & Gering, F., *Documentation of the Food Monitoring Module FoMM in RODOS PV6.0*. Prepared at GSF-Forschungszentrum für Umwelt und Gesundheit, Neuherberg, within the EU program 'Data Assimilation for Off-Site Nuclear Emergency Management', Report No. RODOS(RA5)-TN(03)02, 2003.

Richter, K., Müller, H. & Gering, F., *Documentation of the Food Monitoring Module FoMM in RODOS*. Prepared at GSF-Forschungszentrum für Umwelt und Gesundheit, Neuherberg, within the EU program 'Data Assimilation for Off-Site Nuclear Emergency Management', Report No. RODOS(RA5)-TN(04)02, June 2004.

Richter, K., Müller, H. & Gering, F., *Model description of the Food Monitoring Module FoMM*. Prepared at GSF-Forschungszentrum für Umwelt und Gesundheit, Neuherberg, within the EU program 'Data

Assimilation for Off-Site Nuclear Emergency Management', Report No. RODOS(RA5)-TN(03)01, 2003.

Richter, K., Müller, H. & Gering, F., *Test and validation studies of the Food Monitoring Module*. Prepared at GSF-Forschungszentrum für Umwelt und Gesundheit, Neuherberg, within the EU program 'Data Assimilation for Off-Site Nuclear Emergency Management', Report No. RODOS(RA5)-TN(04)04, June 2004.

Richter, K., Müller, H. & Gering, F., *Uncertainty of measurements in the Food Monitoring Module (FoMM)*. Prepared at GSF-Forschungszentrum für Umwelt und Gesundheit, Neuherberg, within the EU program 'Data Assimilation for Off-Site Nuclear Emergency Management', Report No. RODOS(RA5)-TN(04)01, March 2004.

Richter, K., Müller, H. & Gering, F., *User Guide of the Food Monitoring Module FoMM in RODOS PV6.0*. Prepared at GSF-Forschungszentrum für Umwelt und Gesundheit, Neuherberg, within the EU program 'Data Assimilation for Off-Site Nuclear Emergency Management', Report No. RODOS(RA5)-TN(03)01, 2003.

Richter, K., Müller, H. & Gering, F., *User Guide of the Food Monitoring Module FoMM in RODOS*. Prepared at GSF-Forschungszentrum für Umwelt und Gesundheit, Neuherberg, within the EU program 'Data Assimilation for Off-Site Nuclear Emergency Management', Report No. RODOS(RA5)-TN(04)03, June 2004.

Rojas-Palma, C., Madsen, H., Gering, F., Puch, R., Turcanu, C., Astrup, P., Müller, H., Richter, K., Zheleznyak, M., Treebushny, D., Kolomeev, M., Kamaev, D. & Wynn, H., *Data assimilation in the Decision Support System RODOS*, Radiation Protection Dosimetry, **104(1)**, pp. 31 – 40, 2003.

Rojas-Palma, C., Turcanu, C., Madsen, H., Gering, F., Astrup, P., Puch-Solis, R., Müller, H., Richter, K., Zheleznyak, M., Kolomeev, M. & Kamaev, D., *Data assimilation with Kalman Filters in the Decision Support System RODOS*, Transactions of the American Nuclear Society, Vol. 87, 569-571, 2002.

Sass, B.H.: *The DMI Operational HIRLAM Forecasting System, Version 2.3*. DMI Techical Report 94-8, Danish Meteorological Institute, 1994

Thykier-Nielsen, S.; Deme, S.; Mikkelsen, T., *Description of the Atmospheric Dispersion Module RIMPUFF*. RODOS(WG2)-TN(98)-02, 1998

Todling, R., Cohn, S.E., 1994: Suboptimal schemes for atmospheric data assimilation based on the Kalman filter, *Mon. Weather Rev.*, 122, 2530-2557.

Treebushny, D. and Madsen, H., 2004, Implementation of a new truncation step in the reduced rank square root filter. Subspace Parsing

Enhanced Reduced Rank Square Root filter, DAONEM report, DHI Water & Environment.

Treebushny, D., Madsen, H., 2004, On the construction of a reduced rank square root Kalman filter for efficient uncertainty propagation, *Future Generation of Computer Systems*, In press.

Treebushny, D., Madsen, H., Zheleznyak, M., 2004, Additional testing of the RIVTOX data assimilation module for the Dnieper river case study, RODOS(RA5)-TN(04)-01.

Verlaan, M., Heemink, A.W., 1997, Tidal flow forecasting using reduced rank square root filters, *Stochastic Hydrol. Hydraul*., *11*, 349-368.

Voitsekhovich O.V., Zheleznyak, M., Monte, L., 2002, Comparative analyses of different modelling approaches to simulate radionuclide transport through the Dnieper reservoirs based on extremal flood 1999 scenario. *Radioprotection – colloques*.

Whitaker, J.S., Hamill, T.M. 2002, Ensemble data assimilation without perturbed observations, *Mon. Weather Rev.*, 130, 1913–1924.

Document History

Document Title:	DAONEM Final Report
RODOS number:	RODOS(RA5)-RE(04)-01
Version and status:	Version 1.0 (final)
Authors/Editors:	Carlos Rojas Palma
Address:	Belgian Nuclear Research Center (SCK•CEN) Radiation Protection Division Boeretang 200 B-2400 Mol, Belgium
Issued by:	Carlos Rojas Palma
History:	
Date of Issue:	30 September, 2004
Circulation:	Public
File Name:	
Date of print:	September 2, 2005